Controlling the Bistability of a Trypsin-Based Enzymatic Reaction Network

Master Dissertation Chemical Engineering

(Molecular and Materials Engineering Track)

October 28th, 2024

Pepijn G. de Vries, BSc

Chemical Reaction Networks (CRN) Group

Department of Molecules and Materials

Faculty of Science and Technology

Thesis Committee:

Committee Chair: Dr. Albert S. Y. Wong

External committee member: Dr. Ivana Q. Lin

External committee member: Dr. Hil G. E. Meijer

Daily Supervisor: Dmitrii V. Kriukov, MSc

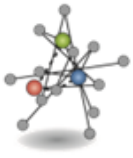

UNIVERSITY OF TWENTE.

Summary

Bistable systems are systems that can exist in one of two stable states and can dynamically switch between these states. Naturally occurring self-regulatory mechanisms such as Turing patterns, homeostasis and cell differentiation all require bistability to exist. Systems chemistry, the field that studies complex chemical networks (CRNs), has recently seen many examples of bistable chemical networks that exhibit interesting properties. Many agree that synthesizing controllable bistable chemical networks will ultimately aid in the creation of artificial life-like systems. For a system to show bistability, it must contain a feedback loop, which is a mechanism where part of the system's output is redirected back into the input. The strength of the feedback directly determines the system's bistable conditions. The most straightforward chemical analogue of feedback is autocatalysis, a type of reaction in which the product of a conversion reaction catalyzes its own formation. In such a case, the strength of the feedback is the rate of autocatalysis. By chemically changing the rate of autocatalysis, the bistability of a network can be controlled. Bistability in CRNs has been widely studied, but experimental demonstrations of control over bistability by tuning the strength of the chemical feedback is rare. In this work, we use a well-known enzymatic autocatalytic chemical network which has been shown to be bistable. Trypsin (Tr) is the central molecule, which is formed autocatalytically by cleavage of its precursor, trypsinogen (Tg). To enable us to control the release of Tr and to switch between steady states, soybean trypsin inhibitor (STI) is added. This network is bistable because it shows two possible states, a high [Tr] state and a low [Tr] state, when placed in the right conditions. Recent work in our group has shown that, by using lanthanide ions such as La^{3+} and Nd^{3+}, the rate of autocatalysis can be controlled. In this work, we introduced La^{3+}, which undergoes the simplest mechanism out of these ions, to the trypsin autocatalytic network. We aimed to address the missing link between chemical feedback and bistability in current systems chemistry by introducing La^{3+} as a control parameter to shift the network's bistability. We performed an experimental investigation of the effect of La^{3+} on the autocatalysis in the presence and absence of constant flow, and on the bistability of the network. We found that La^{3+} increases the rate of autocatalysis until a saturation point around 1.0 mM in batch. From the batch data, we chose experimental conditions to work in flow, where we found that using La^{3+} indeed shifts the bistability. Higher concentrations of La^{3+} caused a need for higher inhibitor concentrations to suppress the high-[Tr] steady state and increased the magnitude of this high-[Tr] state. We envision that the results reported here will inspire more work into the control of various other bistable networks with interesting functionalities by tuning the feedback loops.

Contents

Glossary

Abbreviation/Symbol:	Meaning:
ϵ	Molar absorbance coefficient of pNA. Used to convert absorbance into pNA concentration.
τ	Residence time. Next to the flow rate in µL h^{-1}, this is a measure to quantify the flow of liquid through a CSTR.
BAPNA	Nα-Benzoyl-DL-arginine *p*-nitroanilide hydrochloride. Reporter molecule to track Tr activity.
Ca^{2+}	Calcium ion. Used for stabilization of the proteins in storage conditions.
CRN	Chemical Reaction Network. Group of chemicals that react together. Also the abbreviation of the name of the research group within which this thesis was performed.
CSTR	Continuously Stirred Tank Reactor. Used to create out-of-equilibrium conditions.
La^{3+}	Lanthanum ion. Used as a control knob for the key demonstration in this thesis.
pNA	*p*-nitroaniline. Yellow-colored split-off product when BAPNA is hydrolyzed.
STI	Soybean Trypsin Inhibitor. Inhibits activity of Tr.
Tg	Trypsinogen. One of the core proteins used in the chemical network. Precursor to trypsin.
Tr	Trypsin. The core protein used in the chemical network that is studied in this thesis.
TRIS-HCl	tris(hydroxymethyl)aminomethane buffer adjusted with HCl. Used to buffer reaction conditions (at pH 7.8).

Chapter 1 – Introduction

1.1 – Context

Bistability is a dynamic property in which a system can exist in one of two possible stable states and can switch between these two states [1]. In living systems, bistability is a necessary property for cell differentiation [2] and apoptosis [3], and more broadly, bistability enables memory [4], formation of Turing patterns [5] [6] and homeostasis [7], playing an important role in self-regulation. Inspired by living nature, contemporary research on chemical reaction networks (CRNs) aims to design artificial bistable systems capable of intelligent functions [8]. Systems chemistry, the field that studies complex chemical networks, has seen great recent interest in bistable chemical systems. Recreation, understanding of and gaining control over bistability has been of large interest towards the synthesis of artificial life-like systems [9].

In open systems (i.e., systems where exchange of matter or energy with the environment is possible, see Chapter 2.1), bistability requires the presence of feedback loops within the system [10]. These feedback loops, pathways that reconnect a portion of the output back to the input, enable the system to give nonlinear responses to changes in the environment [11]. In chemistry, the most straightforward form of positive feedback is an autocatalytic reaction (see **Figure 1.1**), which is a specific type of reaction where the product of a reaction (B) catalyzes its own formation from a fuel (A) [12]. The rate of autocatalysis determines the strength of the positive feedback by tuning how fast the catalyst species stimulates its own formation. The strength of the feedback (i.e., the rate constant k), therefore, controls the system output (i.e., the concentration of B).

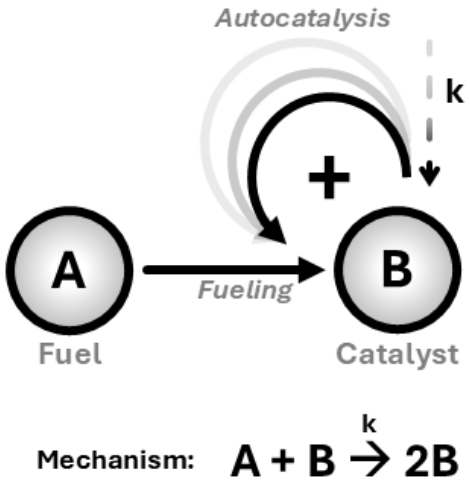

Figure 1.1. Basic motif of a simple autocatalytic reaction. A molecular fuel (A) is converted into a catalyst (B), which speeds up its own formation. The rate of autocatalysis (k) determines the strength of the positive feedback (+).

Significant work has been done on the design of artificial autocatalytic reactions [13] and on the operation of autocatalysis out of equilibrium. Most recent examples include research in the group of Ashkenasy [14] [15] [9], Boekhoven [4] and Huck [12], who have all demonstrated interesting functionalities by manipulating bistable systems out-of-equilibrium. The application of such

functionalities towards synthetic self-regulatory systems requires the design of CRNs that allow for targeted control over the properties of bistable switching. The group of Wong [16] have recently reported a CRN in a continuous flow reactor that can switch freely between two stable states depending on a variety of control parameters such as flowrate, frequency and amplitude of a chemical input. However, in all examples, chemical control over the strength of the feedback which allows for bistability is not demonstrated; environmental control (i.e., by tuning the flow rate) is more common. Typically, a change in the chemical components or physical conditions is required to change the properties of bistability. Tuning of the bistability by direct control over the rate of an autocatalytic reaction can hardly be found.

1.2 – Research Aim

Our work aims to address this gap (i.e., lack of reported chemical control over the feedback to control the bistability) by using a bistable chemical system capable of dynamically switching between two stable states. To achieve this, we took a chemical system already studied in our group under out-of-equilibrium conditions. Briefly, in this CRN the central protein trypsin (Tr) is formed autocatalytically by its precursor trypsinogen (Tg). An inhibitor (Soybean Trypsin Inhibitor, STI) rapidly inhibits the activity of Tr via complexation (**Figure 1.2a**) (see Chapter 2.2 for extended theory). In this system, the network's state is defined as the steady-state concentration of the core compound, Tr. The two observed possible states are a low steady state (Tr inhibition dominates, $[Tr]^{L}_{SS}$) and a high steady state (Tr autocatalysis dominates, $[Tr]^{H}_{SS}$). This CRN is well-known [17] [18], and its bistable behavior under the presence of the inhibitor has been confirmed [12] (**Figure 1.2b**).

A recent publication in our group, which has largely inspired this thesis, has shown [16] that the inhibiting compound can be used as a control parameter to force the system's response to depend critically on its preceding states, so-called history-dependent behavior. However, a link between the strength of the chemical feedback and the bistability is currently missing. A more recent project in our group [11] shows that by introducing trivalent lanthanide ions (i.e., La^{3+}, Nd^{3+}) into the network, the autocatalysis can be significantly sped up by ion-mediation of the trypsin autocatalysis. Our interest is in La^{3+} because La^{3+} undergoes the simplest mechanism, as it only enhances the rate of trypsin autocatalysis, while Nd^{3+} can also slow down this process [11]. We aim to demonstrate control over the bistability (i.e., shift the bistability graph) by using La^{3+} as a control parameter to tune the strength of the positive feedback (i.e. the rate of autocatalytic reaction) (**Figure 1.2c**).

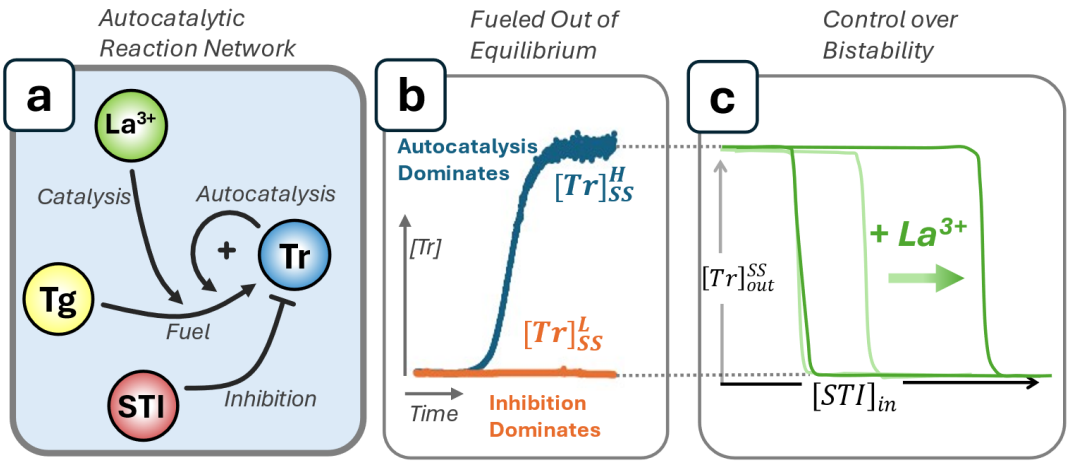

Figure 1.2. Concept figure of this work. **(a)** Motif of the autocatalytic chemical reaction network. Tr cleaves its precursor Tg, catalyzing its own formation. STI inhibits Tr activity. Lanthanum (La^{3+}) promotes Tr autocatalysis. **(b)** The system is constantly fueled out of equilibrium. The response of the system ($[Tr]_{SS}$) depends on the input inhibitor concentration ($[STI]_{in}$). When $[STI]_{in}$ is high, Tr inhibition dominates and the system reaches its low state, $[Tr]^{L}_{SS}$. When $[STI]_{in}$ is low, Tr autocatalysis dominates and the system reaches its high state, $[Tr]^{H}_{SS}$. **(c)** By varying the $[STI]_0$ as a control parameter, the system shows a bistable response. By varying La^{3+}, we aim to demonstrate that the bistability can be controlled.

To achieve our aim, we define three objectives that will lead to the key demonstration. First, to understand the system's behavior, **(i)** the autocatalytic behavior of the present chemical reactions will be studied by means of batch (well-plate) kinetic experiments. These kinetic data will allow us to **(ii)** screen conditions for a bistable behavior experimentally. With a final set of experimental data within these conditions, we will **(iii)** demonstrate the ability to use La^{3+} as a control parameter to control the bistability of the network in flow. This work will provide a crucial demonstration of the possibility to control a chemical network's bistability by tuning the strength of the feedback. By establishing control over the bistability of this chemical network, we lay the foundation to extend our work to different networks with different properties and functionalities, ultimately aiming towards the synthesis of artificial regulatory systems.

Chapter 2 – Theoretical Background

2.1 – Hysteresis and Bistability out-of-equilibrium

A closed system is a system where transfer of energy or matter with the environment is not possible [19]. Closed systems always reach thermodynamic equilibrium, the state where entropy is maximized. Oppositely, an open system is a system where transfer of energy or matter with the environment is possible. Open systems do not necessarily reach thermodynamic equilibrium, as an outside influence can keep the system away from equilibrium. In such open systems, constant flow of matter does not allow for equilibration but may cause the formation of dynamic behaviors. These dynamic behaviors, such as sustained oscillations [17] or bistability [15] [16], are not possible in closed systems [20]. Hence, for a system to exhibit bistability, it must be an open system. In practice, open systems are made by placing the system in flow conditions where constant exchange of matter is possible, so-called out-of-equilibrium conditions.

A bistable system has exactly two stable steady states [10], such as an off state and an on state. (**Figure 2.1a**). For instance, a light switch is a type of bistable system because it can be switched on and off (**Figure 2.1b**). Similarly, a mathematical binary step function is bistable because it either shows 0 or 1. Bistability is therefore a type of nonlinear behavior, as a change in signal (S) will not necessarily yield a linearly proportional change in response (R).

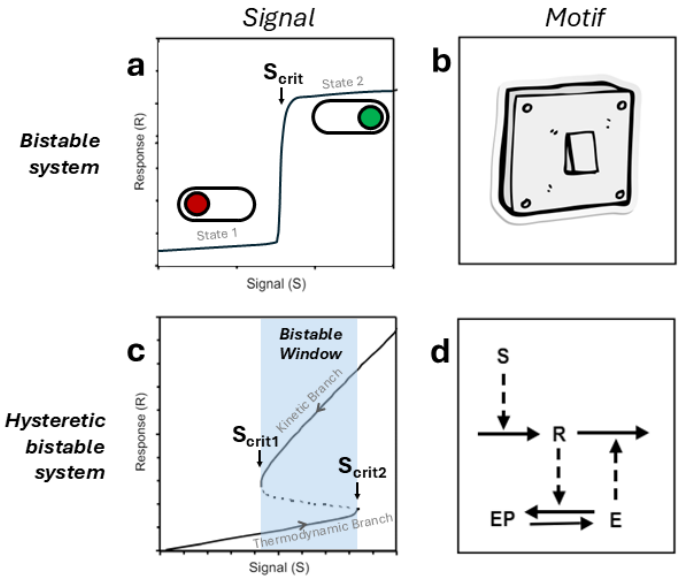

Figure 2.1. Different forms of bistable behaviors (rows) depending on the system motif (columns). **(a)** A typical signal curve of simple bistable systems. **(b)** An example motif of a simple bistable system is a light switch. **(c)** A signal curve of a hysteretic bistable system in which going from low S to high S (thermodynamic branch) means a response switch at S_{crit2}, and going from high S to low S (kinetic branch) means a response switch at S_{crit1}. The region where both the high and the low system steady states are possible (bistable window) is highlighted blue. **(d)** The motif of a simple enzymatic reaction network that exhibits hysteretic bistability. A signal (S) determines the system response (R). In turn, R stimulates an exchange reaction between a protein (E) and its phosphorylated form (EP). Simultaneously, the protein E inhibits the response R. Adapted from [10].

In chemistry, we may consider a system bistable when there are exactly two possible states (responses) from the system when it is left to reach steady state, depending on the input concentrations. If an arbitrary chemical system has two states, say, a high concentration state and a low concentration state, the system will reach the high state when activating compounds are abundant, and the low state when inhibiting compounds are abundant.

Switching from one state to the other is trivial in such bistable systems, as the critical signal (S_{crit}) required for a response change is at a constant value. Adding activating compounds until the critical point is reached will switch the system from the low state to the high state, and vice versa. Consider a system in which switching from the low state to the high state is easily done at some S_{crit2}, but switching from the high state back to the low state happens at a different signal $S_{crit1} < S_{crit2}$ (**Figure 2.1c**). This system is still bistable, but the path that the signal took critically determines the signal at which the response changes. When S starts low (thermodynamic branch), the response changes at S_{crit2}, but when S starts high (kinetic branch), the response changes at S_{crit1}. When the two different paths of S have different effects on the response curve, this is called hysteresis. The system in **Figure 2.1c** is therefore called a hysteretic bistable system. The region of S wherein both responses are possible, depending on the path that S took before, is called the bistable window.

Underlying these types of bistable behaviors are so-called motifs, system representations that highlight the interactions of the individual system components. For the simple on-off bistable system, the motif is a light switch. Chemical networks are often studied and reported using their motifs, and subtle motif changes can completely change a network's behavior. For instance, **Figure 2.1d** depicts the motif of an enzymatic reaction that behaves as in **Figure 2.1c**, which depicts its network components R, S, EP and E to perform different functions and collectively show the bistable behavior. A signal (S) determines the response (R). In turn, R stimulates an exchange reaction of a protein (E), which inhibits the activity of R. The exchange reaction forms EP, the phosphorylated form of E. This feedback between R and E is crucial for, and directly causes, the hysteretic bistable behavior of the system. Without this feedback, the system would be linear and would not exhibit bistability [10].

2.2 – Trypsin Autocatalytic Network

The chemical network that is studied in this thesis is an enzymatic autocatalytic network, as depicted in **Figure 1.2a**. It contains the following components and reactions, trypsinogen (Tg, yellow) is autocatalytically converted to trypsin (Tr, blue). An inhibitor (soybean trypsin inhibitor, STI, red) competes with Tg to suppress Tr activity. The trypsin autocatalysis rate is enhanced by multivalent metal ions such as Ca^{2+} and La^{3+} (green) [21] [11]. Trypsin autocatalysis is the simplest example of positive chemical feedback, and therefore lays the foundation for bistable behavior to emerge under the right conditions [12]. Tracking the concentration of the core protein, trypsin, in the outflow gives the temporal response of the system to different inputs.

Figure 2.2a shows the network with each component depicted as its real structure. Tg is converted into Tr due to cleavage by Tr of the N-terminal hexapeptide tail of Tg (H_2N-Val-Asp_4-Lys-COOH, VDDDDK) [22]. This cleavage results in an inactive form of Tr [23], but in the presence of cations such

as Ca^{2+}, inert Tr formation is negated entirely [24], and the active form of Tr can be retrieved instead. Ca^{2+} sits in the calcium binding loop in trypsin and trypsinogen [25] [21]. Addition of Ca^{2+} enhances the rate of autocatalysis in the presence of Tg since Tr activity accelerates its own formation. Trivalent ions such as La^{3+} bind to the same active pocket as Ca^{2+} and can have similar effects on trypsin autocatalysis [26] [27]. Since Ca^{2+} has a stabilizing role to the proteins [28], we will always add it to reaction solutions in this thesis, and its autocatalysis rate enhancing effect is thus always present. Further tuning of autocatalysis rates is thus most readily done by controlling the presence of La^{3+}. Inhibition of Tr is done by STI, which sits in the catalytic triad pocket of Tr (Asp^{102}-His^{57}-Ser^{195}) [29].

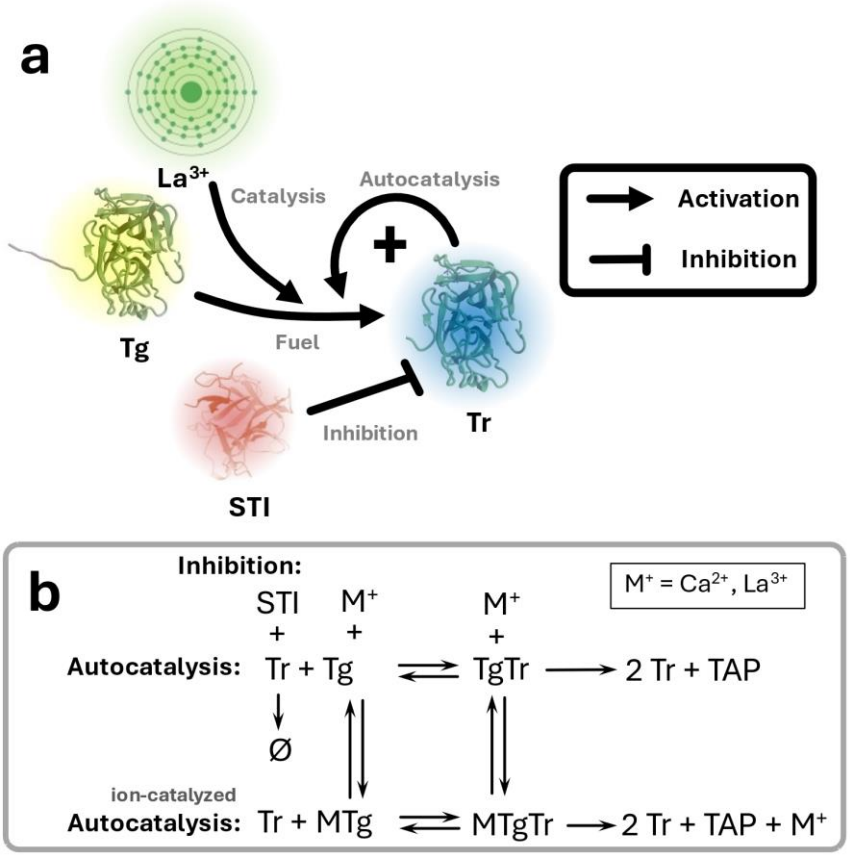

Figure 2.2. Details on the Trypsin-Trypsinogen autocatalytic chemical network. **(a)** Visualization of the reactions of the network, where each species is depicted with their real structures. The insert clarifies the meanings of the arrow types. **(b)** Scheme showing all chemical reactions occurring in the CRN. Ion-catalyzed autocatalysis of Tr is taken generally where M^+ represents either Ca^{2+} or La^{3+}.

The collection of the chemical reactions that occur in the network is shown in **Figure 2.2b**. The predominant reactions that occur are native autocatalysis without a metal ion, ion-catalyzed (M^+) autocatalysis, and inhibition of Tr by STI.

The core proteins of this chemical network are relevant in metabolism and life-like biological systems [23] [30] [22] [31] [12], hence experimental pH values around physiological pH are ideal for the activity of the proteins within the network. Specifically, trypsin and trypsinogen are most active

within pH 7.0 – 9.0 [21]. Storage conditions for these proteins are preferably acidic, as the proteins are inactive and therefore stabilized in these conditions. Furthermore, the addition of Ca^{2+} should ensure that Tr and Tg are stabilized in storage conditions. For details on protein stability, see Chapter 3.2.

A comparison can be made between the Tr-Tg network and the hysteretic bistable network example in **Figure 2.1d**. The motif of the example network resembles the motif of our used CRN in multiple ways. A signal (S, Tg) determines the response (R, Tr), and the response is inhibited by a protein that is involved in inhibition of the response (E, STI). The autocatalysis of Tr provides the necessary positive feedback for nonlinear kinetics [10]. It is therefore reasonable to expect this network to exhibit bistable behavior in out-of-equilibrium conditions. Indeed, this behavior has been experimentally demonstrated previously [12]. However, a key difference with the example system is that the control parameter to determine the system steady state is not Tg, but STI, which is a necessary adjustment needed to control the amount of Tr released without affecting the rate of autocatalysis. The possibility of using STI as a control parameter in the bistability of the system has been previously demonstrated [12] [16] and shows that the network's bistability is manipulable and behaves as we expect.

Chapter 3 – Materials and Methods

3.1 – Materials

All chemicals (trypsin from bovine pancreas, trypsinogen from bovine pancreas, Nα-Benzoyl-DL-arginine p-nitroanilide hydrochloride, $La(NO_3)_3).6H_2O$, soybean trypsin inhibitor) were purchased from Sigma or Roche and used without further purification. Protein solutions (i.e., Tr, Tg, or STI) are made fresh before an experiment is started to minimize degradation.

Batch reactions are monitored in a Tecan Infinite 200 PRO UV-vis plate reader at 400 nm. Batch experiments were performed in Greiner 96 well plates. Flow experiments are performed using a CETONI Base 120 Syringe pump equipped with a QMix Lambda STS-UV flow spectrometer. The syringe pump system is controlled by QMixElements software.

3.2 – Batch Methods

Calibration of Trypsin Activity by BAPNA Hydrolysis in Batch

All chemicals in the Tr-Tg network are not observable in the visible range (380-780 nm), hence, to facilitate the kinetic analysis, a standard BAPNA assay [16] is employed to monitor the activity of Tr during reactions (see Appendix A.1 Exp 1). Calibration of trypsin activity by BAPNA hydrolysis allows the conversion from an absorbance change at λ=400 nm to time-dependent [Tr] [32].

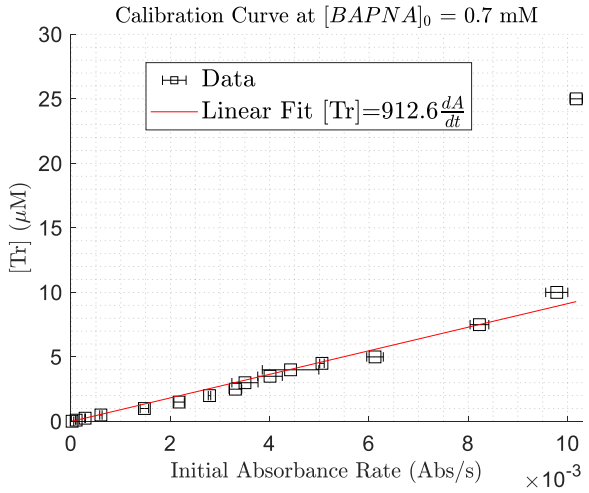

Figure 3.1. Calibration curve of BAPNA hydrolysis. Conditions: $[BAPNA]_0$ = 0.7 mM, $[Tr]_0$ = 0.015 μM, 0.1 μM, 0.25 μM, 0.5 μM, 1.0 μM, 1.5 μM, 2.0 μM, 2.5 μM, 3.0 μM, 3.5 μM, 4.0 μM, 4.5 μM, 5.0 μM, 7.5 μM, 10 μM, 25 μM, $[Ca^{2+}]_0$ = 20 mM. Buffered by 0.5 M TRIS-HCl pH = 7.8. Total well volume 200 μL. Error bars are s.e., n=3. Linear fit R^2= 0.976.

We hydrolyzed BAPNA at varying Tr concentrations and plotted the initial absorbance rates against [Tr] (**Figure 3.1**). The resulting calibration curve is linear between $0 < [Tr]_0 < 10$ μM:

$$[\mathrm{Tr}]_t = 912.6\frac{\mathrm{dA}}{\mathrm{dt}}. \qquad (3.1)$$

Above [Tr] = 10 μM, time restrictions made it impossible to capture the initial regime of BAPNA cleavage, and therefore the calibration curve is not reliable.

To convert absorbance to pNA concentration, we use the molar absorbance coefficient (ϵ) by the law of Lambert-Beer to monitor the active pNA concentration.

$$A = \epsilon bc. \qquad (3.2)$$

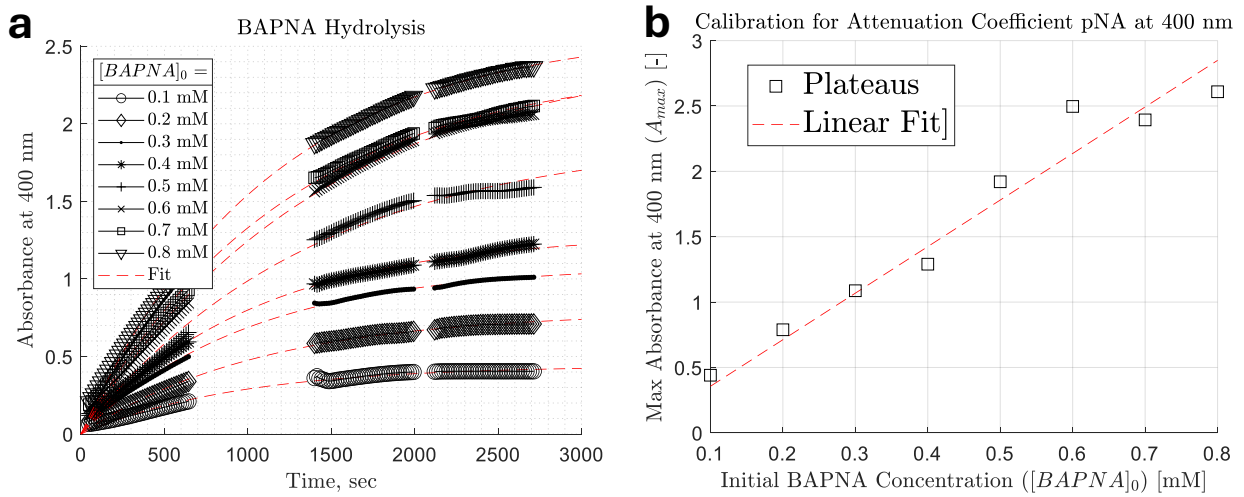

Figure 3.2. Results of gathering molar absorbance coefficient of p-nitroaniline (pNA) at 400 nm. **a.** Reaction curves at varying [BAPNA]$_0$. The data is fitted based on a kinetic model of the system. Conditions: [BAPNA]$_0$ = 0.1 mM, 0.2 mM, 0.3 mM, 0.4 mM, 0.5 mM, 0.6 mM, 0.7 mM and 0.8 mM, [Tr]$_0$ = 1.0 μM, [Tg]$_0$ = 100 μM, [Ca^{2+}]$_0$ = 20 mM. Buffered by 0.5 M TRIS-HCl pH = 7.8. Total well volume 200 μL. **b.** The plateau value of each reaction curve is taken based on the fits and plotted against [BAPNA]$_0$. The molar absorbance coefficient is retrieved from the slope of the Lambert-Beer linear regression. Linear fit R^2 = 0.956.

To measure the molar absorbance coefficient of pNA at 400 nm, we hydrolyzed BAPNA at varying initial BAPNA concentrations and fitted the results using a simple kinetic model of the reactions (**Figure 3.2a**) (see Appendix A.1 Exp 2). The plateaus (full BAPNA hydrolysis) are plotted against [BAPNA]$_0$ and linearly fitted (**Figure 3.2b**). By equation (3.2), the slope of the linear regression was measured to be ϵb = 3.56 mM^{-1}. The path length b = 0.56 cm is estimated based on the volume inside the wells since the absorbance was measured from the bottom of the well plates. Based on this estimate, we find ϵ = 6.36 mM cm^{-1}, which is in a similar range as reported in literature [33] [34].

Effect of La^{3+} on Trypsin Calibration

To check whether La^{3+} affects the hydrolysis of BAPNA, we performed a plate experiment at 400 nm (**Figure 3.3a**) where the rows of the plate had varying [BAPNA]$_0$, and the columns had varying [La^{3+}]$_0$ in triplicate (see Appendix A.1 Exp 3). The initial absorbance slopes were converted into reaction rate using ϵ and plotted against [BAPNA]$_0$ for each [La^{3+}]$_0$ series as Michaelis-Menten plots (**Figure 3.3b**). The [La^{3+}]$_0$ series were not significantly different from each other based on the overlapping standard errors. We conclude that La^{3+} does not affect the hydrolysis of BAPNA. A fit of enzyme-substrate binding (Michaelis-Menten) kinetics to the data indicates if our results are in line with literature reports. The Michaelis-Menten equation is

$$v = \frac{V_{max}[S]}{K_M + [S]}, \qquad (3.3)$$

where the substrate concentration [S] is $[BAPNA]_0$ in our case. Fitting equation (3.3) to the data yielded the kinetic parameters of Tr towards BAPNA: V_{max} = 7.23 · 10^{-4} mM s^{-1}, K_M = 0.6444 mM, and k_{cat} = 0.7234 s^{-1}, which are in the same order of magnitude as reported values in literature [35] [36] [37].

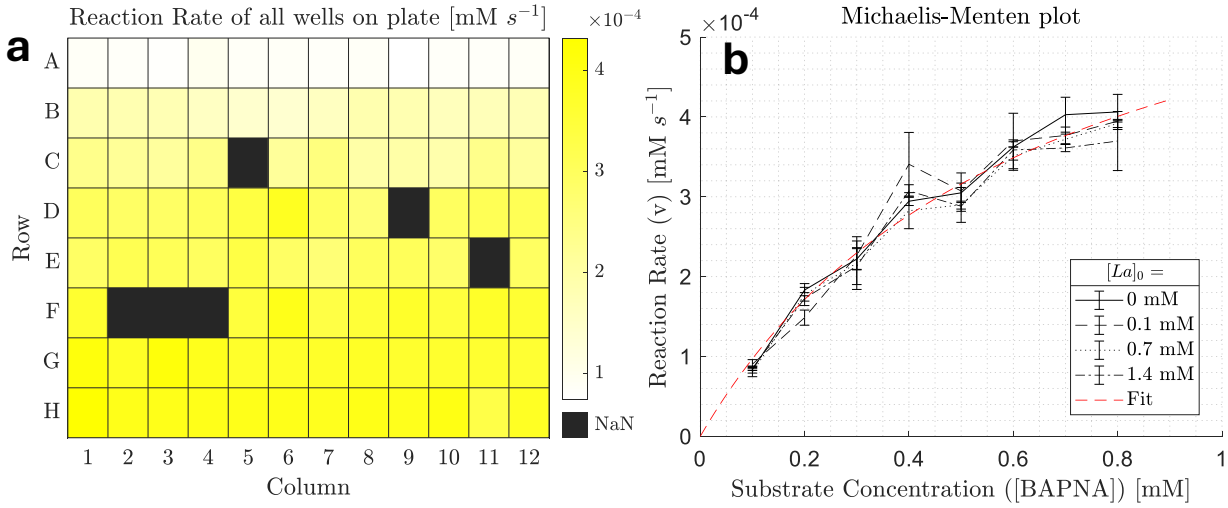

Figure 3.3. Results showing the effect of La^{3+} on BAPNA hydrolysis. **(a)** Reaction rates (in mM s^{-1}) for all wells. Conditions: across the columns, $[La^{3+}]_0$ = 0.0 mM, 0.1 mM, 0.7 mM, and 1.4 mM in triplicates. Across the rows, $[BAPNA]_0$ is varied as $[BAPNA]_0$ = 0.1 mM, 0.2 mM, 0.3 mM, 0.4 mM, 0.5 mM, 0.6 mM, 0.7 mM and 0.8 mM. $[Tr]_0$ = 1 µM, $[Ca^{2+}]_0$ = 20 mM. Buffered by 0.5 M TRIS-HCl pH = 7.8. Total well volume 200 µL. NaN-entry wells (black color) are disregarded due to experimental error. **(b)** Michaelis-Menten plot of the reaction rates across the well plate. The black lines are the $[La^{3+}]_0$ data series. The red dashed line is a nonlinear regression based on the Michaelis-Menten kinetics. Error bars are s.e., n = 3.

Stability of Chemicals in Storage Conditions

To monitor the stability of solutions in storage conditions, we simulated the conditions in which the chemicals are present during multiple-hour long experiments. The standard storage conditions for each compound that are used in this thesis are tabulated in **Table 3.1**. The stability of chemicals in storage conditions has been assumed in previous crucial work in our group [16].

Label:	Solution:	Molarity:	Solvent:
Tr	Tr + Ca^{2+}	30 µM	4 mM HCl + 20 mM $CaCl_2$
Tg	Tg + Ca^{2+}	1000 µM	4 mM HCl + 20 mM $CaCl_2$
La	La^{3+}	5 mM	mQ
STI	STI + Ca^{2+}	50 µM	Buffer
BAPNA	BAPNA	11.2 mM	v:v 0.20 mQ + 0.72 DMF + 0.08 DMSO
Buffer	TRIS-HCl pH 7.8 + Ca^{2+}	200 mM	mQ + 20 mM $CaCl_2$

Table 3.1. Standard storage stock conditions for each compound used throughout experimental work in this thesis. The leftmost column specifies the label of each solution composition (second column), which is used colloquially to refer to each solution more conveniently. Ca^{2+} is added to each protein-containing solution as a stabilizing agent [29]. The third column notes the molarity of the labeled chemical. The fourth column shows the solvent used per solution.

Stability of Tr. Previous work [17] shows that Tr is stable in storage conditions over time scales that are relevant for this thesis.

Stability of STI. Previous crucial work in the group has used STI over long periods of time without reduced activity of STI while in storage conditions. We conclude that no further assessment of the stability of STI in storage conditions is necessary.

Stability of Tg. The missing information on protein stability is that of Trypsinogen, which degrades quickly in neutral and biological conditions [30]. To preserve it as much as possible, it is stored in stabilizing conditions. Under these conditions, we must verify that the degradation of Tg is minimized.

Six small vials containing varying $[Ca^{2+}]_0$ and $[La^{3+}]_0$ are prepared (combinations of $[Ca^{2+}]_0$ = 5, 100 mM and $[La^{3+}]_0$ = 0, 0.2, 2.0 mM), all vials contain $[Tg]_0$ = 200 uM and 4 mM HCl. At 1h, 7.5h, 23h, and 30h after creating these vials, samples are taken and analyzed using a BAPNA assay (see Appendix A.1 Exp 4).

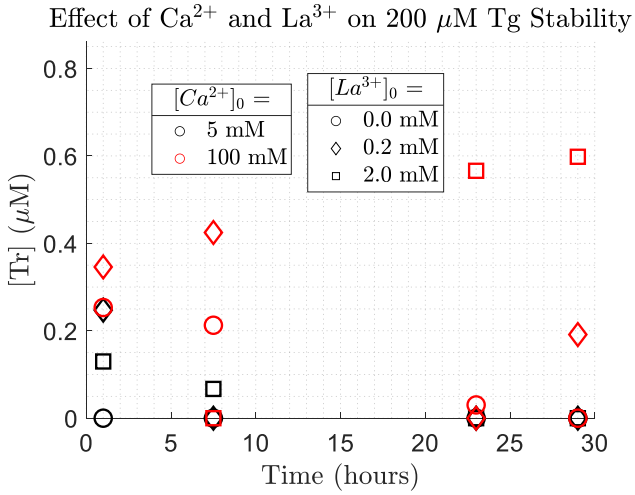

Figure 3.4. Stability of Tg under varying $[Ca^{2+}]_0$ and $[La^{3+}]_0$ conditions over 30 hours. Black colored data points are $[Ca^{2+}]_0$ = 5 mM. Red colored data points $[Ca^{2+}]_0$ = 100 mM. Circle marked data points are $[La^{3+}]_0$ = 0.0 mM. Diamond marked data points are $[La^{3+}]_0$ = 0.2 mM. Square marked data points are $[La^{3+}]_0$ = 2.0 mM.

Figure 3.4 shows no trends. Hence, there is no indication that significant amounts of Tr are produced over 30 hours inside all six vials. No significant difference between the conditions was observed, indicating that as little as 5 mM of Ca^{2+} is sufficient to stabilize Tg in 4mM HCl over 30 hours, which is in line with literature reports [24], and we see that La^{3+} has no effect on the degradation of Tg at these conditions.

Autocatalysis Kinetic Assay

To observe Tr autocatalysis in batch, concentrations of La^{3+} and Tg are changed across the rows and columns of a well plate, respectively (see Appendix A.1 Exp 5). After sequential addition of microvolumes of each reactant (Tr, Tg, and La^{3+}), the reaction is initiated by addition of a mixture of Buffer and BAPNA and placed in the plate reader. Absorbance at 400 nm is monitored in all wells for 90 minutes and thereafter converted into [pNA] concentration using the molar absorbance ϵ and

visualized in a combined plot. We analyze the effects of $[Tg]_0$ and $[La^{3+}]_0$ on Tr autocatalysis by introducing an arbitrary threshold at 50% conversion of BAPNA into pNA [38]. We use this threshold as a measure for autocatalysis rate, and we report it in the form of a heatmap for all conditions. Based on these findings, we will conclude which conditions are optimal to work in flow conditions. For details, see Chapter 4.1.

3.3 – Flow Methods

To perform our demonstrations in flow conditions, we used an experimental strategy which allows us to work in out-of-equilibrium conditions required for the system's bistable behavior. Most experiments in flow in this thesis are performed using a consistent general setup, as shown in **Figure 3.5**. Six syringes filled with chosen stock solutions (containing La, STI, Tr, Tg, Buffer, and BAPNA, see **Table 3.1**) are installed on a syringe pump holder and connected to a series of microfluidic chips using flexible tubing. The first chip (R1) acts as the main reactor. The syringes containing La, STI, and Buffer are directly connected to the entrances to R1. The syringes containing Tr and Tg are first joined using a Y-junction, and subsequently fed into R1. A magnetic stirrer mixes the reaction chamber, and the outflow is fed into the second chip (R2). R2 acts as the detection reactor, where the reaction mixture is combined with BAPNA. The outflow out of R2 is fed into a UV-Vis spectrometer where the absorbance intensity at 450 and 500 nm are recorded over time. The temperature inside the reactors is kept approximately constant by placing the reactors on a small layer of insulating foam, to prevent the stirring plate from heating the solutions.

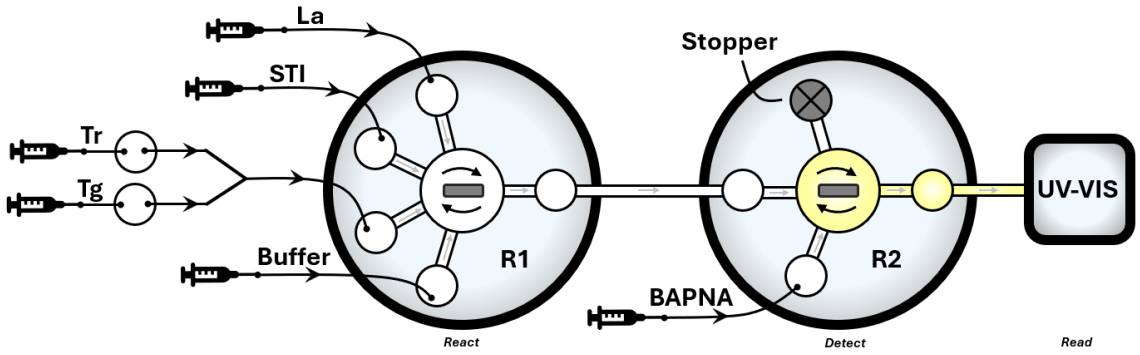

Figure 3.5. Schematic representation of the general experimental setup used for experiments in flow conditions. Six syringes filled with chosen stock solutions (containing La, STI, Tr, Tg, Buffer, and BAPNA) are installed on a syringe pump holder and connected to a series of microfluidic chips using flexible tubing. The first chip (R1) acts as the main reactor. The syringes containing La, STI, and Buffer are directly connected to the entrances to R1. The syringes containing Tr and Tg are first joined using a Y-junction, and subsequently fed into R1. A magnetic stirrer mixes the reaction chamber, and the outflow is fed into the second chip (R2). R2 acts as the detection reactor, where the reaction mixture is combined with BAPNA. The outflow out of R2 is fed into a UV-Vis flow spectrometer where the absorbance intensity at 450 and 500 nm are recorded over time. Total volume of both reactors is 90 µL, of which the magnetic stirrer occupies 14 µL. Thus, the effective reactor volume is 76 µL.

Calibrate BAPNA Hydrolysis to Trypsin Activity in Flow

The system state is defined as the steady-state concentration of Tr in the outflow. Similarly to the batch experiments in this thesis (see Chapter 3.2), a standard BAPNA reporter assay is used to track

the concentration of Tr. For the calibration of the chemical network in flow, we adapt the experimental setup in **Figure 3.5** slightly (see Appendix A.2 Exp 18). Instead of two reactors in series, only R2 is used with three inputs, BAPNA, Tr, and Buffer. Three syringes filled with chosen stock solutions (see **Table 3.1**) are installed on a syringe pump holder and connected to a microfluidic chip using flexible tubing. The chip acts as the detection reactor, where Tr is directly combined with BAPNA and a buffer to initiate the conversion of BAPNA into the detectable pNA. The outflow out of R2 is fed into a UV-Vis spectrometer where the transmittance intensities at 450 and 500 nm are recorded over time.

By controlling the flow rates out of the syringes, the target concentration of Tr inside the reactor is controlled. Monitoring the ratio of transmittance intensity at 500 nm to 450 nm against time for each step of $[Tr]_0$ until a steady state is reached, allows the system to be calibrated in flow conditions. The results of the calibration are shown in **Figure 3.6**, which shows the reached steady state signal values at every [Tr] step. The calibration line for $[BAPNA]_0$ = 2.8 mM in flow is

$$[\mathrm{Tr}] = 3.943\left(\frac{\mathrm{I}(500)}{\mathrm{I}(450)}\right)_{\mathrm{SS}} - 4.595. \qquad (3.1)$$

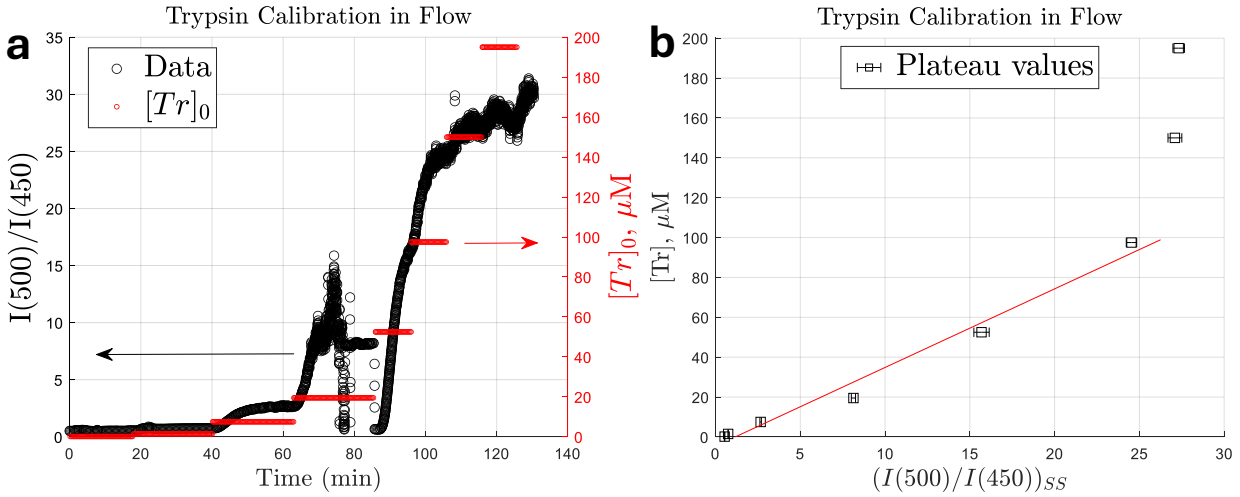

Figure 3.6. Calibration of BAPNA hydrolysis in flow conditions. $[BAPNA]_0$ = 2.8 mM. **(a)** The y-axis shows the ratio between the transmittance intensity at 500 nm divided by the intensity at 450 nm, which are the two intensities directly monitored by the UV-Vis spectrometer. The flow rate of the Tr syringe into the reactor is adjusted manually (and compensated to keep a constant flow rate by adjusting the Buffer syringe) to create Tr-steps, after which the system is allowed to equilibrate. The equilibrium intensity ratio of each step is thus correlated with the concurrent tr concentration in flow. Conditions: flow rate through R1 2000 µL h^{-1} (τ = 2.28 min). **(b)** Calibration curve relating steady state (plateau) signal values to concurrent [Tr]. The values are taken as the average of the last 20% of data points of a Tr step. Error bars are s.e. Signals until I(500)/I(400) = 25 (corresponding to [Tr] = 100 µM) are fitted with a linear fit. Linear fit R^2 = 0.982. Signals where the calibration is nonlinear are typically not achieved in experiments (see Chapter 4.2).

Chapter 4 – Results and Discussion

4.1 – Effect of La^{3+} on the Autocatalysis in batch

We performed experiments in batch conditions to examine the behavior of the autocatalytic network when subjected to changes in La and Tg. **Figure 4.1a** depicts the experimental setup, wherein a 96-well plate is used to test many conditions simultaneously. We varied $[La^{3+}]_0$ and $[Tg]_0$ across rows and columns, respectively, to examine the effect of $[La^{3+}]_0$ and $[Tg]_0$ on the autocatalytic conversion of Tg into Tr. From top to bottom, $[La^{3+}]_0$ increases from 0.0 mM to 2.0 mM (green gradient), and across the columns, $[Tg]_0$ increases from 0 µM to 200 µM (yellow gradient). The experiments are performed with $[Tg]_0$ duplicates, indicated by the dotted grey rectangle. The resulting absorbance curves are depicted per well in the small graphs.

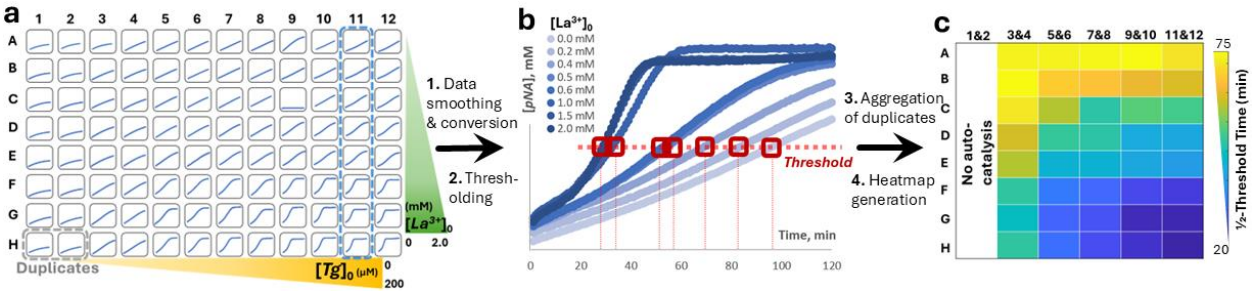

Figure 4.1. Generation and post-processing of data acquired from autocatalysis kinetic assay. Figure structure inspired by and adapted from [39]. **(a)** Autocatalytic data gathered from a 96-well plate experiment. Conditions: $[La^{3+}]_0$ = 0.0 mM, 0.2 mM, 0.4 mM, 0.5 mM, 0.6 mM, 1.0 mM, 1.5 mM, and 2.0 mM across the rows (green gradient). $[Tg]_0$ = 0 µM, 40 µM, 80 µM, 100 µM, 150 µM, and 200 µM across the columns in duplicate (yellow gradient). All wells contained $[Tr]_0$ = 0.25 µM, $[BAPNA]_0$ = 1.0 µM, and $[Ca^{2+}]_0$ = 20 mM. Buffered by 0.5 M TRIS-HCl pH = 7.8. Total well volume 200 µL. Grey dotted rectangle indicates duplicates. Blue dotted rectangle indicates a sample set of data for the next panel. The autocatalysis data is smoothed and converted from absorbance to $[pNA]_t$ (step **1**). The time at which a threshold at 50% of the plateau (½-threshold time) is reached is used as a measure of characteristic autocatalysis speed (step **2**). **(b)** Example set of autocatalysis data (plate column 11, $[Tg]_0$ = 200 µM) with varying $[La^{3+}]_0$. The red dotted line illustrates the ½-threshold. Duplicate measurements are aggregated (step **3**) and a heatmap is generated based on the ½-threshold times (step **4**) to yield the last panel. **(c)** Heatmap showing the ½-threshold times for all wells in duplicates.

Briefly, we analyzed the data for each well as follows. First, we used a MATLAB® built-in data smoothing function to reduce the noise of the data, and we converted the absorbance data to [pNA] concentrations (see Chapter 3.2 for details) (step **1**). We then used an arbitrary threshold (step **2**), in this case at 50% of the maximum [38], to analyze the steepness of the curves. **Figure 4.1b** shows this threshold as a red dotted line. In the same figure, we show at which time each curve crosses this threshold with small, dotted lines. We named the time at which each curve reaches this threshold the ½-theshold time, and we use it as a measure of autocatalysis rate. **Figure 4.1b** depicts a sample set of autocatalysis data (wells in column 11, $[Tg]_0$ = 200 µM), where we see that an increase in $[La^{3+}]_0$ (indicated by the color change) causes the curves to shift to the left, and thus causes the ½-theshold time to shift to the left, which indicates an increase in activation of the steep part of the curve. This activation of the steep part of the curve confirms that autocatalysis occurs.

To further quantify the increase in activation caused by an increase in $[La^{3+}]_0$, we used the threshold at 50% of the [pNA] plateau value for all wells [38] and gathered the experimental duplicates (step **3**). Based on the ½-threshold time values for each well, we generated a heatmap (step **4**) which summarizes the autocatalysis behavior of all wells. **Figure 4.1c** depicts this heatmap, where we see that an increase in $[La^{3+}]_0$ (from top to bottom) causes the halfway time to drop, indicating an increase in autocatalysis speed. An increase in $[Tg]_0$ (from left to right) has a similar effect. Columns 1 and 2 with $[Tg]_0$ = 0 µM did not reach the threshold, as no autocatalysis was observed.

The observations from the heatmap serve as the basis for our choice of conditions for experiments in flow. For every value of $[Tg]_0$, the effect of La^{3+} on $t_{½}$ saturated after $[La^{3+}]_0$ = 1.0 mM, hence using higher values than $[La^{3+}]_0$ = 1.0 mM is unnecessary. Varying $[La^{3+}]_0$ had the largest effect within the region $[La^{3+}]_0$ = 0.2 – 1.0 mM. Preliminary experiments in flow conditions have indicated that significant precipitation of La^{3+} occurs for $[La^{3+}]_0$ > 0.5 mM due to the limited solubility of La^{3+} at pH = 7.6 [40]. Hence, we conclude that the optimum region of $[La^{3+}]_0$ to observe changes in bistability is between 0.2 and 0.5 mM in flow conditions.

4.2 – Control over Bistability in Out-Of-Equilibrium Conditions with La^{3+}

To demonstrate our aimed ability to control bistability using La^{3+} as a controlling parameter, we used an experimental working strategy to familiarize ourselves with the setup which allows us to work in out-of-equilibrium conditions required for the system's bistable behavior. The conditions we work in (e.g., $[Tr]_0$, $[Tg]_0$, $[La^{3+}]_0$) are based on the system's autocatalytic behavior in batch (Chapter 4.1). The flow setup is described in Chapter 3.3. Briefly, we use a programmable syringe pump in which syringes filled with chemicals are connected to a series of CSTRs by flexible tubing. By setting the flow rates of each syringe, the concentration of that chemical can be controlled. The outflow out of the system is analyzed by UV-vis spectrometry and the signal is converted into [Tr] by a calibration curve.

We screened optimal flow rates to study bistability (See Appendix A.2, Exp 11-17). We tested flow rates of 250 µL h^{-1} (τ = 18.24 min), 500 µL h^{-1} (τ = 9.12 min), 1500 µL h^{-1} (τ = 3.04 min), 2000 µL h^{-1} (τ = 2.28 min), and 3000 µL h^{-1} (τ = 1.52 min). We found that flow rates of 1500-2000 µL h^{-1} provided optimal conditions for bistability to emerge and were sufficiently fast so that an experiment can be performed within a working day. Flow rates lower than 1500 µL h^{-1} took too long to reach steady states and did not remove partially precipitated La^{3+} fast enough. Flow rates higher than 2000 µL h^{-1} were too fast to allow for bistability [16].

The system's bistability is given by the response to different $[STI]_0$ conditions, where $[STI]_0$ is suddenly changed from a baseline value $[STI]_{-1}$ to a desired $[STI]_0$. To demonstrate the system's bistability, we programmed the syringe pump to vary the flow of STI accordingly (See Appendix A.2, Exp 21-26). **Figure 4.2** depicts a sample response of the system (black points) when subjected to sudden $[STI]_0$ changes (red points). After every $[STI]_0$ step, the system is brought back to a baseline state ($[STI]_{-1}$ = 23 µM), where we were confident that virtually all Tr is inhibited, to reset the system. Each set of two

STI values ($[STI]_{-1}$ to $[STI]_0$) can be seen separately from the rest of the experiment. The bistability is clearly visible, as only two states are reached, $[Tr]^L_{SS}$ (e.g., at t = 10 min) and $[Tr]^H_{SS}$ (e.g., at t = 70 min). $[Tr]^L_{SS}$ is reached for high $[STI]_0$ (e.g., 8 µM), and $[Tr]^H_{SS}$ is reached for low $[STI]_0$ (e.g., 0.5 µM). For $[STI]_0$ = 4 µM, the low state is reached, but for $[STI]_0$ = 3 µM, the signal suddenly shoots up, indicating that the switching point between $[Tr]^H_{SS}$ and $[Tr]^L_{SS}$ is somewhere in between these two values.

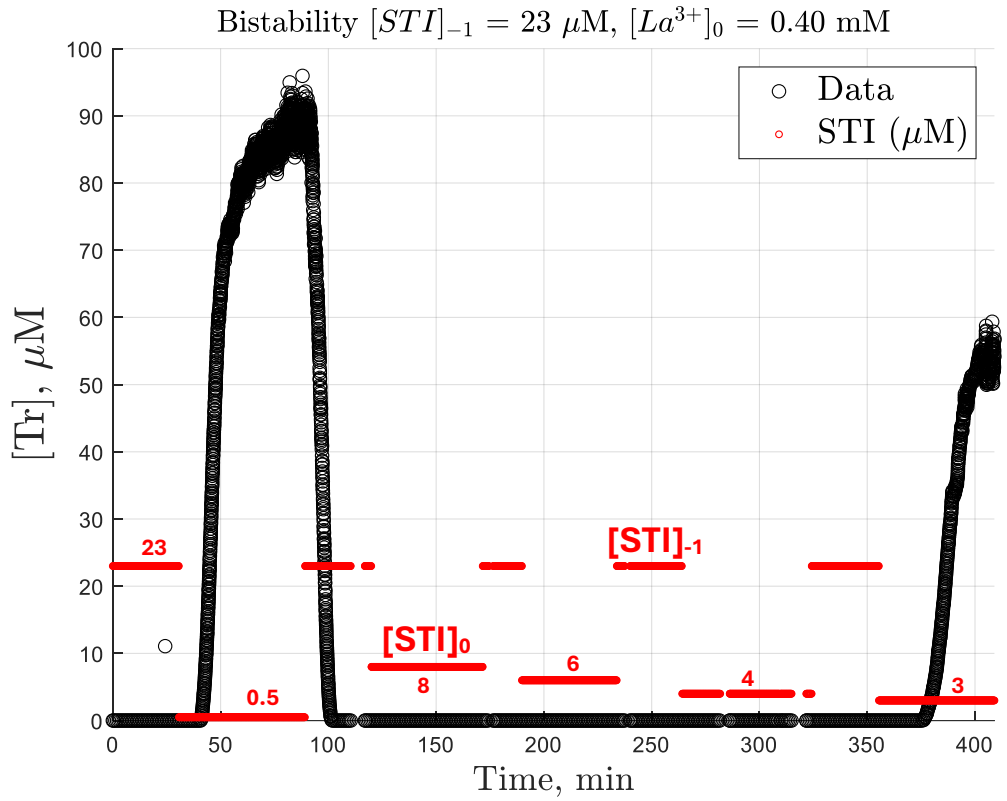

Figure 4.2. Sample data of system bistable response to sudden changes in $[STI]_0$ input steps. Conditions: flow rate through R1 = 2000 µL h^{-1}, $[La^{3+}]_0$ = 0.40 mM, $[Tr]_0$ = 6 µM, $[Tg]_0$ = 250 µM, $[Ca^{2+}]_0$ = 100 mM, buffered by TRIS-HCl 0.2 M pH 7.8. Flow rate through R2 = 2667 µL h^{-1}, $[BAPNA]_0$ = 2.8 mM. Note that any regions where bubbles caused unusable data have been removed. For raw data, see Appendix A.2 Exp 24.

To better visualize the switching from low to high states, we noted the value of the signal at the end of each STI step and plotted this signal against $[STI]_0$ (see **Figure 4.3**). This gave the conventional form of a bistability plot [41] where the system state ($[Tr]_{SS}$) is plotted against an input parameter ($[STI]_0$). We performed the experiment in **Figure 4.2** for two different $[La^{3+}]_0$ to investigate the effect of changing $[La^{3+}]_0$ on the bistable response of the system (filled squares), which is our aimed demonstration. **Figure 4.3** shows the bistability of the system when subjected to sudden STI changes at varying $[La^{3+}]_0$. We also performed both $[La^{3+}]_0$ series in the reverse direction, i.e., the baseline is $[STI]_{-1}$ = 0.5 µM where close to no Tr is inhibited (empty squares). The figure shows that low $[STI]_0$ generally gives a high-Tr state, and high $[STI]_0$ gives a low-Tr state response. Addition of La^{3+} shifts the high-Tr state to higher values. The value of $[Tr]^H_{SS}$ was increased from ~20 µM to ~80 µM when we increased $[La^{3+}]$ from 0.10 mM to 0.40 mM. We hypothesize that this increase is due to an increase

in the rate of autocatalysis caused by the addition of La^{3+}. More Tr is formed in flow, which shifts the high-Tr state upwards.

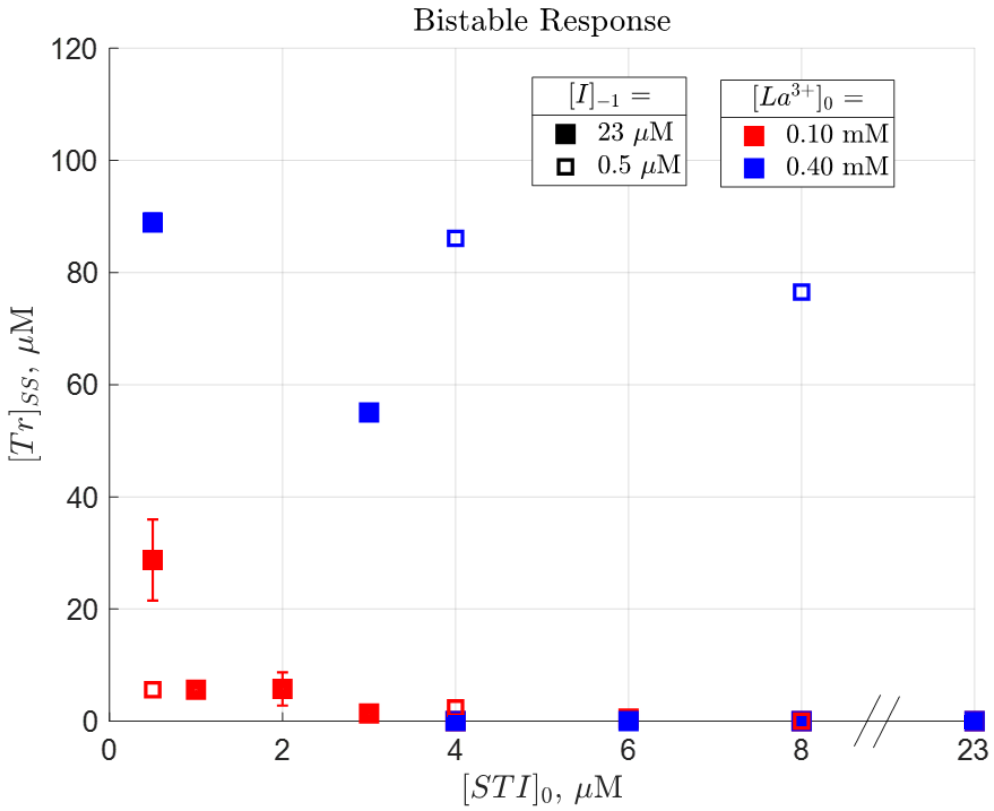

Figure 4.3. Bistability plot of system steady states ($[Tr]_{SS}$). $[Tr]_{SS}$ is plotted against the input parameter $[STI]_0$ when $[STI]_0$ is changed suddenly from a baseline ($[STI]_{-1}$ = 23 μM, filled squares or $[STI]_{-1}$ = 0.5 μM, empty squares) to $[STI]_0$, at varying $[La^{3+}]_0$. Red points ▪: $[La^{3+}]_0$ = 0.10 mM, blue points ▪: $[La^{3+}]_0$ = 0.40 mM. Conditions: Flow Rate through R1 = 2000 μL h^{-1}, $[Tg]_0$ = 250 μM, $[Tr]_0$ = 6 μM, flow rate through R2 = 2667 μL h^{-1} $[BAPNA]_0$ = 2.8 mM for both data series. The series $[La^{3+}]_0$ = 0.10 mM was performed twice and averaged, therefore the error bars are s.e. (n=2).

We also see that the forward and reverse direction of changing $[STI]_0$ ($[STI]_{-1}$ = 23 μM and $[STI]_{-1}$ = 0.5 μM, respectively) follow different paths, which confirms the hysteretic behavior of the system. At $[La^{3+}]_0$ = 0.40, the system can be in both states when $[STI]_0$ = 4 μM, depending on the direction of change from $[STI]_{-1}$ to $[STI]_0$. The bistable window is clearly visible for the $[La^{3+}]$ = 0.40 series (blue points). Within this window, both states are possible, and the $[STI]_0$ path taken critically determines the system state. However, for $[La^{3+}]_0$ = 0.10 mM, this is harder to see. This is because lower values of $[Tr]_{SS}$ are reached when $[La^{3+}]_0$ is 0.10 mM. Briefly, in the forward direction ($[STI]_{-1}$ = 23 μM, red filled squares), the low state is reached above $[STI]_0$ = 3 μM, and the high state is reached below this point. In the reverse direction ($[STI]_{-1}$ = 0.5 μM, red empty squares), this switching point is between 4-8 μM. The switching point between $[Tr]^H_{SS}$ and $[Tr]^L_{SS}$ for $[La^{3+}]_0$ = 0.40 mM is between $[STI]_0$ = 8-23 μM. Thus, we see that the addition of La^{3+} shifts the bistability by shifting the $[STI]_{-1}$ = 0.5 μM branch to the right.

To further investigate the effect of La^{3+} on the bistable behavior of the network, we looked at the history dependent behavior, which has been previously demonstrated [16]. When STI is gradually

changed in stairs, the system retains information about the previous path taken and gives a different response than the bistability we observed.

To check the system response to gradual STI concentration variation, we adapted the STI steps. We started at a very low value ($[STI]_0$ = 0.5 μM) where almost no Tr is inhibited. The steps increased to a very high value ($[STI]_0$ = 23 μM) where we were confident that most Tr is inhibited, and back down in a staircase shape (See Appendix A.2, Exp 19-20). The results are shown in **Figure 4.4**, which shows the series where $[La^{3+}]$ = 0.40 mM. The results again show that a high-Tr state is reached at the lowest STI steps where autocatalysis dominates, and a low-Tr state is reached at the highest STI step where inhibition dominates. When $[STI]_0$ is increased to 15 μM, the high steady state is reached, but when $[STI]_0$ is decreased to 15 μM, the low steady state is reached. The system can thus give two responses at the same condition, depending on the path taken, again demonstrating the hysteretic response of the system to $[STI]_0$ as the input parameter.

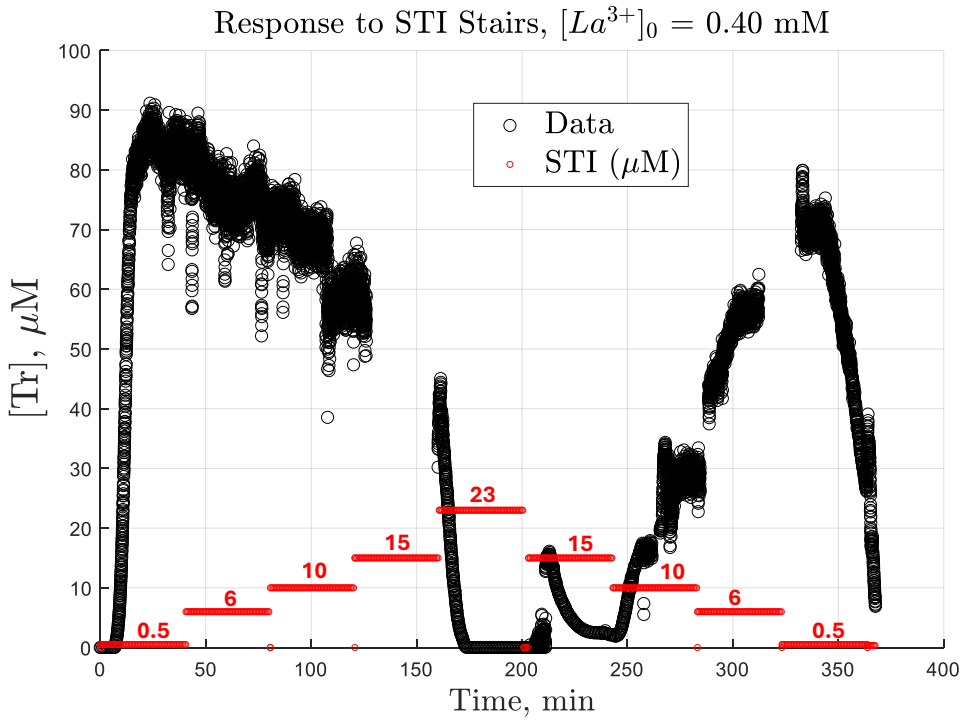

Figure 4.4. System response to gradually changing $[STI]_0$ input steps. Conditions: flow rate through R1 = 1500 μL h^{-1}, $[La^{3+}]_0$ = 0.40 mM, $[Tr]_0$ = 6 μM, $[Tg]_0$ = 250 μM, $[Ca^{2+}]_0$ = 20 mM, buffered by TRIS-HCl 0.5 M pH 7.8. Flow rate through R2 = 2000 μL h^{-1}, $[BAPNA]_0$ = 2.8 mM. Note that any regions where bubbles caused unusable data have been removed. For raw data, see Appendix A.2 Exp 20.

We performed the experiment in **Figure 4.4** for two different $[La^{3+}]_0$ to observe the effect of adding La^{3+} to the system's response to gradual $[STI]_0$ changes. To visualize the hysteretic behavior more clearly, we again noted the value of the signal at the end of each STI step and plotted this signal against $[STI]_0$. **Figure 4.5** shows the system's response to gradual $[STI]_0$ changes at two different concentrations of La^{3+} (0.10 mM and 0.40 mM). The direction of $[STI]_0$ change is indicated with the colored arrows. The figure shows that low $[STI]_0$ generally leads to a high-Tr response from the system, and high $[STI]_0$ generally leads to a low-Tr response. Addition of La^{3+} changes the behavior of the

system by shifting the high-Tr state to higher values. We again hypothesize that this change is due to an increase in the rate of autocatalysis when $[La^{3+}]_0$ is increased. Therefore, more Tr is formed in flow, which shifts the high-Tr state upwards.

We also see a change in the amount of STI needed to suppress the high-Tr state when La^{3+} is added, which shifts the curve to the right. For $[La^{3+}]$ = 0.10 mM, the point at which the system switches from the low to the high state is between 6 μM < $[STI]_0$ < 10 μM, whereas for $[La^{3+}]$ = 0.40 mM, the switch from the low state to the high state happens between 10 μM < $[STI]_0$ < 15 μM. There is a similar change in the high-to-low state switch point when La^{3+} is added.

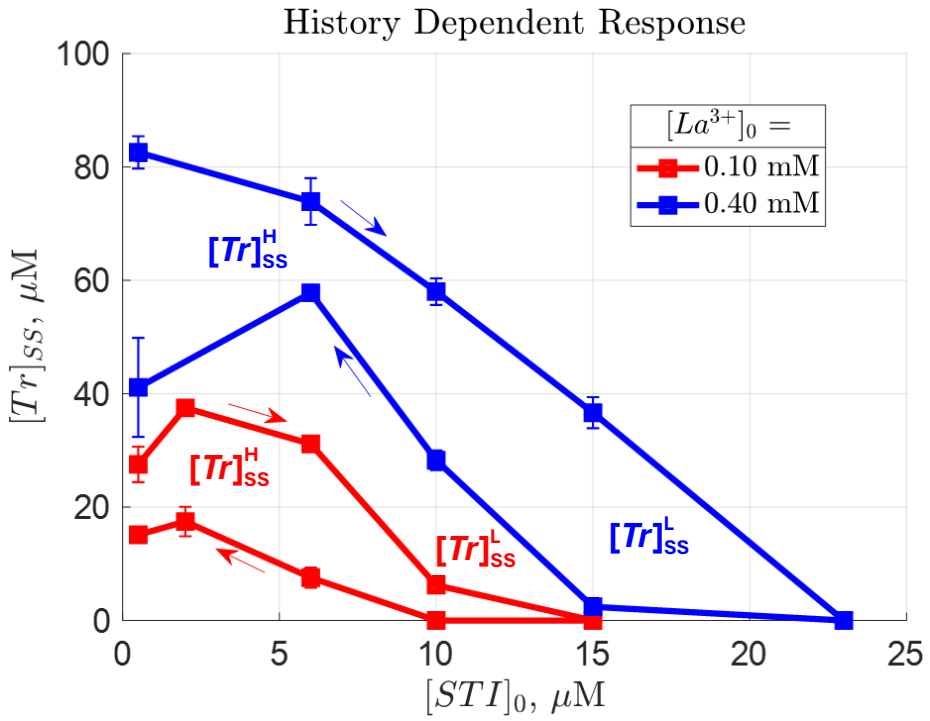

Figure 4.5. Plot of the history dependent response. The system state ($[Tr]_{SS}$) is plot against the input ($[STI]_0$). $[STI]_0$ is gradually changed from low to high values and back (STI steps), at varying $[La^{3+}]_0$. ■: $[La^{3+}]_0$ = 0.10 mM, ■: $[La^{3+}]_0$ = 0.40 mM. The arrows indicate the direction of change of $[STI]_0$. The value of $[Tr]^H_{SS}$ is taken as the average of the last 30% of data points per $[STI]_0$ step. Error bars are s.e. Conditions for both data series: Flow Rate through R1 = 1500 μL h^{-1}, $[Tg]_0$ = 250 μM, $[Tr]_0$ = 6 μM, flow rate through R2 = 2000 μL h^{-1}, $[BAPNA]_0$ = 2.8 mM.

For both methods of $[STI]_0$ variation, we have demonstrated that addition of La^{3+} in flow significantly affects the response of the system. Addition of La^{3+} increases the rate of autocatalysis, which shifts the high-Tr steady state to higher values, without affecting the low-Tr state. The system's history dependent response to stepwise $[STI]_0$ variation is strongly affected by addition of La^{3+}, as the switch between the low and the high state in both directions required more $[STI]_0$ when $[La^{3+}]_0$ was increased. When $[STI]_0$ is changed to desired values after reaching a baseline value, which is the bistable response, addition of La^{3+} increased $[Tr]^H_{SS}$ and shifted the switch between the low and high state of the kinetic branch ($[STI]_{-1}$ = 0.5 μM) towards higher $[STI]_0$. The switch between the low and high state of the thermodynamic branch ($[STI]_{-1}$ = 23 μM) was not affected.

Chapter 5 – Conclusion

This thesis was aimed at the control of the bistability of an enzymatic autocatalytic reaction network. Contemporary research in systems chemistry has proven that chemical networks are highly diverse and can exhibit intelligent functional properties in the right conditions. One such property is bistability, a property in which a system can exist in two stable states and can switch between them, which is omnipresent in natural and artificial regulatory systems. Bistable chemical systems are caused by feedback loops and are widely researched and manipulated to perform interesting functions. However, there has existed a wide lack of control over the bistability of these systems by controlling the feedback.

In this thesis, we employed a chemical network based on the autocatalysis of trypsinogen (Tg) to trypsin (Tr), in competition with a fast trypsin inhibitor (STI), and demonstrated control over this system's bistability by tuning the concentration of a trivalent lanthanum ion (La^{3+}), which enhances the rate of autocatalysis. We demonstrated control over the bistability of a chemical system by tuning the strength of the chemical feedback loop. We achieved this by **(i)** monitoring the autocatalytic kinetic behavior of the system in batch, which provided us knowledge about the kinetics of the network under varying conditions. This knowledge of the system's kinetics allowed us to **(ii)** screen the right conditions for bistability when the system is placed in out-of-equilibrium conditions. These out-of-equilibrium conditions were necessary for bistability to exist, which we achieved by studying the network in flow. Finally, we **(iii)** demonstrated that the addition of the lanthanum ion allows us to control the system's bistable behavior. Our results show that the system is indeed bistable and shows a hysteretic response to variations in the inhibitor concentration. We saw that an increase of La^{3+} in flow affected the bistability and the history dependent response of the network by shifting the curves to higher $[STI]_0$. Previously, demonstrations of control over bistability by direct tuning of the chemical feedback were rare. Hence, this work addresses the current gap in systems chemistry by providing a demonstration of the control over the bistability of a chemical system by controlling the strength of the feedback with La^{3+}.

To further solidify the control over the bistability of this specific network, we would require more extensive work on a wide range of lanthanum concentrations. In batch, we saw that the effect of adding lanthanum saturated above a certain value, so there is likely a similar effect in flow conditions, which we have not investigated. We did not test the system without the presence of lanthanum, so we are unsure what range of concentrations would be optimal, while minimizing the precipitation of the barely soluble La^{3+}. Still, our findings address a gap in current systems chemistry, and we envision that the findings presented here will inspire research into controlling the bistable behaviors of different networks. Such research is crucial if we, ultimately, aim to synthesize artificial life-like regulatory mechanisms.

Chapter 6 – Outlook

We believe that the work presented in this thesis has several different unexplored paths. Most notably, we envision the integration of the bistable network into a chemical analogue of a Schmitt trigger (**Figure 6.1a**). A Schmitt trigger is a type of analog-to-digital signal comparator which, differently from a regular comparator, filters noise out of a noisy analog signal (top panel) [42]. Such a comparator is a typical example of a bistable system, as the digital output is binary. A regular comparator (middle panel) has one signal threshold S_{crit} (red line), above which the response is 1, and below which the response is 0. A Schmitt Trigger (bottom panel) has two different thresholds, depending on the direction that the signal is changing in (green lines). While the signal decreases, the threshold signal is S_1 and while the signal increases, the signal is S_2, where $S_1 < S_2$. This difference in signal threshold depending on the path taken beforehand means that a Schmitt trigger has a hysteretic response. This hysteretic behavior means that a sudden decrease or increase in signal (noise) does not disturb the response, hence noise is filtered out of the analog data, depending on the magnitude of the noise. When we plot the signal-response (input-output) curve of such a Schmitt trigger (see **Figure 6.1b**), we see a strong resemblance with the chemical bistability we have studied in this work. Due to this resemblance, we were urged to investigate whether a chemical analogue of the Schmitt trigger is possible using our system.

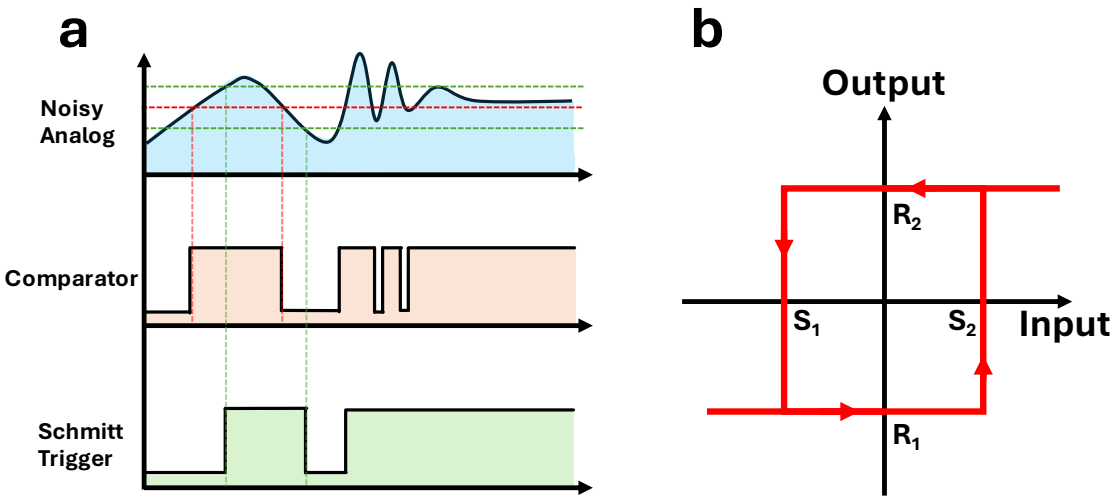

Figure 6.1. Description of a Schmitt trigger. **(a)** A noisy analog signal (top) is converted into a binary digital response, a typical example of a bistable system. A regular comparator (middle) has a threshold at a constant value. Noise in the analog is kept in the response. A Schmitt trigger (bottom) has two different thresholds, depending on the signal path taken beforehand. The threshold when the signal is increasing is S_2, the threshold when the signal is decreasing is S_1, where $S_1 < S_2$. A Schmitt trigger is thus hysteretic. The hysteresis filters noise out of the analog data. **(b)** Plot of the signal-response (input-output) curve of a Schmitt trigger.

To investigate whether a chemical Schmitt trigger is possible using our trypsin autocatalytic CRN, we planned to dedicate a part of this thesis to the analysis of the stability of the steady states. That is, how resilient are the system's steady states to sudden perturbations in signal? By performing a so-called stability analysis of nonlinear systems, we planned to evaluate the mathematical stability of our steady states, and to study the effect of La^{3+} thereon. However, due to time constraints, our

focus shifted away from this study. We still envision that such an analysis may provide key insights into the development of a chemical noise filter, using a chemical analogue of a Schmitt trigger. We are yet unsure to what extent the Schmitt trigger quantitively matches with our chemical system in terms of scale, sensitivity to signals, or the range in which the thresholds can be tuned.

A significant portion of time spent on this project was aimed at the creation of a mathematical model in MATLAB based on the network's kinetic equations, which are listed in **Figure 2.2b**. We made several draft versions of the model, but we did not manage to reach a state where the model was finished enough to include in the main text. For the model to be accurate to our system, we require values of the kinetic parameters of the reactions, or at minimum good guesses of them. Some values are reported in literature, but some values are not or have a wide spread of reported values. We thus aimed to measure these parameters ourselves by fitting kinetic data in batch. However, this proved difficult, and we were not able to perform this fitting while also keeping our focus on the key demonstration. The main purpose of the mathematical model that we envisioned was to predict under which conditions bistability would be best to study in flow conditions. However, we later decided that our decision for the working conditions in flow should be a general guess based on the autocatalytic behavior in batch. From this guess of parameters, we performed several experiments to familiarize ourselves with the system (see Appendix A.2, Exp 11-14), and to converge towards correct conditions. We have developed most of the model, but due to a lack of confirmed rate constants, the model is not yet optimized. However, developing this model further would enable a comparison between bistability in theory and in practice.

To observe the output of the CRN, we used the reporter molecule BAPNA, which should not interfere with the autocatalytic kinetics. However, since the conversion of BAPNA requires Tr to participate, we were interested in whether the presence of BAPNA significantly affected the rate of the other chemical reactions or not. To this end, we performed a set of preliminary experiments in batch, similar to the kinetic assay that was described in Chapter 4.1, but without the presence of BAPNA (see Appendix A.1, Exp 6-10). We tracked the autocatalytic increase in Tr by a standard aliquoting procedure. Our preliminary results indicate that the binding of Tr to Tg follows substrate inhibition kinetics [43]. The addition of La^{3+} did not seem to affect this behavior. To investigate the results of these experiments further, we planned to fit a substrate inhibition Michaelis-Menten kinetic model to our data to extract kinetic parameters. However, this proved difficult, and we no longer aimed for the kinetic parameters for the model, so we did not follow through on this. We instead focused on the demonstrations in the main text. The experimental data is available.

We have described several possible pathways that we could take this project after the finalization of this thesis. We described a few specific features of the project that were unexplored or partially explored. More generally, by using our autocatalytic bistable network, and by controlling the bistability with La^{3+}, we envision that the creation of a chemical analogue of a Schmitt trigger is the next step in this project.

Acknowledgements

Saying that the past 9 months have been a rollercoaster would be an understatement. Oh yes- 9 months instead of the usual 6. I tried to do Honors during my thesis, but that ended up being… not entirely for me, so I quit that right before it was about to finish. Combined with some other delays, this project ended up running from February 2nd, 2024, until November 4th, 2024, on which I finally hope to defend this thesis publicly in Carré 3D from 15:00-16:00. If you are reading this, please consider yourself invited to my defense! Everyone I have spoken to during my thesis time has contributed to my process in one way or another. But in particular, I would like to thank several people and put them in the spotlight for a bit.

First and foremost, a big thank you to my supervisors, Albert and Dmitrii. Albert, thank you for all the thesis-related and non-thesis related professional guidance. Thanks for giving direction and purpose to this project when sometimes there seemed to be none on the horizon. Ever since we started working together during my bachelor's thesis two and a half years ago, you have made it clear that you understand my long-term goals and want to contribute to my process. It's clear that your heart is in the right place. Dmitrii, thanks for being the exact opposite of myself in almost every aspect. Your pragmaticism and dryness has been a great antidote for my indecisiveness and worries at times, and I want to thank you for always remaining cool and collected. Notice how I'm not using the word 'organized' here. You should really keep your fume hood organized! Hazal would agree. Thanks for being simultaneously the most appreciative and the most critical of my work. You're honest and correct, which are necessary features of a project that was fuzzy for me at times. Also, thanks for growing the best moustache I have ever seen.

Hazal, you're up next. Thanks for being a supervisor in disguise. Actually, I think I talked to you more than anyone during my thesis, which is slightly concerning. But thanks for being there for me anyway. Thanks for becoming my ex-supervisor turned friend and someone I feel like I can relate to on both a personal and a professional level; For always being available for both stupid questions in the lab, and intellectual conversations outside of the lab; For being someone that can almost be described as a mother figure when I was feeling demotivated [insert old-age joke here].

A unique thank you to Thomas for being the best thing that has happened to me in my professional and academic career. Meeting each other 5 years ago at that table in Technohal during a tutorial for Inorganic Chemistry sparked a half-decade long collaboration in quite literally anything. Over these many years, we must have spent somewhere around €1000 on Subway sandwiches (if not more…) to help us through the rough weeks which kept getting rougher and rougher. As I write this, you have long graduated, started your new job, and engaged to your soon-to-be wife. Congratulations! It gives me such joy that we were able to work together so efficiently and effectively for so many years, and now seeing you about to start this new chapter of your life that you have been dreaming about for years. Know that, soon, I will do the same. When in doubt, always go Mimic.

Thank you, Calista, for being the best girlfriend I could have wished for, for the past four years, and hopefully many more to come. Coming home to you every day has been a gift from the world that I

never thought would impact me as much as it has. These past months have been professionally draining, but every time I come home, I have a loving shoulder to rest on, and I hope I can provide you with the same. As we both start this new chapter of our lives and careers, let us look forward to what is to come. Next up: a dog. Sammy, right?

Thanks, Ivanna, for being a great and somewhat unexpected friend. I told you this story several times of the first time we met, during that online call in 2022, where you were starting your Module 3 project, and I was your Learning Assistant. After the call ended, I said out loud "well, she definitely hates me." Now, almost three years later, we have spent countless hours laughing together in the lab talking about all kinds of nonsense and serious topics at the same time. Please know that you are highly appreciated, and a kind soul such as yourself deserves all the best that life has to offer. Слава Україні!

To my parents and the rest of my family: thank you for providing me with the best basis that any student could hope for. Providing me with not only a safe environment to go back to in Ermelo, but also with a beautiful apartment in Enschede to complete my studies in, was the biggest blessing I have ever received. You have assumed your mission to be: "make it as smooth as possible for our children to develop themselves as much as possible." Well, mission accomplished, times a million. I love you all so much.

Special thanks to Leonie Krab–Hüsken for being a great mentor and an even better program coordinator of the amazing Chemical Science and Engineering program here at the University of Twente. Over the years, we have had so many great conversations about the program, and you have endured countless hours of my rambling and feedback directed at the program. I plan to continue in academia, and, who knows, maybe I may even stand in your shoes one day! Although they probably would not fit because you are much taller than I am.

Combined thanks to Erna Brus, Renilde Bonthuis–van Seters and all other members of the Chemical Science and Engineering program, thank you for shaping the future of science and caring about the experience and enjoyment of students as much as their learning trajectories. Science should be both enjoyable and productive, which you all realize more than anyone.

Special thanks to Martin van der Hoef for being, first and foremost, an amazing lecturer and an inspiring teacher over the many courses you have taught me. But also, for being a great collaborator in the many Teaching Assistant jobs that I have done under your guidance. I have enjoyed our conversations very much, and I hope to continue this trend better and stronger than ever.

And thanks to Jeffery Wood, Hil Meijer, Ivana Lin and others for professional guidance and advice of all shapes and sizes over my thesis time.

If your name was not mentioned, you may assume that your name has been thrown into a pit and forgotten for eternity. Either that, or I did not have enough time or space to mention everyone. You may choose. See ya.

"Progress, not perfection." – Theo Von

Literature References

1. Ferrell, J. E.; Ha, S. H. Ultrasensitivity Part III: Cascades, Bistable Switches, and Oscillators. Trends in Biochemical Sciences 2014, 39 (12), 612–618. DOI: 10.1016/j.tibs.2014.10.002.
2. Süel, G. M.; Garcia-Ojalvo, J.; Liberman, L. M.; Elowitz, M. B. An Excitable Gene Regulatory Circuit Induces Transient Cellular Differentiation. Nature 2006, 440 (7083), 545–550. DOI: 10.1038/nature04588.
3. Bagci, E. Z.; Vodovotz, Y.; Billiar, T. R.; Ermentrout, G. B.; Bahar, I. Bistability in Apoptosis: Roles of Bax, Bcl-2, and Mitochondrial Permeability Transition Pores. Biophysical journal 2006, 90 (5), 1546–1559. DOI: 10.1529/biophysj.105.068122.
4. Schnitter, F.; Rieß, B.; Jandl, C.; Boekhoven, J. Memory, Switches, and an OR-Port through Bistability in Chemically Fueled Crystals. Nature Communications 2022, 13 (1). DOI: 10.1038/s41467-022-30424-2.
5. Szalai, I.; De Kepper, P. Turing Patterns, Spatial Bistability, and Front Instabilities in a Reaction-Diffusion System. The journal of physical chemistry. A, Molecules, spectroscopy, kinetics, environment & general theory. 2004, 108 (25), 5315. DOI: 10.1021/jp049168n.
6. Kaminaga, A.; Vanag, V. K.; Epstein, I. R. A Reaction-Diffusion Memory Device. Angewandte Chemie International Edition 2006, 45 (19), 3087–3089. DOI: 10.1002/anie.200600400.
7. Wang, G. Optimal Homeostasis Necessitates Bistable Control. Journal of the Royal Society, Interface 2012, 9 (75), 2723–2734. DOI: 10.1098/rsif.2012.0244.
8. Kaspar, C.; Ravoo, B. J.; van der Wiel, W. G.; Wegner, S. V.; Pernice, W. H. P. The Rise of Intelligent Matter. Nature: International weekly journal of science 2021, 594 (7863), 345–355. DOI: 10.1038/s41586-021-03453-y.
9. Maity, I.; Dev, D.; Cohen-Luria, R.; Wagner, N.; Ashkenasy, G. Engineering Reaction Networks by Sequential Signal Processing. Chem 2024, 10 (4), 1132–1146. DOI: 10.1016/j.chempr.2023.10.017.
10. Tyson, J. J.; Chen, K. C.; Novak, B. Sniffers, Buzzers, Toggles and Blinkers: Dynamics of Regulatory and Signaling Pathways in the Cell. Current opinion in cell biology 2003, 15 (2), 221–231. DOI: 10.1016/S0955-0674(03)00017-6.
11. Kriukov, D. V.; Huskens, J.; Wong, A. S. Y. Exploring the Programmability of Autocatalytic Chemical Reaction Networks. Nature communications 2024, 15 (1), 8289. DOI: 10.1038/s41467-024-52649-z.
12. Postma, S. G. J.; te Brinke, D.; Vialshin, I. N.; Wong, A. S. Y.; Huck, W. T. S. A Trypsin-Based Bistable Switch. Tetrahedron 73 (33), 4896–4900. DOI: 10.1016/j.tet.2017.04.053.
13. Hanopolskyi, A. I.; Smaliak, V. A.; Novichkov, A. I.; Semenov, S. N. Autocatalysis: Kinetics, Mechanisms and Design. ChemSystemsChem 2021, 3 (1). DOI: 10.1002/syst.202000026.
14. Maity, I.; Wagner, N.; Mukherjee, R.; Dev, D.; Peacock-Lopez, E.; Cohen-Luria, R.; Ashkenasy, G. A Chemically Fueled Non-Enzymatic Bistable Network. Nature communications 2019, 10 (1), 4636. DOI: 10.1038/s41467-019-12645-0.
15. Maity, I.; Dev, D.; Basu, K.; Wagner, N.; Ashkenasy, G. Signaling in Systems Chemistry: Programing Gold Nanoparticles Formation and Assembly Using a Dynamic Bistable Network. Angewandte Chemie 2021, 133 (9), 4562–4567. DOI: 10.1002/ange.202012837.

16. Kriukov, D. V.; Koyuncu, A. H.; Wong, A. S. Y. History Dependence in a Chemical Reaction Network Enables Dynamic Switching. Small (Weinheim an der Bergstrasse, Germany) 2022, 18 (16), e2107523. DOI: 10.1002/smll.202107523.
17. Semenov, S. N.; Wong, A. S. Y.; van der Made, R. M.; Postma, S. G. J.; Groen, J.; van Roekel, H. W. H.; de Greef, T. F. A.; Huck, W. T. S. Rational Design of Functional and Tunable Oscillating Enzymatic Networks. Nature chemistry 2015, 7 (2), 160–165. DOI: 10.1038/nchem.2142.
18. Maguire, O. R.; Wong, A. S. Y.; Westerdiep, J. H.; Huck, W. T. S. Early Warning Signals in Chemical Reaction Networks. Chemical Communications 2020, 56 (26), 3725–3728. DOI: 10.1039/d0cc01010c.
19. Nicolis, G.; Prigogine, I. Self-Organization in Nonequilibrium Systems: From Dissipative Structures to Order through Fluctuations; Wiley: New York, 1977. Chapter 1, ISBN 9780471024019 or 0471024015.
20. Semenov, S. N.; Kraft, L. J.; Ainla, A.; Zhao, M.; Baghbanzadeh, M.; Campbell, V. E.; Kang, K.; Fox, J. M.; Whitesides, G. M. Autocatalytic, Bistable, Oscillatory Networks of Biologically Relevant Organic Reactions. Nature 2016, 537 (7622), 656–660. DOI: 10.1038/nature19776.
21. Sipos, T.; Merkel, J. R. An Effect of Calcium Ions on the Activity, Heat Stability, and Structure of Trypsin. Biochemistry 1970, 9 (14), 2766–2775. DOI: 10.1021/bi00816a003.
22. Zdeněk Perutka; Marek Šebela. Pseudotrypsin: A Little-Known Trypsin Proteoform. Molecules 2018, 23 (10), 2637. DOI: 10.3390/molecules23102637.
23. Rick Wirnt, Trypsin, Methods of Enzymatic Analysis, Academic Press, 1965, Pages 807-818, ISBN 9780123956309, DOI: 10.1016/B978-0-12-395630-9.50146-8.
24. McDonald, M. R.; Kunitz, M. The Effect of Calcium and Other Ions on the Autocatalytic Formation of Trypsin from Trypsinogen. The Journal of general physiology 1941, 25 (1), 53–73. DOI: DOI: 10.1085/jgp.**25**.1.53.
25. Andreas H. Simon; Sandra Liebscher; Ariunkhur Kattner; Christof Kattner; Frank Bordusa. Rational Design of a Calcium-Independent Trypsin Variant. Catalysts 2022, 12 (9), 990. DOI: 10.3390/catal12090990.
26. Abbott, F.; Gomez, J. E.; Birnbaum, E. R.; Darnall, D. W. The Location of the Calcium Ion Binding Site in Bovine Alpha-Trypsin and Beta-Trypsin Using Lanthanide Ion Probes. Biochemistry 1975, 14 (22), 4935–4943. DOI: 10.1021/bi00693a024.
27. Darnall, D. W.; Abbott, F.; Gomez, J. E.; Birnbaum, E. R. Fluorescence Energy-Transfer Measurements between the Calcium Binding Site and the Specificity Pocket of Bovine Trypsin Using Lanthanide Probes. Biochemistry 1976, 15 (23), 5017–5023. DOI: DOI: 10.1021/bi00668a011.
28. Strynadka, N. C. J.; N.G. James, M. Towards an Understanding of the Effects of Calcium on Protein Structure and Function. Current Biology 2 (1), 13–14. DOI: 10.1016/0960-9822(92)90405-Y.
29. T.T. Baird, C.S. Craik, Chapter 'Trypsin', Encyclopedia of Genetics, Academic Press, 2001, Pages 2071-2075, ISBN 9780122270802, DOI: 10.1006/rwgn.2001.1342.
30. Whitcomb, D. C. Early Trypsinogen Activation in Acute Pancreatitis. Gastroenterology 116 (3), 770–772. DOI: 10.1016/S0016-5085(99)70205-2.

31. Gomez, J. E.; Birnbaum, E. R.; Darnall, D. W. The Metal Ion Acceleration of the Conversion of Trypsinogen to Trypsin. Lanthanide Ions as Calcium Ion Substitutes. Biochemistry 1974, 13 (18), 3745–3750. DOI: DOI: 10.1021/bi00715a020.
32. Lottenberg, R.; Jackson, C. M. Solution Composition Dependent Variation in Extinction Coefficients for P-Nitroaniline. Biochimica et Biophysica Acta (BBA)/Protein Structure and Molecular Enzymology 742 (3), 558–564. DOI: 10.1016/0167-4838(83)90273-X.
33. Woolwine, S. C.; Sprinkle, A. B.; Wozniak, D. J. Loss of Pseudomonas Aeruginosa PhpA Aminopeptidase Activity Results in Increased algDTranscription. Journal of Bacteriology 2001, 183 (15), 4674–4679. DOI: 10.1128/JB.183.15.4674-4679.2001.
34. Bru, R.; Walde, P. Product Inhibition of α-Chymotrypsin in Reverse Micelles. European Journal of Biochemistry 1991, 199 (1), 95–103. DOI: 10.1111/j.1432-1033.1991.tb16096.x.
35. França, R. C. d. P.; Assis, C. R. D.; Santos, J. F.; Torquato, R. J. S.; Tanaka, A. S.; Hirata, I. Y.; Assis, D. M.; Juliano, M. A.; Cavalli, R. O.; Carvalho, L. B. d.; Bezerra, R. S. Bovine Pancreatic Trypsin Inhibitor Immobilized onto Sepharose as a New Strategy to Purify a Thermostable Alkaline Peptidase from Cobia (Rachycentron Canadum) Processing Waste. Journal of chromatography. B, Analytical technologies in the biomedical and life sciences 2016, 1033-1034, 210–217. DOI: 10.1016/j.jchromb.2016.08.028.
36. Murphy, A. Chemical modification of bovine trypsin for use in peptide synthesis. PhD Thesis, Dublin City Univ. 1996, Available at URL: doras.dcu.ie/19109/.
37. Ásgeirsson, B.; Cekan, P. Microscopic Rate-Constants for Substrate Binding and Acylation in Cold-Adaptation of Trypsin I from Atlantic Cod. FEBS Letters 2006, 580 (19), 4639–4644. DOI: 10.1016/j.febslet.2006.07.043.
38. Arcadia, C. E.; Dombroski, A.; Oakley, K.; Chen, S. L.; Tann, H.; Rose, C.; Kim, E.; Reda, S.; Rubenstein, B. M.; Rosenstein, J. K. Leveraging Autocatalytic Reactions for Chemical Domain Image Classification. Chemical Science 2021, 12 (15), 5464–5472. DOI: 10.1039/d0sc05860b.
39. Sánchez-Morán, H.; Kaar, J. L.; Schwartz, D. K. Combinatorial High-Throughput Screening of Complex Polymeric Enzyme Immobilization Supports. Journal of the American Chemical Society 2024, 146 (13), 9112–9123. DOI: 10.1021/jacs.3c14273.
40. KONG, G.; LIU, L.; LU, J.; CHE, C.; ZHONG, Z. Study on Lanthanum Salt Conversion Coating Modified with Citric Acid on Hot Dip Galvanized Steel. Journal of Rare Earths 28 (3), 461–465. DOI: 10.1016/S1002-0721(09)60134-4.
41. Scheffer, M.; Carpenter, S.; Foley, J. A.; Folke, C.; Walker, B. Catastrophic Shifts in Ecosystems. Nature 2001, 413 (6856), 591–596. DOI: DOI: 10.1038/35098000
42. Otto H Schmitt. A Thermionic Trigger. Journal of Scientific Instruments 1938, 15 (1), 24–26. DOI: 10.1088/0950-7671/15/1/305
43. Sonnad, J. R.; Goudar, C. T. Solution of the Haldane Equation for Substrate Inhibition Enzyme Kinetics Using the Decomposition Method. Mathematical and Computer Modelling 40 (5), 573–582. DOI: 10.1016/j.mcm.2003.10.051

Appendices

MATLAB scripts and raw data are available from the author by request.

Appendix A – Detailed Experimental Procedures, Conditions and Data

Extended information including procedures, conditions and data for a selection of successful experiments throughout the course of this thesis.

A.1 – Batch Experiments

Experiment 1 – Calibrate Trypsin Activity by BAPNA Hydrolysis in Batch

To calibrate trypsin concentration by BAPNA in batch, we performed a well plate experiment at varying trypsin concentrations. A wide range of [Tr] should be used, across at least 2-3 orders of magnitude. Hence, several Tr stock solutions should be prepared to make the required additions of volume realistic in size and to keep approximately the same total well volume in all the wells. The stock solutions used for this experiment are as follows.

- **Tr** stocks
  - **Tr_1** = 250 uM Tr in [4 mM HCl + 20 mM $CaCl_2$]
  - **Tr_2** = 50 uM Tr in [4 mM HCl + 20 mM $CaCl_2$]
  - **Tr_3** = 5 uM Tr in [4 mM HCl + 20 mM $CaCl_2$]
- **BAPNA** stock (25 mM BAPNA in DMSO)
- **Buffer** stock (0.5 M TRIS-HCl pH 7.8 + 20 mM $CaCl_2$)

The conditions for the calibration of the BAPNA cleavage reporter reaction are tabulated in **Table A1.1**. All wells contain $[BAPNA]_0$ = 0.7 mM, and $[Ca^{2+}]_0$ = 20 mM and are buffered by 0.5 mM TRIS-HCl pH = 7.8. $[Tr]_0$ is varied in the wells in triplicates.

In all wells: $[BAPNA]_0$ = 0.7 mM $[Ca]_0$ = 20 mM	1, 2 & 3	4, 5 & 6	7, 8 & 9	10, 11 & 12
A	15 nM Tr	100 nM Tr	250 nM Tr	500 nM Tr
B	1.0 µM Tr	1.5 µM Tr	2.0 µM Tr	2.5 µM Tr
C	3.0 µM Tr	3.5 µM Tr	4.0 µM Tr	4.5 µM Tr
D	5.0 µM Tr	7.5 µM Tr	10 µM Tr	25 µM Tr

Table A1.1. Experimental conditions for the calibration of the BAPNA cleavage reaction. The table represents the dimensions of half of a 96-well plate. $[Tr]_0$ is varied as triplicates across the wells, from left to right and from top to bottom. All wells contain $[BAPNA]_0$ = 0.7 mM, and $[Ca^{2+}]_0$ = 20 mM, and are buffered by 0.5 mM TRIS-HCl pH = 7.8.

The volumes added of each stock solution are tabulated in **Table A1.2**. First, all wells are filled with the appropriate volume of the appropriate Tr stock, and subsequently the reactions are initiated by addition of 190 of a bath of BAPNA and buffer.

	1, 2 & 3	4, 5 & 6	7, 8 & 9	10, 11 & 12	Bath composition
A	0.4 µL **Tr_3** 190 µL Bath	4.0 µL **Tr_3** 190 µL Bath	10.0 µL **Tr_3** 190 µL Bath	20.0 µL **Tr_3** 190 µL Bath	280 µL **BAPNA** + 9720 µL **Buffer**
B	4.0 µL **Tr_2** 190 µL Bath	6.0 µL **Tr_2** 190 µL Bath	8.0 µL **Tr_2** 190 µL Bath	10.0 µL **Tr_2** 190 µL Bath	
C	12.0 µL **Tr_2** 190 µL Bath	14.0 µL **Tr_2** 190 µL Bath	16.0 µL **Tr_2** 190 µL Bath	18.0 µL **Tr_2** 190 µL Bath	
D	4.0 µL **Tr_1** 190 µL Bath	6.0 µL **Tr_1** 190 µL Bath	8.0 µL **Tr_1** 190 µL Bath	20.0 µL **Tr_1** 190 µL Bath	

Table A1.2. All volumes of stocks added for the calibration of the BAPNA cleavage reaction. The table represents the dimensions of half of a 96-well plate. The stock names refer to the list of stocks for this experiment. All reactions are initiated by the addition of 190 µL of the bath mixture, of which the composition is listed in the rightmost column. $[Tr]_0$ is varied across the wells, from left to right and from top to bottom ($[Tr]_0$ = 0.015, 0.1, 0.25, 0.5, 1.0, 1.5, 2.0, 2.5, 3.0, 3.5, 4.0, 4.5, 5.0, 7.5, 10, and 25 µM).

The data of this experiment contains many BAPNA hydrolysis curves. The initial rate of change of the absorbance is taken for each curve. The triplicates are averaged, and these averages are plotted against the value of $[Tr]_0$ as in **Table A1.2**. This is shown in **Figure A1.1**. The points below [Tr] = 10 µM behaved linearly and are thus fitted with a linear matrix regression, the result is $[\mathrm{Tr}]_t = 912.6\frac{dA}{dt}$.

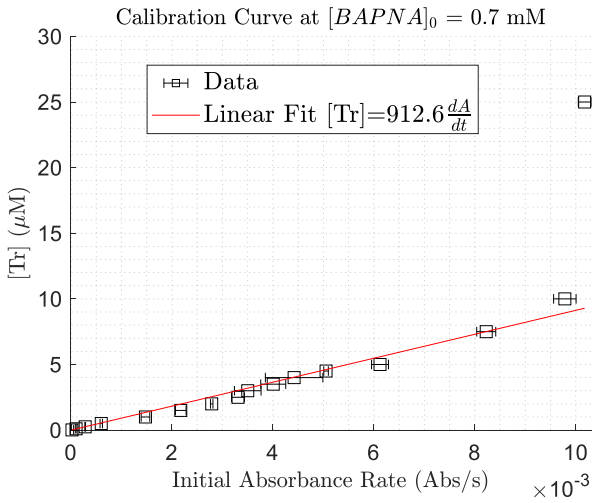

Figure A1.1. Data from calibration curve of BAPNA hydrolysis. Linear fit $[\mathrm{Tr}]_t = 912.6\frac{dA}{dt}$.

Experiment 2 – Determine Molar Absorbance of pNA

To convert absorbance values directly to pNA concentration, we determined the molar absorbance of pNA by means of well plate experiments. The stock solutions used for this experiment are as follows.

- **Tr** stock (40 µM Tr in [4 mM HCl + 20 mM $CaCl_2$])
- **Tg** stock (5 mM Tg in [4 mM HCl + 20 mM $CaCl_2$])
- **BAPNA** stock (25 mM BAPNA in DMSO)
- **Buffer** stock (0.5 M TRIS-HCl pH 7.8 + 20 mM $CaCl_2$)

The conditions for the experiment are shown in **Table A2.1**. All wells contain $[Tr]_0$ = 1 µM, $[Tg]_0$ = 100 µM and $[Ca^{2+}]_0$ = 20 mM and are buffered by 0.5 mM TRIS-HCl pH = 7.8. $[BAPNA]_0$ is varied in the wells in triplicates.

We pipetted Tr in one corner of all wells, then the appropriate BAPNA in the opposite corner. The Tg was mixed with Buffer in a bath to achieve appropriate concentrations in the wells. We then pipetted this bath using a 12-fold multi pipette into all wells and quickly entered the plate into the plate reader. Absorbance was measured at 400 nm for 10 minutes, waited for 12.5 minutes, measured again for 10 min, waited for 2 min, then measured for 10 more minutes.

	1, 2 & 3	4, 5 & 6	7, 8 & 9	10, 11 & 12	Bath composition
C	5 µL **Tr** 0.8 µL **BAPNA** 190 µL Bath	5 µL **Tr** 1.6 µL **BAPNA** 190 µL Bath	5 µL **Tr** 2.4 µL **BAPNA** 190 µL Bath	5 µL **Tr** 3.2 µL **BAPNA** 190 µL Bath	100 µL **Tg** 5000 µL **Buffer**
D	5 µL **Tr** 4.0 µL **BAPNA** 190 µL Bath	5 µL **Tr** 4.8 µL **BAPNA** 190 µL Bath	5 µL **Tr** 5.6 µL **BAPNA** 190 µL Bath	5 µL **Tr** 6.4 µL **BAPNA** 190 µL Bath	

Table A2.1. Experimental conditions for the retrieval of the molar absorbance of pNA. $[BAPNA]_0$ is varied as triplicates across the wells, from left to right and from top to bottom ($[BAPNA]_0$ = 0.1, 0.2, 0.3, 0.4, 0.5, 0.6, 0.7, and 0.8 mM). All wells contain $[Tr]_0$ = 1 µM, $[Tg]_0$ = 100 µM and $[Ca^{2+}]_0$ = 20 mM and are buffered by 0.5 mM TRIS-HCl pH = 7.8.

The raw data of this experiment contains many curves of BAPNA hydrolysis at varying $[BAPNA]_0$. We averaged the triplicates and fitted a basic model ($A = A_{max}(1 - e^{(-kt)})$) to the data. The fitted values of A_{max} are plotted against $[BAPNA]_0$, by the law of Lambert-Beer ($A = \epsilon bc$) (**Figure A2.1a**). The slope a linear fit through these data (**Figure A2.1b**) divided by the path length b = 0.56 cm yields the molar absorbance of pNA, ϵ = 6.36 mM cm^{-1}.

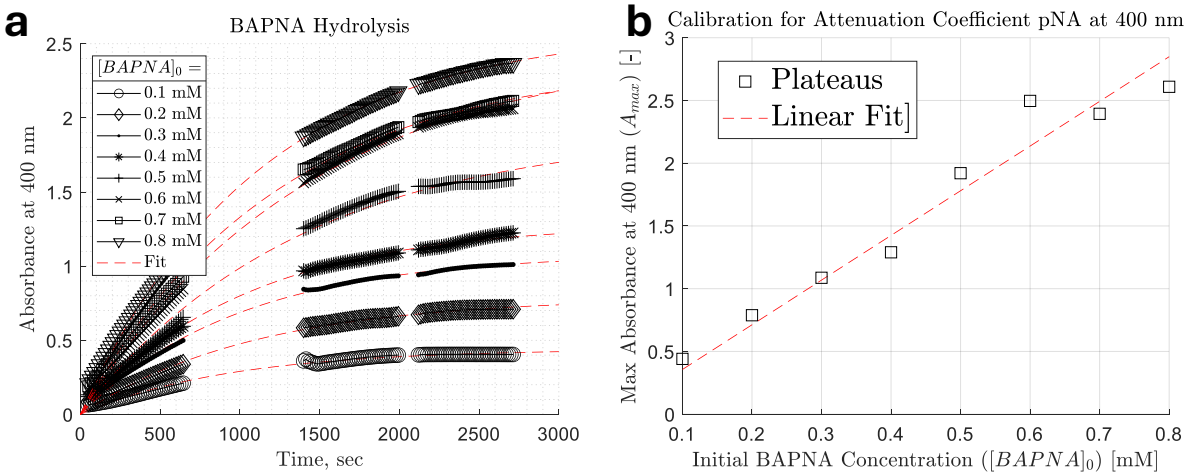

Figure A2.1. Data from the experiment to gather the molar absorbance coefficient of p-nitroaniline (pNA) at 400 nm. **a.** Reaction curves at varying $[BAPNA]_0$. The data is fitted based on a kinetic model of the system. **b.** The fitted maximum absorbance of each reaction curve is taken based on the fits and plotted against $[BAPNA]_0$. The molar absorbance coefficient is retrieved from the slope of the Lambert-Beer linear regression. Linear fit R^2 = 0.956.

Experiment 3 – Monitor Effect of La^{3+} on Trypsin Calibration

To check whether the calibration curve can be used for real experiments with La^{3+} present, we investigated whether the presence of La^{3+} affects the calibration of trypsin by BAPNA. The stock solutions used for this experiment are as follows.

- **Tr** stock (40 µM Tr in [4 mM HCl + 20 mM $CaCl_2$])
- **La** stock (50 mM in mQ)
    - **La_1** = 50 mM in mQ
    - **La_2** = 10 mM in mQ
- **BAPNA** stock (25 mM BAPNA in DMSO)
- **Buffer** stock (0.5 M TRIS-HCl pH 7.8 + 20 mM $CaCl_2$)

The conditions for the experiment are shown in **Table A3.1**.

	1, 2 & 3 ($[La^{3+}]_0$ = 0.0 mM)	4, 5 & 6 ($[La^{3+}]_0$ = 0.1 mM)	7, 8 & 9 ($[La^{3+}]_0$ = 0.7 mM)	10, 11 & 12 ($[La^{3+}]_0$ = 1.4 mM)	Bath composition
A	5 µL **Tr** 0 µL **La_1** 190 µL $Bath_A$	5 µL **Tr** 2 µL **La_2** 190 µL $Bath_A$	5 µL **Tr** 2.8 µL **La_1** 190 µL $Bath_A$	5 µL **Tr** 5.6 µL **La_1** 190 µL $Bath_A$	3 mL **Buffer** 12 µL **BAPNA** ($[BAPNA]_0$ = 0.1 mM)
B	5 µL **Tr** 0 µL **La_1** 190 µL $Bath_B$	5 µL **Tr** 2 µL **La_2** 190 µL $Bath_B$	5 µL **Tr** 2.8 µL **La_1** 190 µL $Bath_B$	5 µL **Tr** 5.6 µL **La_1** 190 µL $Bath_B$	3 mL **Buffer** 24 µL **BAPNA** ($[BAPNA]_0$ = 0.2 mM)
C	5 µL **Tr** 0 µL **La_1** 190 µL $Bath_C$	. . .	. . .	. . .	3 mL **Buffer** 36 µL **BAPNA** ($[BAPNA]_0$ = 0.3 mM)
D	5 µL **Tr** 0 µL **La_1** 190 µL $Bath_D$	. . .	. . .	. . .	3 mL **Buffer** 48 µL **BAPNA** ($[BAPNA]_0$ = 0.4 mM)
E	5 µL **Tr** 0 µL **La_1** 190 µL $Bath_E$	. . .	. . .	. . .	3 mL **Buffer** 60 µL **BAPNA** ($[BAPNA]_0$ = 0.5 mM)
F	5 µL **Tr** 0 µL **La_1** 190 µL $Bath_F$	. . .	. . .	. . .	3 mL **Buffer** 72 µL **BAPNA** ($[BAPNA]_0$ = 0.6 mM)
G	5 µL **Tr** 0 µL **La_1** 190 µL $Bath_G$	. . .	. . .	. . .	3 mL **Buffer** 84 µL **BAPNA** ($[BAPNA]_0$ = 0.7 mM)
H	5 µL **Tr** 0 µL **La_1** 190 µL $Bath_H$	. . .	. . .	. . .	3 mL **Buffer** 96 µL **BAPNA** ($[BAPNA]_0$ = 0.8 mM)

Table A3.1. Experimental conditions for the investigation of the effect of La^{3+} on the calibration of trypsin by BAPNA. $[La^{3+}]_0$ is varied as triplicates across the columns and from $[BAPNA]_0$ is varied across the rows. All wells contain $[Tr]_0$ = 1 µM, and $[Ca^{2+}]_0$ = 20 mM and are buffered by 0.5 mM TRIS-HCl pH = 7.8.

We pipetted the appropriate amount of **La** one corner of all wells, then **Tr**. The bath mixture for one row was mixed, and added to the wells of that row, and afterwards the plate was placed in the plate reader to be measured for 4 minutes. This procedure was repeated for all rows. The absorbance profile of each well was converted into [pNA] using the molar absorbance, and the initial reaction rate was taken for each well, the results are shown in **Figure A3.1a**. The averages of the triplicates were taken, along with the standard deviations, and plotted in **Figure A3.2b**, which shows no significant difference at different $[La^{3+}]$.

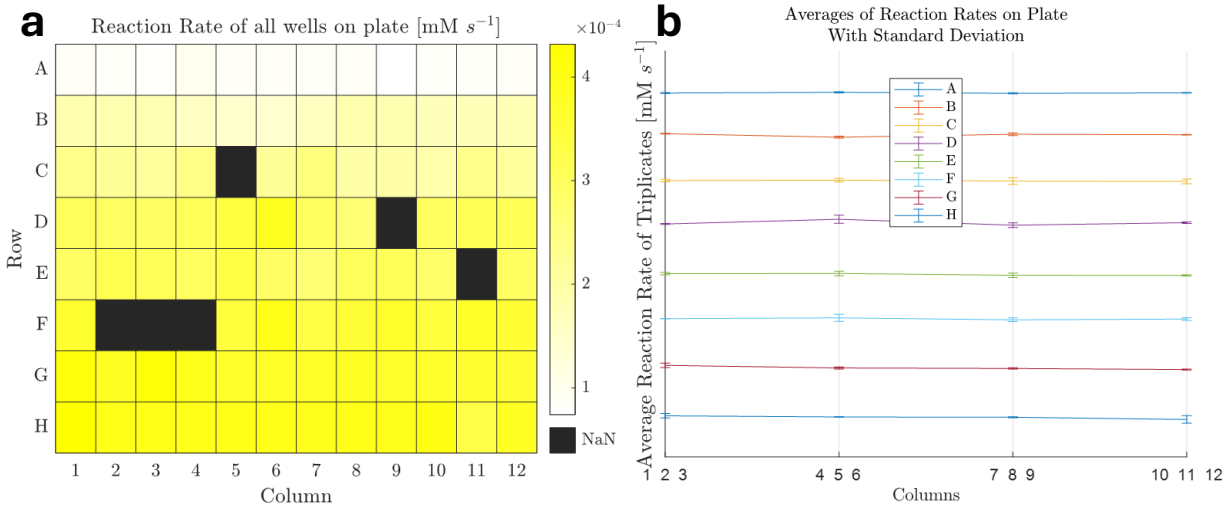

Figure A3.1. Data from the experiment to investigate the effect of La^{3+} on the calibration of trypsin by BAPNA. **a.** The full 96-well plate as a heatmap, where the color of each well corresponds to the initial reaction rate of BAPNA hydrolysis. $[BAPNA]_0$ is changed row-wise, and $[La^{3+}]_0$ is changed column-wise in triplicates. **b.** The averages of the triplicates of the 96-well plate shown with their standard deviations.

To retrieve the kinetic parameters, and to solidify the conclusion, we converted the data into a Michaelis-Menten plot (reaction rate versus substrate concentration). We fitted a nonlinear Michaelis-Menten model to this data, $v = \frac{V_{max}[S]}{K_M+[S]}$, where v is the reaction rate and [S] is the substrate concentration ([BAPNA]). The resulting fitted parameters are V_{max} = 7.23 · 10^{-4} mM s^{-1}, K_M = 0.6444 mM, and k_{cat} = 0.7234 s^{-1}.

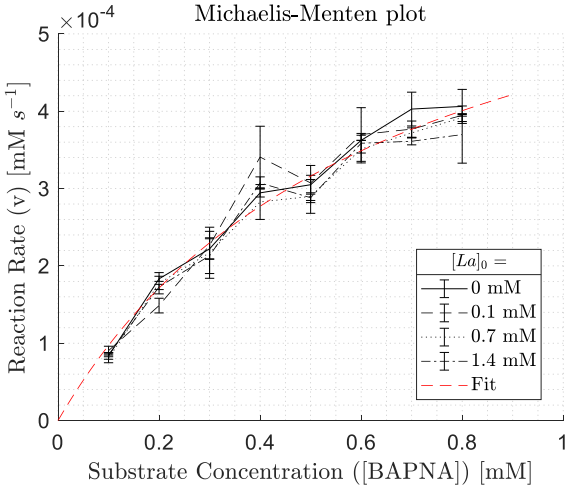

Figure A3.2. Michaelis-Menten plot of the reaction rates across the well plate. The black lines are the $[La^{3+}]_0$ data series. The red dashed line is a nonlinear regression based on the Michaelis-Menten kinetics. Error bars are s.e., n = 3.

Experiment 4 – Monitor Stability of Trypsinogen in Storage Conditions

To determine whether our chemicals stay active during several hour-long experiments, we tested the stability of trypsinogen in relevant conditions. Trypsin and STI are assumed stable for our purposes, based on literature reports. The stock solutions used for this experiment are as follows.

- **La** stock (10 mM in mQ)
- **BAPNA** stock (25 mM BAPNA in DMSO)
- **Buffer** stock (0.5 M TRIS-HCl pH 7.8 + 20 mM $CaCl_2$)

The conditions for the experiment are shown in **Table A4.1**.

	$[La^{3+}]$ = 0.0 mM	$[La^{3+}]$ = 0.2 mM	$[La^{3+}]$ = 2.0 mM
$[Ca^{2+}]$ = 5 mM	1	2	3
$[Ca^{2+}]$ = 100 mM	4	5	6

Table A4.1. Experimental conditions for the determination of the stability of Tg in relevant conditions over many hours. Six vials are prepared with combinations of two $[Ca^{2+}]$ values and three $[La^{3+}]$ values. All vials contain $[Tg]_0$ = 200 µM and 4 mM HCl.

We prepared six vials with the conditions as tabulated in **Table A4.1** and took 5 µL aliquots from each vial at 1h, 7.5h, 23h and 30h after the vials were prepared, and placed these aliquots into empty wells in a well plate. To these aliquots, I added 195 µL of a bath (0.7 mM **BAPNA** in **Buffer**) to initiate the hydrolysis of BAPNA. The formed Tr from degradation should cleave BAPNA and give an absorbance signal. The plate is placed in the plate reader, and the initial absorbance change rate is measured and related to the current Tr concentration using the calibration curve. The results are shown in **Figure A4.1**. Some wells produced initial absorbance rates that were very noisy but indistinguishable from zero, and therefore sometimes negative. These values were set to zero. From the data, we see no significant formation of Tr in the vials, and therefore conclude that Tg is likely stable over 30 hours in these conditions.

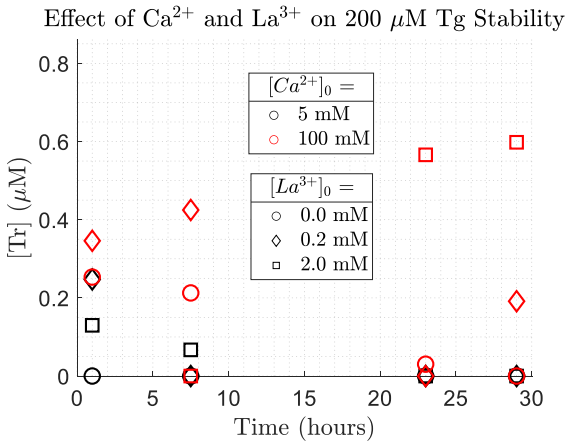

Figure A4.1. Plot of the amount of trypsin produced at each condition, over 30 hours.

Experiment 5 – Perform Autocatalysis Kinetic Assay with BAPNA

To maintain a constant volume of 200 µL in all wells, a number of La^{3+} and Tg stock solutions equal to the number of different concentration data points of these respective compounds is prepared to compensate for the dilution factors. All other compounds are prepared as single stocks. The stock solutions used for this experiment are as follows.

- **La** stocks (variable molarity in mQ)
  - Row A: 0.0 mM La^{3+} in mQ
  - Row B: 16 mM La^{3+} in mQ

- Row C: 32 mM La^{3+} in mQ
- Row D: 40 mM La^{3+} in mQ
- Row E: 48 mM La^{3+} in mQ
- Row F: 80 mM La^{3+} in mQ
- Row G: 120 mM La^{3+} in mQ
- Row H: 160 mM La^{3+} in mQ

- **Tg** stocks (variable molarity in [4 mM HCl + 20 mM $CaCl_2$])
  - Columns 1&2: 0.0 mM Tg in [4 mM HCl + 20 mM $CaCl_2$]
  - Columns 3&4: 1.6 mM Tg in [4 mM HCl + 20 mM $CaCl_2$]
  - Columns 5&6: 3.2 mM Tg in [4 mM HCl + 20 mM $CaCl_2$]
  - Columns 7&8: 4.0 mM Tg in [4 mM HCl + 20 mM $CaCl_2$]
  - Columns 9&10: 6.0 mM Tg in [4 mM HCl + 20 mM $CaCl_2$]
  - Columns 11&12: 8.0 mM Tg in [4 mM HCl + 20 mM $CaCl_2$]
- **Tr** stock (20 µM in [4 mM HCl + 20 mM $CaCl_2$])
- **BAPNA** stock (25 mM BAPNA in DMSO)
- **Buffer** stock (0.5 M TRIS-HCl pH 7.8 + 20 mM $CaCl_2$)

The conditions for the autocatalytic kinetic assay of the chemical network with BAPNA are tabulated in **Table A5.1**. All wells contain $[Tr]_0$=0.25 µM, $[BAPNA]_0$ = 1.0 mM, and $[Ca^{2+}]_0$ = 20 mM and are buffered by 0.5 mM TRIS-HCl pH = 7.8. $[La^{3+}]_0$ and $[Tg]_0$ are varied across the rows and columns, respectively, with $[Tg]_0$ varied in duplicates.

In all wells: $[BAPNA]_0$ = 1.0 mM $[Tr]_0$ = 0.25 µM $[Ca]_0$ = 20 mM		$[Tg]_0$ =					
		0 µM 1 & 2	40 µM 3 & 4	80 µM 5 & 6	100 µM 7 & 8	150 µM 9 & 10	200 µM 11 & 12
$[La^{3+}]_0$ =	0.0 mM A						
	0.2 mM B						
	0.4 mM C						
	0.5 mM D						
	0.6 mM E						
	1.0 mM F						
	1.5 mM G						
	2.0 mM H						

Table A5.1. Experimental conditions for studying the effect of $[La^{3+}]_0$ and $[Tg]_0$ on the autocatalysis reaction kinetic constants. The table represents the dimensions of a 96-well plate. Across the rows, $[La^{3+}]_0$ is varied as 0.0 mM, 0.2 mM, 0.4 mM, 0.5 mM, 0.6 mM, 1.0 mM, 1.5 mM, and 2.0 mM. Across the columns, [Tg] is varied as 0 µM, 40 µM, 80 µM, 100 µM, 150 µM, and 200 µM in duplicates. All wells contain $[Tr]_0$=0.25 µM, $[BAPNA]_0$ = 1.0 mM, and $[Ca^{2+}]_0$ = 20 mM and are buffered by 0.5 mM TRIS-HCl pH = 7.8. The volume in all wells is kept constant at 200 µL.

Each well is filled with 2.5 µL **Tr** stock, 2.5 µL of the appropriate **La** stock, 5 µL of the appropriate **Tg** stock, and filled until 200 µL with **BAPNA** stock and **Buffer** until [BAPNA] = 1.0 mM. All wells are initiated simultaneously, and starting all the reactions took approximately 70 seconds due to delays in pipetting each row separately using a multi pipette. The plate was placed in a plate reader and the absorbance at 400 nm was measured for 90 minutes. The resulting absorbance curves were converted to [pNA] using the molar absorbance of pNA, the curves were smoothed using a

built-in MATLAB data smoothing tool, and the duplicates were aggregated. **Figure A5.1** shows a set of sample curves that span the range of conditions for this experiment.

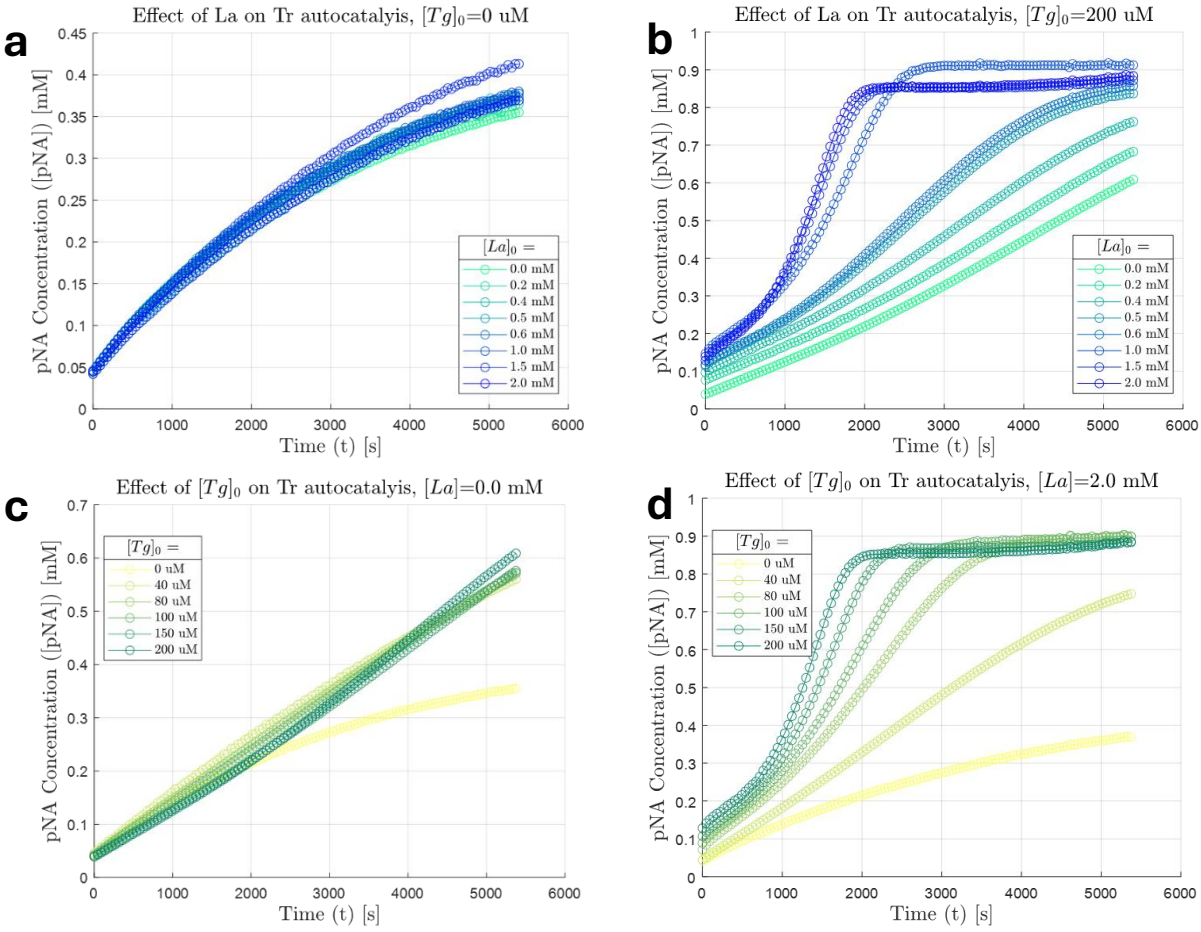

Figure A5.1. Four example plots of kinetic graphs of the autocatalytic conversion of Tg to Tr, assayed by BAPNA in batch. **(a)** Varying $[La^{3+}]_0$ for $[Tg]_0$ = 0 μM (leftmost column in **Table A5.1**). **(b)** Varying $[La^{3+}]_0$ for $[Tg]_0$ = 200 μM (rightmost column). **(c)** Varying $[Tg]_0$ for $[La^{3+}]_0$ = 0.0 mM (top row). **(d)** Varying $[Tg]_0$ for $[La^{3+}]_0$ = 2.0 mM (bottom row).

To visualize all the 96 graphs simultaneously, we employed an arbitrary threshold value of 50% of the plateau values, which we use as a measure of the rate of autocatalysis (**Figure A5.2a**). Alternatively, we also examined the time at which the reaction rate (slope) is maximum (**Figure A5.2b**).

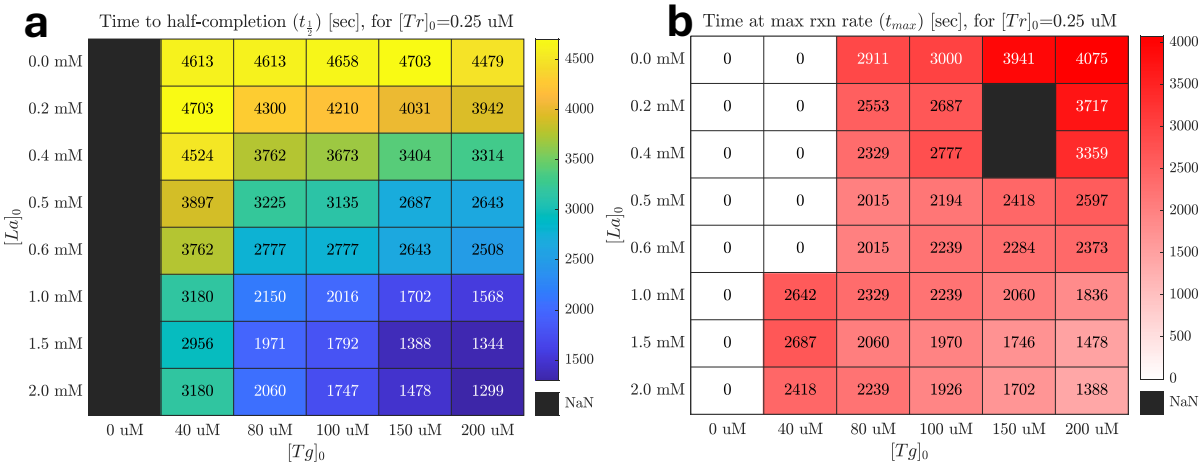

Figure A5.1. Two visualizations of all autocatalysis kinetic data in the 96-well plate. **(a)** Heat map of the times at which each curve reached 50% of the plateau. **(b)** Heat map of the times at which each curve reached its maximum reaction rate.

From the heat maps, we indeed see that adding Tg and La^{3+} consistently increases the speed of autocatalysis. From these results, and using preliminary knowledge from the group, we conclude which conditions are optimal for autocatalysis in flow to observe the bistable behavior.

Experiments 6–10 – Autocatalysis Kinetic Assay without BAPNA

To observe the effect of BAPNA on the autocatalysis kinetics, we performed a set of preliminary experiments in batch without BAPNA present in the autocatalysis reaction mixture. We performed these experiments by a standard aliquoting assay. This method directly means that each experiment is time-consuming. Hence, each series of $[Tg]_0$ data is to be done by itself, to minimize the time delay. Each $[Tg]_0$ data point is thus a separate experiment. The stock solutions prepared for this experiment are as follows and are the same throughout this set of experiments.

- **La** stocks (variable molarity in mQ):
  - Row A: **La_A** 0 mM La^{3+} in mQ
  - Row B: **La_B** 4 mM La^{3+} in mQ
  - Row C: **La_C** 8 mM La^{3+} in mQ
  - Row D: **La_D** 16 mM La^{3+} in mQ
  - Row E: **La_E** 24 mM La^{3+} in mQ
  - Row F: **La_F** 32 mM La^{3+} in mQ
  - Row G: **La_G** 40 mM La^{3+} in mQ
  - Row H: **La_H** 80 mM La^{3+} in mQ
- **Tg** stocks (variable molarity in [4 mM HCl + 20 mM $CaCl_2$]):
  - For series $[Tg]_0$ = 50 µM (Exp 6): **Tg_{50}**: 1000 µM Tg in [4 mM HCl + 20 mM $CaCl_2$]
  - For series $[Tg]_0$ = 100 µM (Exp 7): **Tg_{100}**: 2000 µM Tg in [4 mM HCl + 20 mM $CaCl_2$]
  - For series $[Tg]_0$ = 200 µM (Exp 8): **Tg_{200}**: 4000 µM Tg in [4 mM HCl + 20 mM $CaCl_2$]
  - For series $[Tg]_0$ = 400 µM (Exp 9): **Tg_{400}**: 4000 µM Tg in [4 mM HCl + 20 mM $CaCl_2$]
  - For series $[Tg]_0$ = 600 µM (Exp 10): **Tg_{600}**: 4000 µM Tg in [4 mM HCl + 20 mM $CaCl_2$]
- **Tr** stock (2 µM in [4 mM HCl + 20 mM $CaCl_2$])
- **BAPNA** stock (25 mM BAPNA in DMSO)
- **Buffer** stock (0.1 M TRIS-HCl pH 7.8 + 20 mM $CaCl_2$)

The experimental conditions for the determination of the effect of BAPNA absence on autocatalysis by aliquoting are tabulated in **Table A6.1**. Each column represents a $[Tg]_0$ series, and thus an entire experiment. For each experiment series, we prepared the wells with the appropriate conditions. As often as possible, we took 10 µL aliquots from each well and placed them in a separate 96-well plate. In practice, this was approximately one aliquot every 2-5 minutes, getting quicker with practice. We added 190 µL of a bath mixture (0.7 mM **BAPNA** in **Buffer**) to these wells to initiate the detection reaction, and quickly placed this detection plate in the plate reader for 1.5 minutes. The initial rate of absorbance change is related to concurrent Tr concentration in the main reactor well via the calibration curve. This Tr concentration is then plotted over time.

In all wells: $[Tr]_0$ = 0.05 µM $[Ca]_0$ = 20 mM $[BAPNA]_0$ = 0 mM		$[Tg]_0$ = 50 µM (***Experiment 6***)	$[Tg]_0$ = 100 µM (***Experiment 7***))	$[Tg]_0$ = 200 µM (***Experiment 8***)	$[Tg]_0$ = 400 µM (***Experiment 9***)	$[Tg]_0$ = 600 µM (***Experiment 10***)
$[La^{3+}]_0$ =	0.0 mM A	5 µL **La_A** 5 µL **Tr** 10 µL **Tg_{50}** 180 µL **Buffer**	5 µL **La_A** 5 µL **Tr** 10 µL **Tg_{100}** 180 µL **Buffer**	2.5 µL **La_A** 2.5 µL **Tr** 5 µL **Tg_{200}** 90 µL **Buffer**	2.5 µL **La_A** 2.5 µL **Tr** 10 µL **Tg_{400}** 85 µL **Buffer**	2.5 µL **La_A** 2.5 µL **Tr** 15 µL **Tg_{600}** 80 µL **Buffer**
	0.1 mM B	5 µL **La_B** 5 µL **Tr** 10 µL **Tg_{50}** 180 µL **Buffer**	5 µL **La_B** 5 µL **Tr** 10 µL **Tg_{100}** 180 µL **Buffer**	2.5 µL **La_B** 2.5 µL **Tr** 5 µL **Tg_{200}** 90 µL **Buffer**	2.5 µL **La_B** 2.5 µL **Tr** 10 µL **Tg_{400}** 85 µL **Buffer**	2.5 µL **La_B** 2.5 µL **Tr** 15 µL **Tg_{600}** 80 µL **Buffer**
	0.2 mM C	.	.	.	.	.
	0.4 mM D	.	.	.	.	.
	0.6 mM E	.	.	.	.	.
	0.8 mM F	.	.	.	.	.
	1.0 mM G	.	.	.	.	.
	2.0 mM H	.	.	.	.	.

Table A6.1. All concentrations and volumes of stocks added for the experiment to determine the effect of absence of BAPNA on the autocatalysis reactions. The table represents a number of columns of a 96-well plate, where each $[Tg]_0$ series in the table represents two columns of a well plate. Each $[Tg]_0$ series is thus in duplicate.

The results of each experiment are summarized in **Figure A6.1a-e**. We clearly see an autocatalytic shape of the curves, implying that we observe what we expect. Our aim was to capture the region of the curve in which less than 10% of Tg has been converted. After this point, the true rate of autocatalysis can no longer be captured. We see that adding Tg and La^{3+} increases the speed of the autocatalysis, but after a certain point (**Figure A6.1c**), adding Tg makes the curves slower again. According to literature procedure [42], the apparent rate of autocatalysis can be extracted by first taking the ratio of the rate at each data point and dividing it by the initial rate, $\frac{v}{v_0}$. Then, a linearization of $\ln\frac{v}{v_0}$ versus time gives a straight line of which the fitted slope, δ, is the apparent rate of autocatalysis. By plotting δ against $[Tg]_0$, the substrate binding kinetics can be characterized in a Michaelis-Menten plot, see **Figure A6.1f**. We note that the shape of the Michaelis-Menten plot is unconventional and represents that of a substrate-inhibition reaction [1]. The data indicates that adding Tg over ~200 µM leads to a significant reduction to autocatalysis rate. By fitting such a substrate-inhibition model, we can fit the kinetic Michaelis-Menten parameters of the reaction. Due to time restrictions, we did not follow through with this.

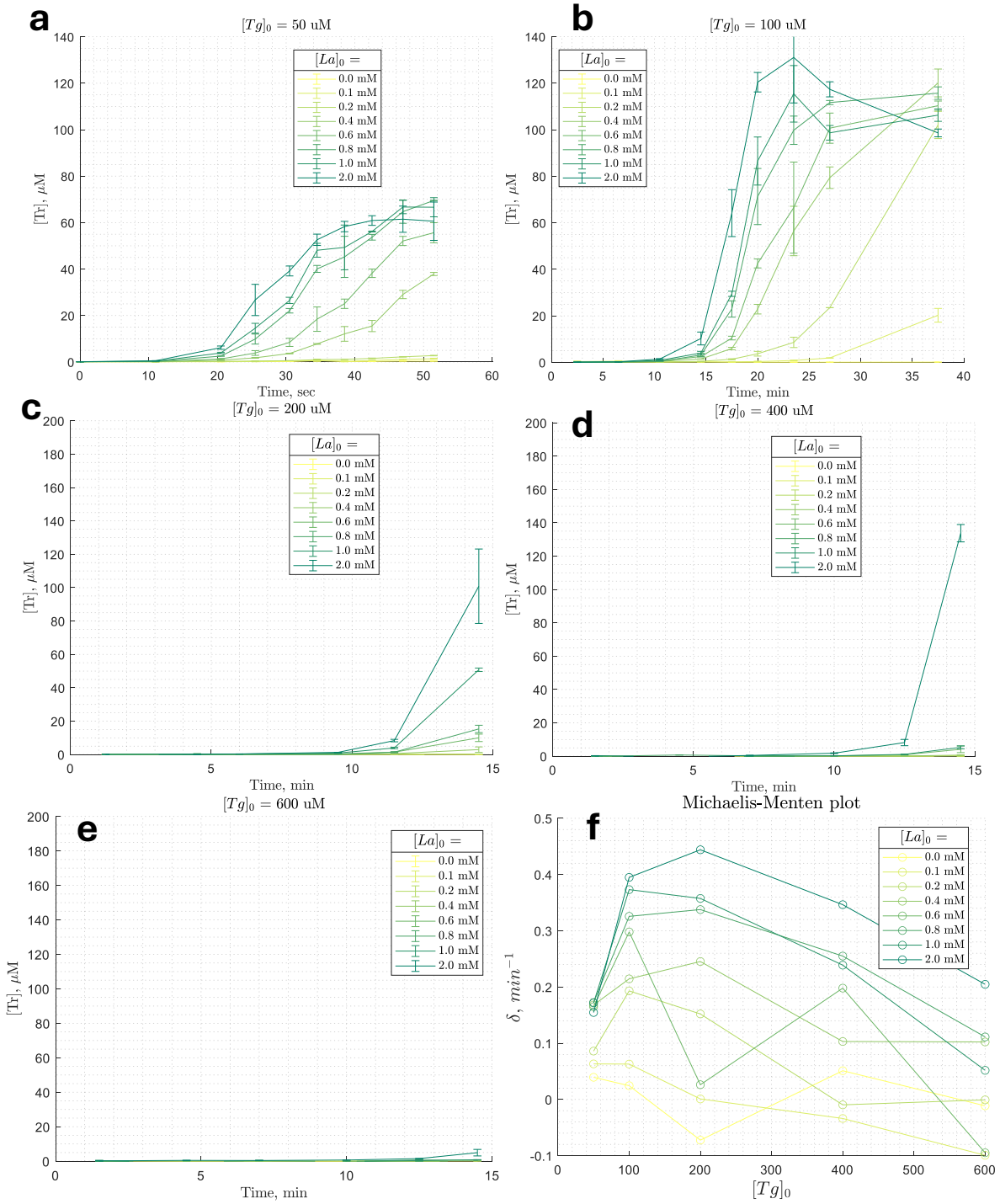

Figure A6.1. Autocatalytic trypsin concentration over time, in the absence of BAPNA, with varying [La^{3+}]. **(a)** Series $[Tg]_0$ = 50 μM (Exp 6). **(b)** Series $[Tg]_0$ = 100 μM (Exp 7). **(c)** Series $[Tg]_0$ = 200 μM (Exp 8). **(d)** Series $[Tg]_0$ = 400 μM (Exp 9). **(e)** Series $[Tg]_0$ = 600 μM (Exp 10). **(f)** Combined Michaelis-Menten plot of panels **(a)**-**(e)**.

A.2 – Flow Experiments

Experiments 11–14 – Familiarize with Flow Setup and Develop Flow Protocol

Experiment 11. To familiarize myself with the flow setup, we performed several experiments to test the behavior and limits of the setup. Each experiment thus did not have an explicit goal, and was

mostly aimed to gain experience with using the setup. First, we aimed to develop a written protocol for the group, the protocol is reported in Appendix B.1. To this end, we set up two CSTRs in series. We prepared stock solutions according to our desired concentrations in flow, and filled syringes with these stock solutions. We connected the syringes to the CSTRs according to the scheme shown in **Figure A11.1**. Note that this experimental setup is different from the setup reported in the main text (Chapter 3.3) because we improved on this setup later (see Exp 15).

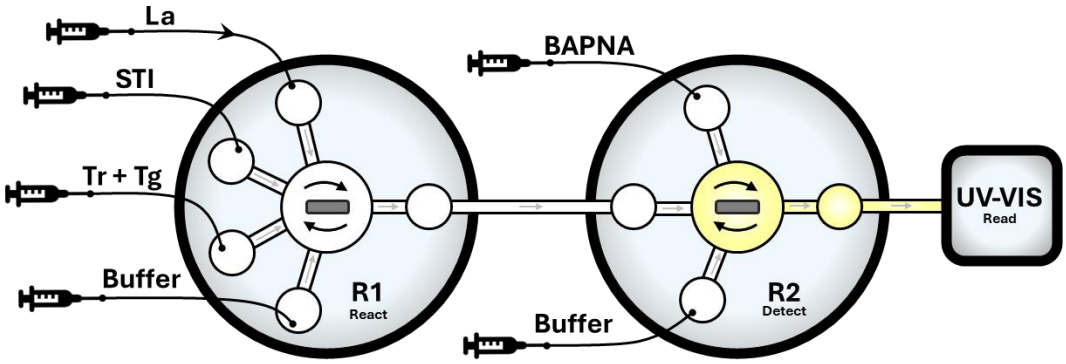

Figure A11.1. Schematic representation of the experimental setup used for familiarization with the flow setup

The stock syringe solutions used for this experiment are as follows. The name of each syringe is highlighted in bold for ease of reference.

- **Tr + Tg** (15 uM Tr + 400 uM Tg dissolved in [4 mM HCl + 20 mM $CaCl_2$])
- **STI** (50 uM STI dissolved in **Buffer1**)
- **Buffer1** (0.5 M TRIS-HCl pH 7.8 + 20 mM $CaCl_2$)
- **Buffer2** (0.5 M TRIS-HCl pH 7.8 + 20 mM $CaCl_2$)
- **La** (5 mM $La(NO_3)_3.6H_2O$ dissolved in mQ)
- **BAPNA** (11.2 mM BAPNA dissolved in [0.20 mQ + 0.72 DMFA + 0.08 DMSO v:v])

Note that Tr and Tg are dissolved together in the same stock solution. Due to a limited number of syringe slots in the syringe holder, we were forced to combine two stock solutions. Since Tr and Tg are stabilized under stock conditions (see Chapter 3.2), we considered it safe to store them together. The experimental procedure, the programmed flow rates of each syringe, is tabulated in **Table A11.1**.

(Values in µL/h)		High La^{3+}	Low La^{3+}	Flush	High La^{3+}	Low La^{3+}		
		High $[STI]_{-1}$	High $[STI]_{-1}$		High $[STI]_{-1}$	High $[STI]_{-1}$	Low $[STI]_0$	High [STI]
R1	**Tr + Tg**	50	50	50	50	50	50	50
	La	50	10	0	50	10	10	10
	STI	50	50	0	50	50	10	50
	Buffer1	100	140	200	100	140	180	140
R2	R1 Out	250	250	250	250	250	250	250
	BAPNA	100	100	100	100	100	100	100
	Buffer2	1250	1250	1250	1250	1250	1250	1250
	R2 Out	1600	1600	1600	1600	1600	1600	1600

Table A11.1. Design of the experiment (Exp 11) to familiarize with the flow setup.

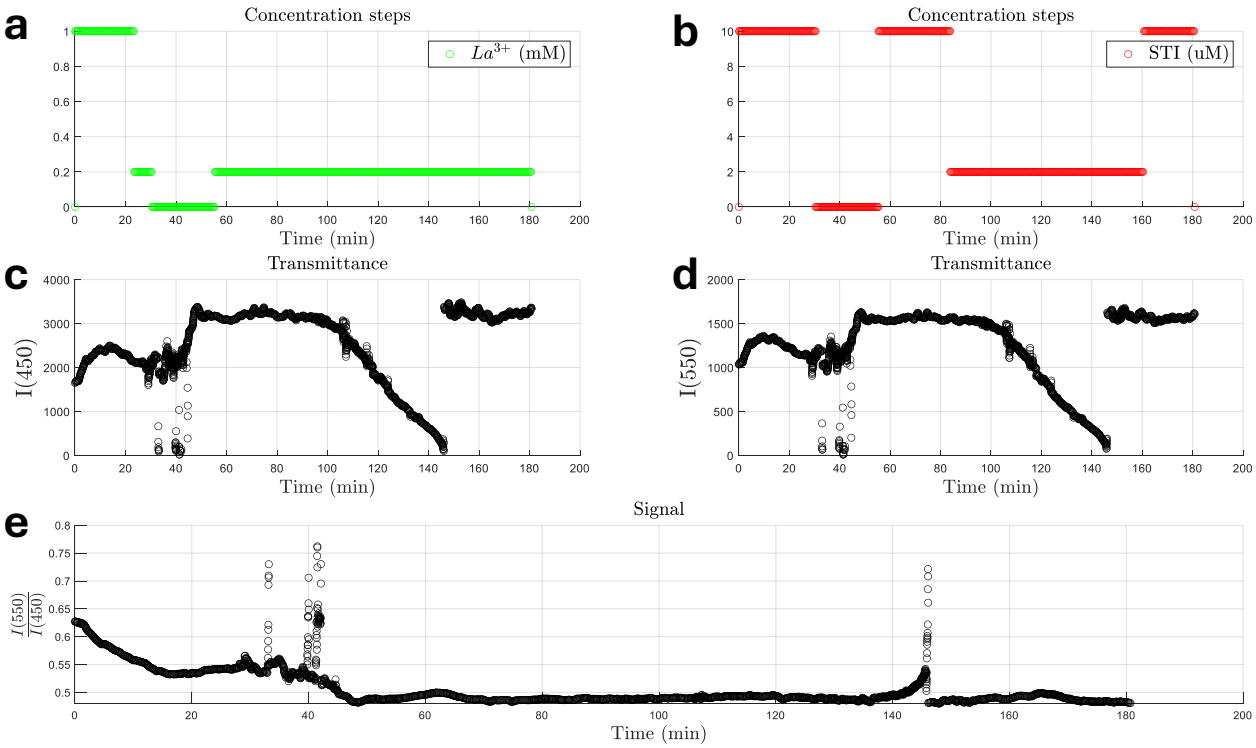

Figure A11.2. Experimental data for the familiarization of the flow setup. **(a)** Experimental variation of [La^{3+}] over time. **(b)** Experimental variation of $[STI]_0$ over time. **(c)** Transmittance at 450 nm. **(d)** Transmittance at 550 nm. **(e)** Experimental signal over time, defined as the transmittance at 550 nm divided by the transmittance at 450 nm over time.

The experimental data is reported in **Figure A11.2**. This figure shows the general format of raw flow data that we report in this text. **Figure A11.2a-b** show the programmed concentration steps of La^{3+} and STI in flow. **Figure A11.2c-d** show the crude transmittance at 450 nm and 500 nm, respectively, as measured by the UV-vis spectrometer. **Figure A11.2e** shows the 'signal' of the system, which we considered as the transmittance at 550 nm divided by the transmittance at 450 nm. Using a calibration curve in flow (see Exp 18), we could relate this signal to the current trypsin concentration. In later experiments we measure the transmittance at 500 nm instead of 550 nm as a more accurate internal standard. These results do not show any significant findings. The concentration steps caused the system to reach its low state and remain there throughout the experiment. From minute 100 to 145, significant bubbles were present in the tubes, which caused problems for the spectrometer and the available volume in the CSTRs. Bubble formation is typically indicated by large noise in the signal curve. The result of this experiment is the protocol as reported in Appendix B.1, and this experiment provided me with experience in how to operate the system.

Experiment 12. Next, we aimed to test a very low flow rate to see what effect this would have on the signal (Exp 12). This low flow rate of 250 µL h^{-1} was also used in Exp 11, but those results are not usable due to improper variation of the concentrations. The stock syringe solutions used for this experiment are as follows.

- **Tr + Tg** (15 µM Tr + 400 uM Tg dissolved in [4 mM HCl + 20 mM $CaCl_2$])
- **STI** (50 µM STI dissolved in **Buffer1**)

- **Buffer1** (0.5 M TRIS-HCl pH 7.8 + 20 mM $CaCl_2$)
- **Buffer2** (0.5 M TRIS-HCl pH 7.8 + 20 mM $CaCl_2$)
- **La** (5 mM $La(NO_3)_3.6H_2O$ dissolved in mQ)
- **BAPNA** (11.2 mM BAPNA dissolved in [0.20 mQ + 0.72 DMFA + 0.08 DMSO v:v])

The experimental procedure, the programmed flow rates of each syringe, is tabulated in **Table A12.1**.

(Values in µL/h)		Flush	Low La^{3+} (= 0.2 mM)		Flush	High La^{3+} (= 1.0 mM)	
			High $[STI]_{-1}$	Low $[STI]_0$		High $[STI]_{-1}$	Low $[STI]_0$
R1	**Tr + Tg**	50	50	50	50	50	50
	La	0	10	10	0	50	50
	STI	0	50 [10 µM]	10 [2 µM]	0	50 [10 µM]	10 [2 µM]
	Buffer1	200	140	180	200	100	140
R2	R1 Out	250	250	250	250	250	250
	BAPNA	100	100	100	100	100	100
	Buffer2	1250	1250	1250	1250	1250	1250
	R2 Out	1600	1600	1600	1600	1600	1600

Table A12.1. Design of the experiment (Exp 12) to test the effect of a very low flow rate (250 µL h^{-1}).

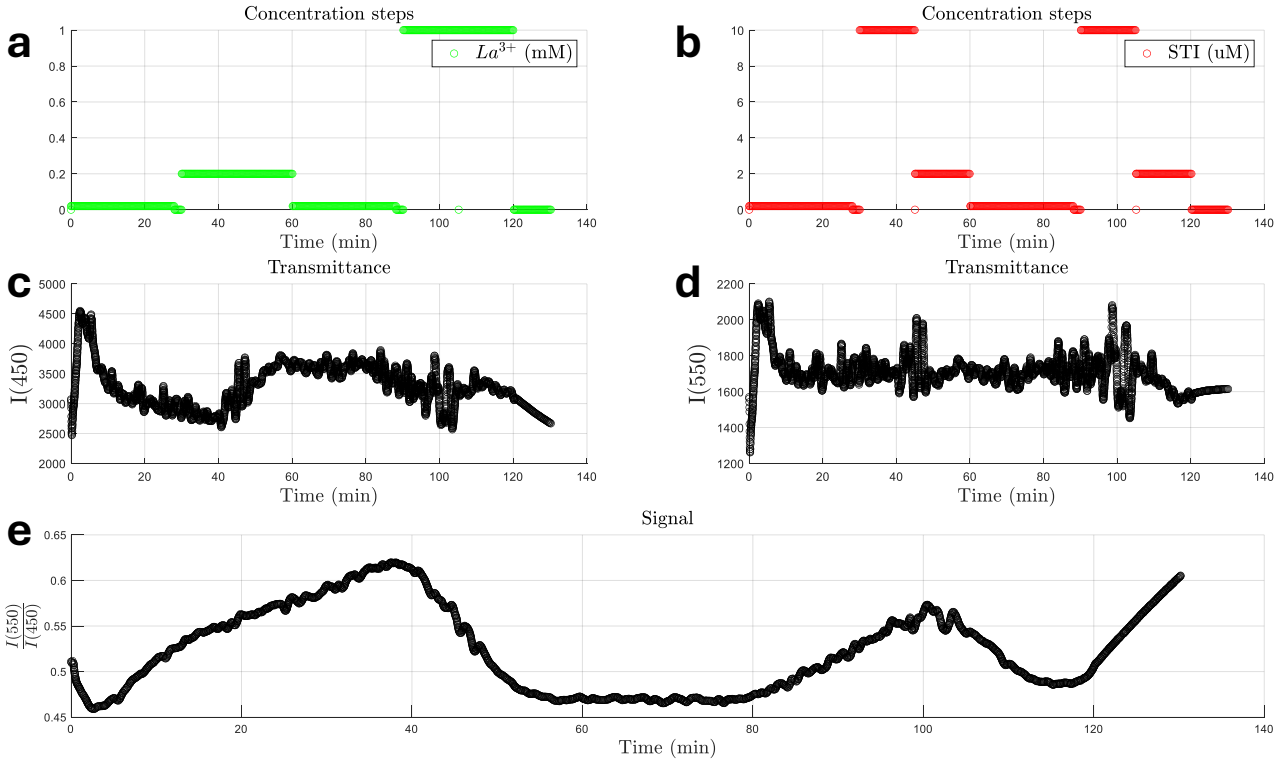

Figure A12.1. Experimental data for the experiment to test a very low flow rate. **(a)** Experimental variation of $[La^{3+}]$ over time. **(b)** Experimental variation of $[STI]_0$ over time. **(c)** Transmittance at 450 nm. **(d)** Transmittance at 550 nm. **(e)** Experimental signal over time, defined as the transmittance at 550 nm divided by the transmittance at 450 nm over time.

The results of this experiment are shown in **Figure A12.1**. We tested the effect of going from a high STI concentration to a low one (**Figure A12.1b**), at two different La^{3+} concentrations (**Figure A12.1a**). The signal shows some variation, indicating that a low and a high state are likely reached. However, we did not take enough time to let the system reach a steady state at each step, which makes it

difficult to reach conclusions. Furthermore, we noticed that this very low flow rate caused significant noise in the raw transmittance data (**Figure A12.1c-d**). We hypothesize that this noise is due to small, precipitated lanthanum salt particles forming in the CSTRs due to the limited solubility of La^{3+} at pH = 7.8. We conclude that higher flow rates are needed to effectively prevent as much La^{3+} from precipitating as possible.

Experiment 13. We were still interested in the experimental design of Exp 12, at double the flow rate (500 µL h^{-1}) through the first reactor. To this end, we used the same syringes as in Exp 12, and the experimental design is the same, but with all individual flow rates doubled.

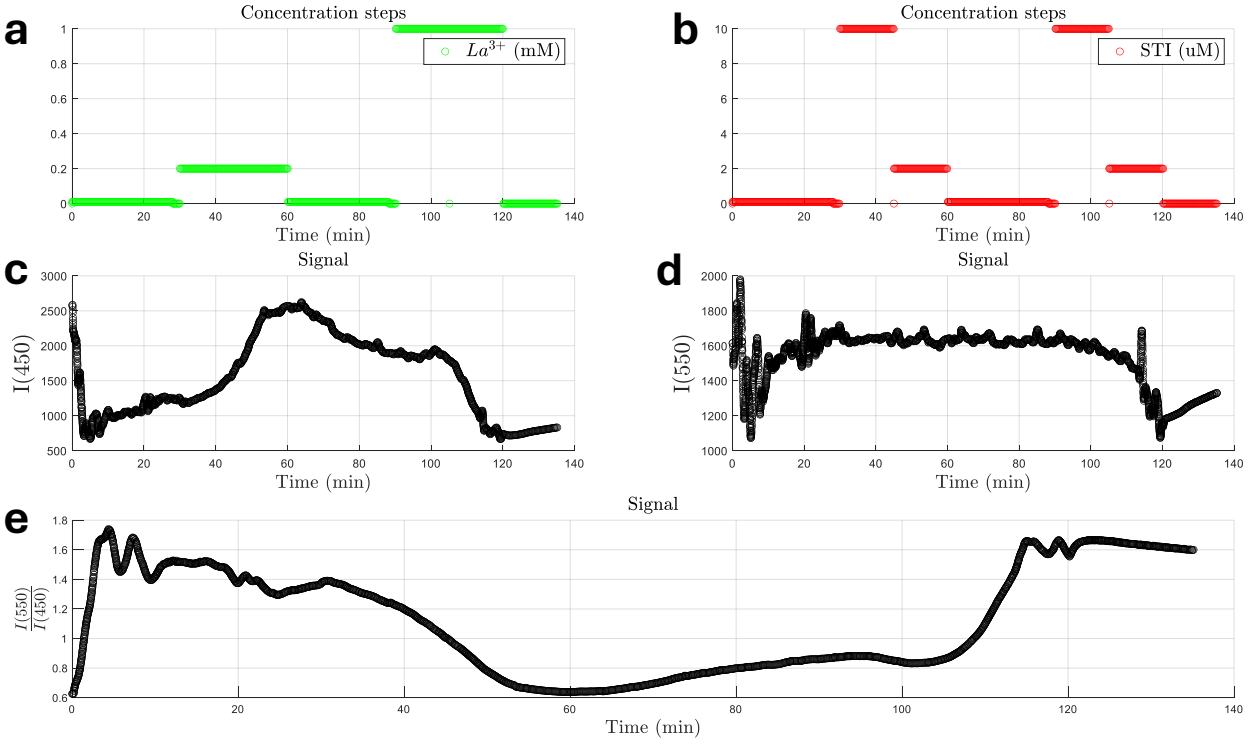

Figure A13.1. Experimental data for the experiment to test very short time steps. **(a)** Experimental variation of [La^{3+}] over time. **(b)** Experimental variation of $[STI]_0$ over time. **(c)** Transmittance at 450 nm. **(d)** Transmittance at 550 nm. **(e)** Experimental signal over time, defined as the transmittance at 550 nm divided by the transmittance at 450 nm over time.

The results are shown in **Figure A13.1**. Similarly to Exp 12, the system seems to travel between two states, but the time allocated for each concentration step was not sufficient for the system to reach steady state. We conclude that we must take more time per step to allow the system to reach its steady states.

Experiment 14. We were still interested in the response of the system to STI steps at varying La^{3+} concentrations, so we repeated Exp 13 but with longer time steps, namely we programmed one hour for the system to reach its steady states. The syringes used are the same as Exp 13. The experimental procedure is tabulated in **Table A14.1**.

(Values in µL/h)		Flush	Low La^{3+} (= 0.2 mM)		Flush	Low La^{3+} (= 0.2 mM)	
			High $[STI]_{-1}$	Mid $[STI]_0$		High $[STI]_{-1}$	Low $[STI]_0$
R1	**Tr + Tg**	100	100	100	100	100	100
	La	0	20	20	0	20	20
	STI	0	100 [10 µM]	60 [2 µM]	0	100[10 µM]	20 [2 µM]
	Buffer1	400	280	320	400	280	360
R2	R1 Out	500	500	500	500	500	500
	BAPNA	100	100	100	100	100	100
	Buffer2	1000	1000	1000	1000	1000	1000
	R2 Out	1600	1600	1600	1600	1600	1600

Flush	High La^{3+} (= 1.0 mM)		Flush	High La^{3+} (= 1.0 mM)	
	High $[STI]_{-1}$	Mid $[STI]_0$		High $[STI]_{-1}$	Low $[STI]_0$
100	100	100	100	100	100
0	100	100	0	100	100
0	100 [10 µM]	60 [2 µM]	0	100[10 µM]	20 [2 µM]
400	200	240	400	200	280
500	500	500	500	500	500
100	100	100	100	100	100
1000	1000	1000	1000	1000	1000
1600	1600	1600	1600	1600	1600

Table A14.1. Design of the experiment (Exp 14) to test the response of the system to longer time steps and several STI steps.

The results of the experiment above are shown in **Figure A14.1**. After 280 minutes, major bubble formation created significant noise. We thus render the data after this point unreliable. Bubbles were able to form because we programmed the system to perform the concentration steps automatically. We conclude that, going forward, we must manually operate the system throughout the experiments to ensure that bubbles are removed on time, as they can get stuck inside the system for extended periods of time. Furthermore, to keep each experiment focused, we conclude that we must keep $[La^{3+}]$ constant for an experiment. Before bubbles occurred, the data showed promising results. Namely, a clear, stable low-state signal is retrieved. The high state was not observed. Lastly, to improve efficiency, we aim to increase the flow rate even further.

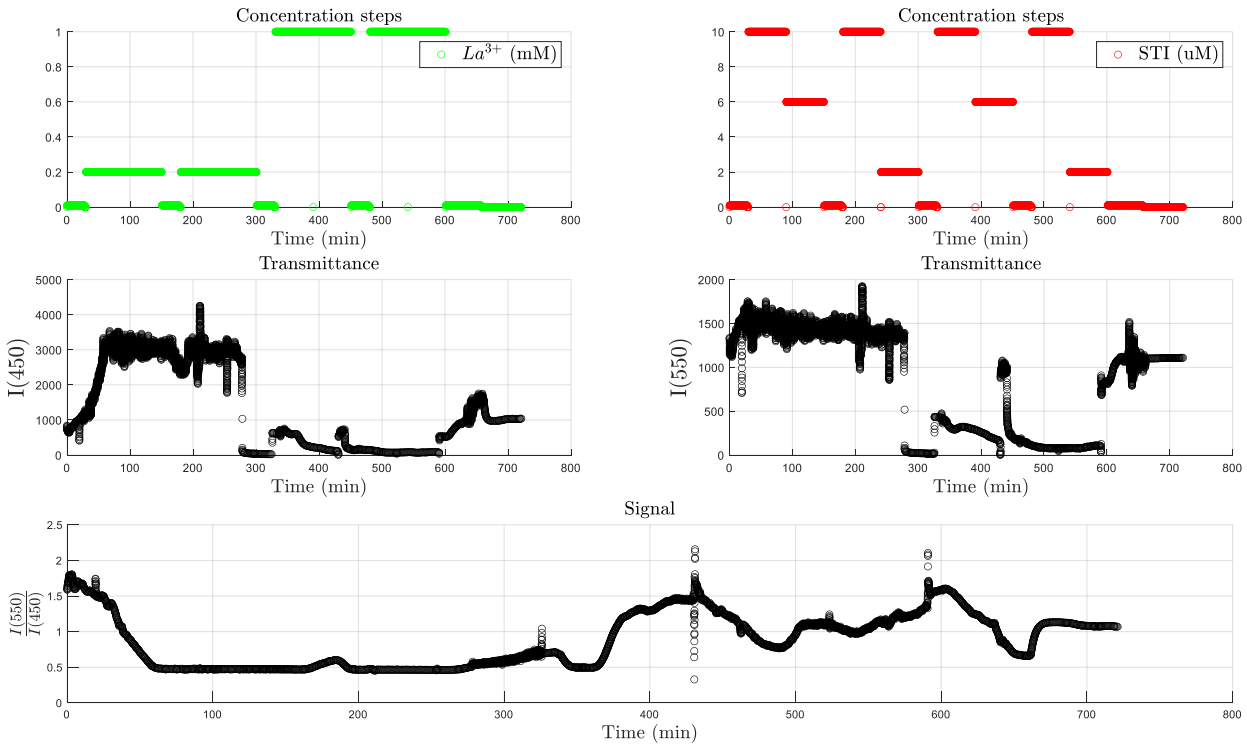

Figure A14.1. Experimental data for the experiment to test very short time steps. **(a)** Experimental variation of [La^{3+}] over time. **(b)** Experimental variation of $[STI]_0$ over time. **(c)** Transmittance at 450 nm. **(d)** Transmittance at 550 nm. **(e)** Experimental signal over time, defined as the transmittance at 550 nm divided by the transmittance at 450 nm over time.

Experiment 15 – Determine System Response to Gradual STI Increase and Sudden Drop

To determine the system response to a gradual increase in STI followed by a sudden decrease, we performed an adapted form of STI steps. We adjusted the experimental setup slightly to the scheme shown in **Figure A15.1**. We separated **Tr** and **Tg** into two separate syringes and removed the second **Buffer** syringe from R2 and combined it with **BAPNA** instead.

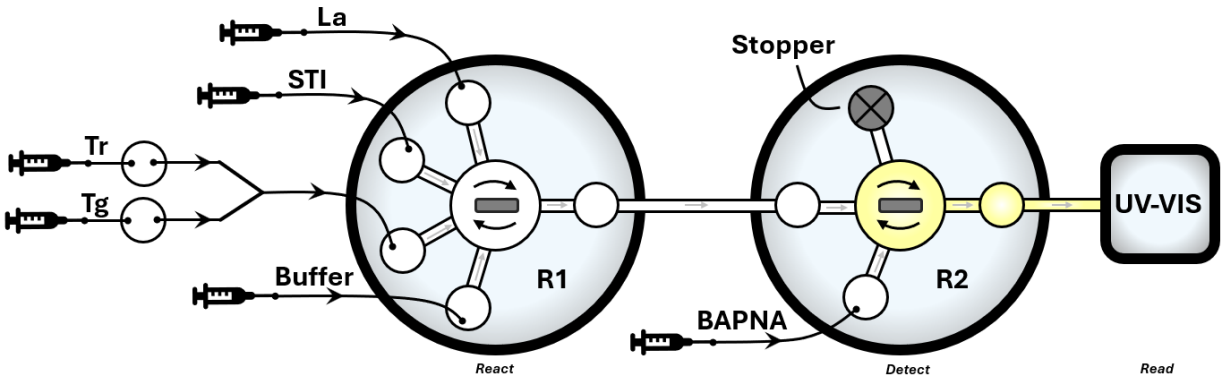

Figure A15.1. Schematic representation of the experimental setup for flow experiments.

The stock syringe solutions used for this experiment are as follows. The name of each syringe is highlighted in bold for ease of reference.

- **Tr** (30 µM in [4 mM HCl + 20 mM $CaCl_2$])
- **Tg** (1000 µM in [4 mM HCl + 20 mM $CaCl_2$])
- **STI** (50 µM STI dissolved in Buffer)
- **Buffer** (0.5 M TRIS-HCl pH 7.8 + 20 mM $CaCl_2$)
- **La** (5 mM $La(NO_3)_3.6H_2O$ dissolved in mQ)
- **BAPNA** (11.2 mM BAPNA dissolved in [0.20 mQ + 0.72 DMFA + 0.08 DMSO v:v])

The experimental procedure, the programmed flow rates of each syringe, is tabulated in **Table A15.1**. Note that the flow rate is now 1500 µL h^{-1}.

(Values in µL/h)		$[La^{3+}]_0$ = 0.66 mM				
		$[STI]_0$=0.83 µM	$[STI]_0$=5.83 µM	$[STI]_0$ = 12.5 µM	$[STI]_0$=15 µM	$[STI]_0$=0.83 µM
R1	**Tr**	300	300	300	300	300
	Tg	375	375	375	375	375
	La	200	200	200	200	200
	STI	25	175	375	450	25
	Buffer	600	450	275	200	600
R2	R1 Out	1500	1500	1500	1500	1500
	BAPNA + **Buffer**	500	500	500	500	500
	R2 Out	2000	2000	2000	2000	2000

Table A15.1. Design of the experiment to observe the system response to gradual STI increases followed by a sudden drop.

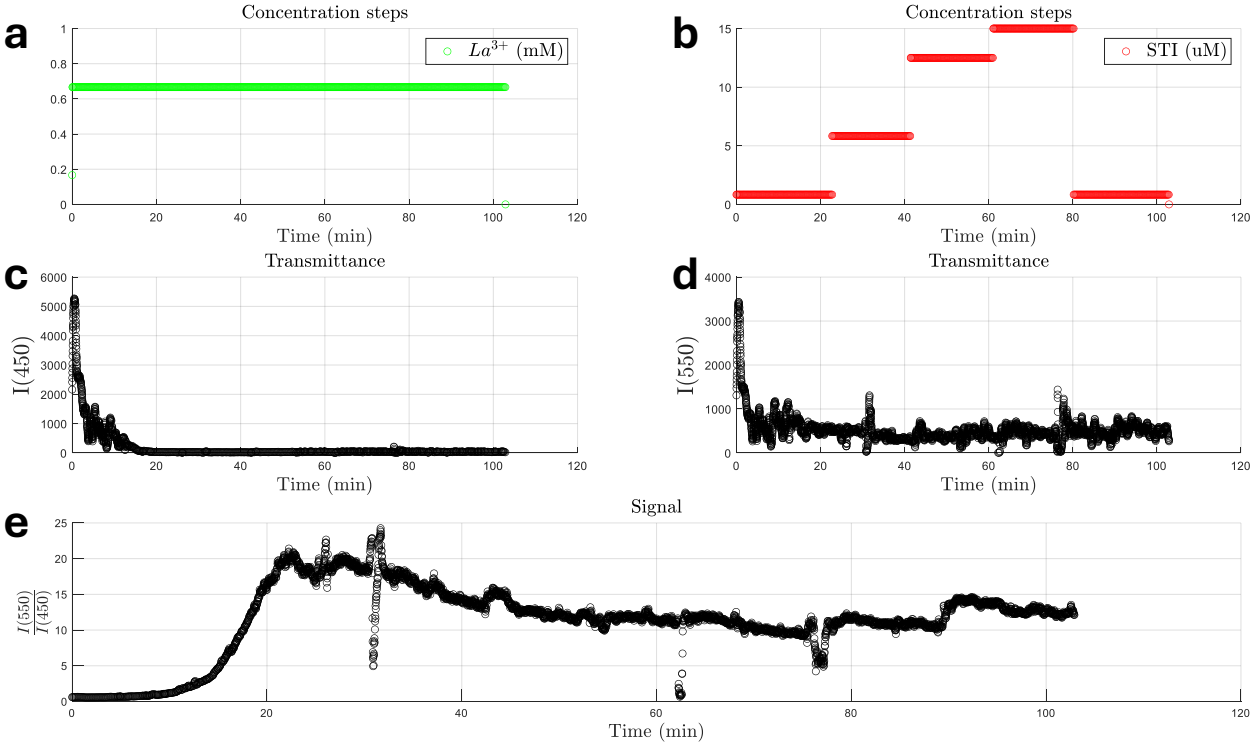

Figure A15.2. Experimental data of system response to gradual STI increase followed by a sudden drop. **(a)** Experimental variation of $[La^{3+}]$ over time. **(b)** Experimental variation of $[STI]_0$ over time. **(c)** Transmittance at 450 nm. **(d)** Transmittance at 550 nm. **(e)** Experimental signal over time, defined as the transmittance at 550 nm divided by the transmittance at 450 nm over time.

The experimental data is reported in **Figure A15.2**. This figure shows that the gradual increase in $[STI]_0$ starting from $[STI]_0$ = 0.83 μM causes the system to remain in the high state, $[Tr]^H_{SS}$. The low state, $[Tr]^L_{SS}$, was not observed. We note that the value of $[Tr]^H_{SS}$ was not the same for both instances of $[STI]_0$ = 0.83 μM, which we hypothesize is due to degradation of Tg inside the syringe, despite our results (see Chapter 3.2) indicating that Tg is stabilized in the storage conditions. **Figure A15.2d** shows significant noise in the data, and during the experiment, we observed the formation of particles inside the **BAPNA** + **Buffer** syringe, indicating that some BAPNA precipitated. We hypothesize that the addition of the buffer to this solution diluted the organic solvents for BAPNA, which reduced its solubility. We conclude that we should remove the buffer from this syringe, as there should be enough buffer from the R1out stream. We also conclude that a gradual increase in $[STI]_0$ keeps the system in its high state until a higher $[STI]_0$ than would be the case if we suddenly changed $[STI]_0$. For instance, see **Figure A12.1**, where $[STI]_0$ = 10 μM placed the system in its low state, whereas in this experiment (Exp 15), $[STI]_0$ = 15 μM was still not enough to suppress Tr activity to the low state.

Experiment 16 – Capture the Two Steady States

Thus far, we have not properly captured both the high and the low steady states in one experiment. To capture both $[Tr]^H_{SS}$ and $[Tr]^L_{SS}$, we performed the following experiment. The stock syringe solutions used for this experiment are the same as in Exp 15. The experimental procedure is shown in **Table A16.1**.

(Values in μL/h)		$[La^{3+}]_0$ = 0.66 mM					
		$[STI]_0$=15 μM	$[STI]_0$=0.66 μM		$[STI]_0$=15 μM	$[STI]_0$=0.66 μM	$[STI]_0$=15 μM
R1	**Tr**	300	300	Flushing	300	300	300
	Tg	375	375		375	375	375
	La	200	200		200	200	200
	STI	450	20		450	20	450
	Buffer	175	605		175	605	175
R2	R1 Out	1500	1500		1500	1500	1500
	BAPNA	500	500		500	500	500
	R2 Out	2000	2000		2000	2000	2000

Table A16.1. Design of the experiment to capture both steady states.

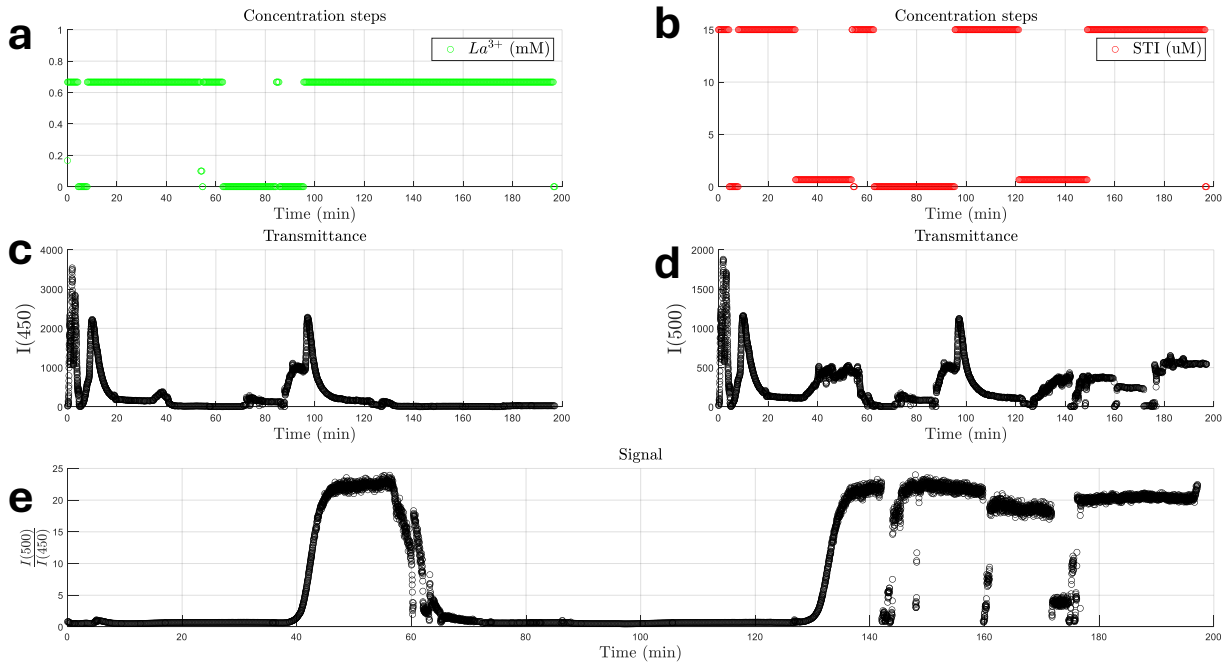

Figure A16.1. Experimental data for the experiment to capture both steady states. **(a)** Experimental variation of $[La^{3+}]$ over time. **(b)** Experimental variation of $[STI]_0$ over time. **(c)** Transmittance at 450 nm. **(d)** Transmittance at 500 nm. **(e)** Experimental signal over time, defined as the transmittance at 500 nm divided by the transmittance at 450 nm over time.

Figure A16.1 shows the experimental results. The two steady states ($[Tr]^H_{SS}$ and $[Tr]^L_{SS}$) are clearly visible. Furthermore, in the latter half of the experiment, we see that $[STI]_0$ = 15 µM gives $[Tr]^L_{SS}$, and going to $[STI]_0$ = 0.66 µM gives $[Tr]^H_{SS}$. Once $[Tr]^H_{SS}$ is reached, returning to $[STI]_0$ = 15 µM does not return the system to $[Tr]^L_{SS}$, which is a clear proof of hysteretic bistability. The conditions in which this experiment was performed will serve as a starting point for more robust, strategic and quantitative experiments on the bistability of our system.

Experiment 17 – Test an Extremely High Flow Rate

To test how the system would respond to an extremely high flow rate, we performed an experiment where STI is gradually increased at a flow rate of 3000 µL h^{-1}. The syringe solutions were the same as in Exp 15. **Table A17.1** shows the experimental procedure.

(Values in µL/h)		$[STI]_0$=0.42 µM	$[STI]_0$=3.33 µM	$[STI]_0$=6.67 µM	$[STI]_0$=10 µM	$[STI]_0$=11.67 µM
R1	**Tr**	800	800	800	800	800
	Tg	600	600	600	600	600
	La	400	400	400	400	400
	STI	25	200	400	600	700
	Buffer	1175	1000	800	600	500
R2	R1 Out	3000	3000	3000	3000	3000
	BAPNA	1000	1000	1000	1000	1000
	R2 Out	4000	4000	4000	4000	4000

Table A17.1. Design of the experiment to test an extremely high flow rate.

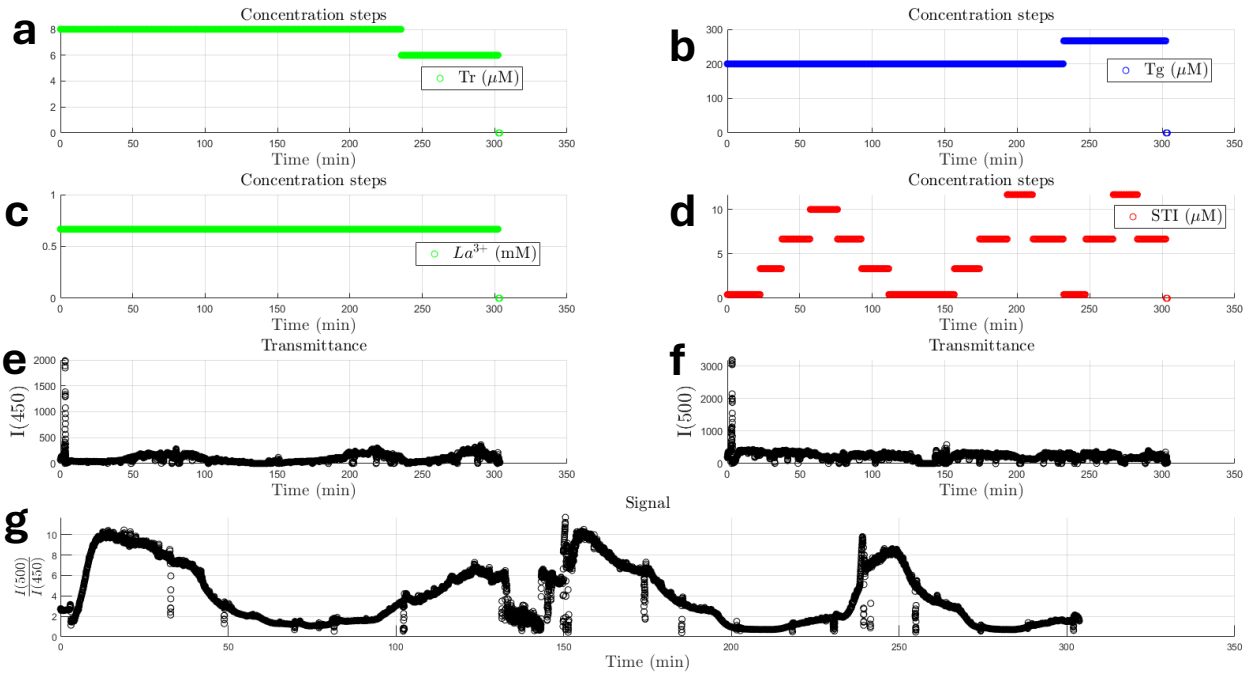

Figure A17.1. Experimental results for the experiment to test very short time steps. **(a)** Experimental variation of $[Tr]_0$ over time. **(b)** Experimental variation of $[Tg]_0$ over time **(c)** Experimental variation of $[La^{3+}]$ over time. **(d)** Experimental variation of $[STI]_0$ over time. **(e)** Transmittance at 450 nm. **(f)** Transmittance at 500 nm. **(g)** Experimental signal over time, defined as the transmittance at 500 nm divided by the transmittance at 450 nm over time.

The results are shown in **Figure A17.1**. It is difficult to state that we observe clear bistability under these conditions. The signal does not seem to vary between two clear states. Instead, it seems that intermediate states are also possible, although the response to $[STI]_0$ variations is still nonlinear. We decide that this flow rate is too high to reliably observe bistability under the conditions we use, although it is difficult to say conclusively with this limited test. We will stick to flow rates between 1500-2000 μL h^{-1} through R1, but more testing could be promising for this flow rate. We conclude that we have tested enough parameters, and that we want to start working towards the final demonstrations using consistent conditions.

Experiment 18 – Calibrate Trypsin Activity by BAPNA assay in Flow

To be able to convert the transmittance data to current Tr concentration in flow, we performed a calibration for trypsin concentration using BAPNA. We adapted the flow setup as introduced in Exp 15 slightly, to the schematic shown in **Figure A18.1**. This setup is only used for this experiment. All subsequent experiments thus use the setup as in Exp 15 again. We keep $[BAPNA]_0$ constant, while varying $[Tr]_0$. Each step of $[Tr]_0$ will give a different steady state signal.

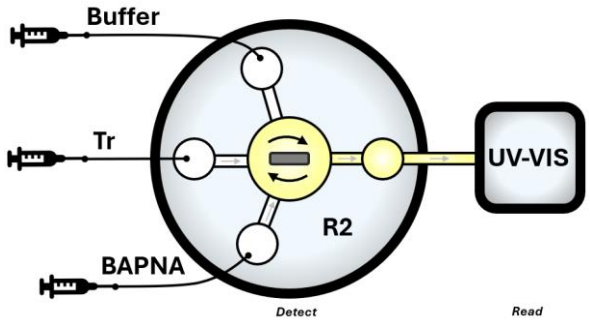

Figure A18.1. Schematic representation of the experimental setup for the calibration of trypsin by BAPNA in flow.

The syringe solutions for this experiment are as follows. The experimental procedure is tabulated in **Table A18.1**.

- **Tr** stocks:
  - **Tr_1**: 30 µM in [4 mM HCl + 20 mM $CaCl_2$] (first 4 $[Tr]_0$ points)
  - **Tr_2**: 300 µM in [4 mM HCl + 20 mM $CaCl_2$] (last 4 $[Tr]_0$ points)
- **Buffer** (0.1 M TRIS-HCl pH 7.8 + 20 mM $CaCl_2$)
- **BAPNA** (11.2 mM BAPNA dissolved in [0.20 mQ + 0.72 DMFA + 0.08 DMSO v:v])

(Values in µL/h)		$[Tr]_0$ = 0.15 µM	$[Tr]_0$ = 1.5 µM	$[Tr]_0$ = 7.5 µM	$[Tr]_0$ = 19.5 µM	$[Tr]_0$ = 52.5 µM	$[Tr]_0$ = 97.5 µM	$[Tr]_0$ = 150 µM	$[Tr]_0$ = 195 µM
R2	**BAPNA**	500	500	500	500	500	500	500	500
	Tr_1 or Tr_2	10	100	500	1300	350	650	1000	1300
	Buffer	1490	1400	1000	200	1150	850	500	200
	R2 Out	2000	2000	2000	2000	2000	2000	2000	2000

Table A18.1. Design of the experiment to calibrate trypsin concentration by BAPNA in flow.

Figure A18.2a shows the experimental results (in black) combined with the Tr steps (in red). We took the steady state (final) value of the signal for each Tr step and plotted this signal against Tr to create the calibration curve in **Figure A18.2b**. The calibration is linear below $[Tr]_0$ = 100 µM. We use this calibration curve to convert transmittance signal data into [Tr].

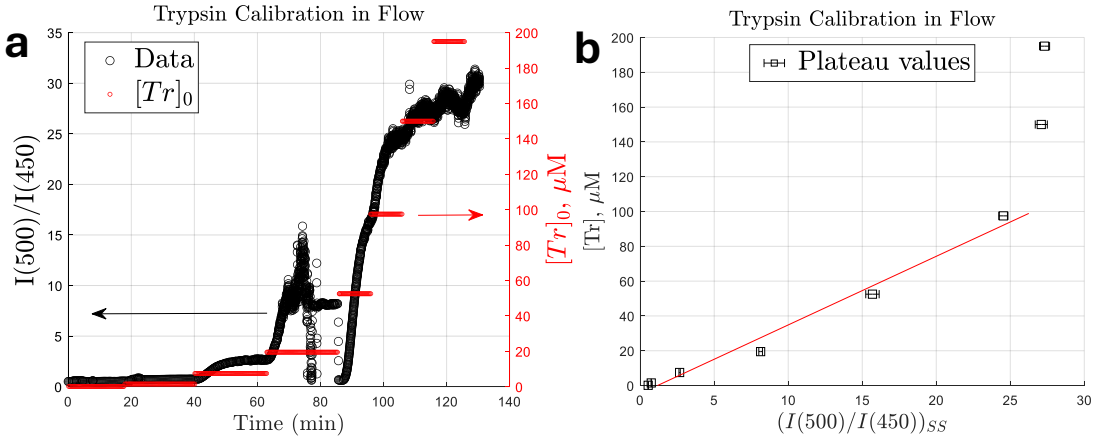

Figure A18.2. Experimental results of trypsin calibration in flow. **(a)** Signal data (black) at each Tr step (red). **(b)** Final calibration curve for trypsin by BAPNA in flow.

Experiments 19–20 – Determine System Response to Gradual STI Steps

We wanted to visualize the system response to gradual $[STI]_0$ changes at varying $[La^{3+}]_0$ to observe the effect of La^{3+} on the history dependent behavior of the network. To this end, we performed two experiments, one $[La^{3+}]_0$ per experiment. Both experiments use the same syringe solutions as Exp 15.

Experiment 19 – La^{3+} = 0.10 mM. The experimental procedure is tabulated in **Table A19.1**. We use a staircase-wise combination of these conditions.

(Values in µL/h)		$[STI]_0$=0.5 µM	$[STI]_0$=2 µM	$[STI]_0$=6 µM	$[STI]_0$=10 µM	$[STI]_0$=15µM
R1	**Tr**	300	300	300	300	300
	Tg	375	375	375	375	375
	La	30	30	30	30	30
	STI	15	60	180	300	450
	Buffer	780	735	615	495	345
R2	R1 Out	1500	1500	1500	1500	1500
	BAPNA	500	500	500	500	500
	R2 Out	2000	2000	2000	2000	2000

Table A19.1. Design of the experiment to vary STI gradually with $[La^{3+}]_0$ = 0.10 mM.

Experiment 20 – La^{3+} = 0.40 mM. The experimental procedure is tabulated in **Table A20.1**. We use a staircase-wise combination of these conditions.

(Values in µL/h)		$[STI]_0$=0.5 µM	$[STI]_0$=6 µM	$[STI]_0$=10 µM	$[STI]_0$=15 µM	$[STI]_0$=23 µM
R1	**Tr**	300	300	300	300	300
	Tg	375	375	375	375	375
	La	120	120	120	120	120
	STI	15	180	300	450	690
	Buffer	690	525	405	255	15
R2	R1 Out	1500	1500	1500	1500	1500
	BAPNA	500	500	500	500	500
	R2 Out	2000	2000	2000	2000	2000

Table A20.1. Design of the experiment to vary STI gradually with $[La^{3+}]_0$ = 0.40 mM.

The results of both experiments (Exp 19 & 20) are shown in **Figure A20.1a-b**. Addition of La^{3+} affects the system by increasing the value of the high steady state. Both $[Tr]^H_{SS}$ and $[Tr]^L_{SS}$ were reached by variation of $[STI]_0$ stepwise for both $[La^{3+}]_0$. Low $[STI]_0$ causes $[Tr]^H_{SS}$, and high $[STI]_0$ causes $[Tr]^L_{SS}$. The state that is reached depends on the $[STI]_0$ path taken beforehand, so called history dependent behavior. To visualize the specific state reached by each STI step better, we noted the steady state value per $[STI]_0$, see **Figure A20.1c**. We conclude that addition of La^{3+} increases the magnitude of $[Tr]^H_{SS}$ and shifts the switch from $[Tr]^H_{SS}$ to $[Tr]^L_{SS}$ to higher $[STI]_0$, and the switch from $[Tr]^L_{SS}$ to $[Tr]^H_{SS}$ was affected in the same way. We have thus demonstrated that addition of La^{3+} provides control over the history dependent bistable behavior of the system.

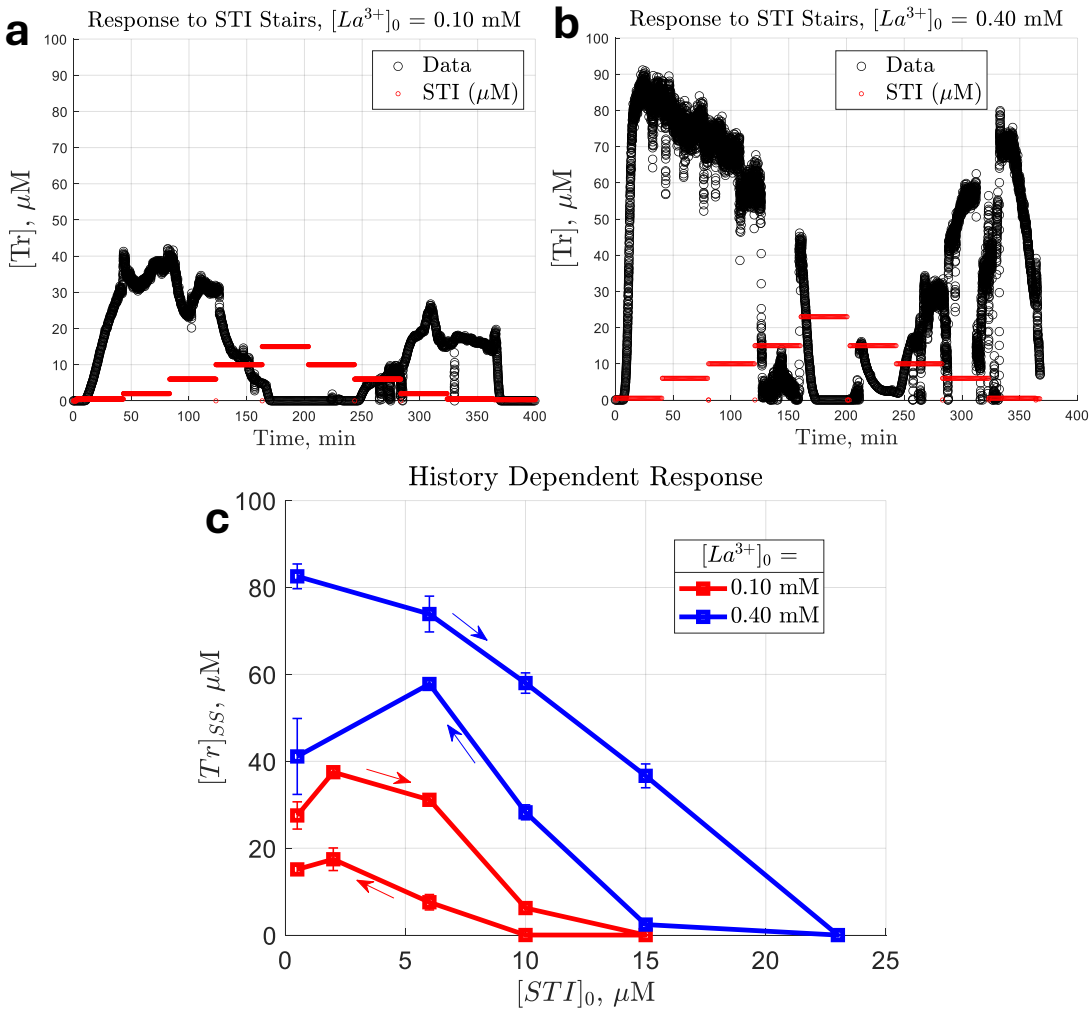

Figure A20.1. Experimental results of gradual variation of $[STI]_0$ in stairs for two different $[La^{3+}]_0$. **(a)** System response to gradual variation of $[STI]_0$ in stairs, for $[La^{3+}]_0$ = 0.10 mM. **(b)** $[La^{3+}]_0$ = 0.40 mM. **(c)** History dependent bistability plot. Each point is the steady state value of the response to the $[STI]_0$ step. The arrows indicate the direction of change of $[STI]_0$. Error bars are s.e. of the last 30% of the data per $[STI]_0$ step.

Experiments 21–26 – Perform Final Demonstration: Bistability Control by La^{3+}

Thus far we have demonstrated the ability to control the history dependent behavior of the system by tuning the La^{3+} concentration. For the final demonstration of this thesis, and to complete the aim thereof, we performed a final set of experiments in flow. Each experiment is covered individually, and their results are combined in a final bistability plot after Exp 26. For these experiments, the syringe solutions are as follows.

- **Tr** (30 µM in [4 mM HCl + 20 mM $CaCl_2$])
  - 100 mM $CaCl_2$ instead of 20 mM for Exp 25 and Exp 26
- **Tg** (1000 µM in [4 mM HCl + 20 mM $CaCl_2$])
  - 100 mM $CaCl_2$ instead of 20 mM for Exp 25 and Exp 26
- **STI** (50 µM STI dissolved in **Buffer**):
- **Buffer** (0.2 M TRIS-HCl pH 7.8 + 20 mM $CaCl_2$).

- 100 mM $CaCl_2$ instead of 20 mM for Exp 25 and Exp 26

- **La** (5 mM $La(NO_3)_3.6H_2O$ dissolved in mQ).
- **BAPNA** (11.2 mM BAPNA dissolved in [0.20 mQ + 0.72 DMFA + 0.08 DMSO v:v]):

To demonstrate the ability to control the bistability by controlling $[La^{3+}]_0$, the system must be placed in the desired $[STI]_0$ conditions while ensuring that the system does not recall information about the $[STI]_0$ path taken beforehand. Before and after each $[STI]_0$ step, we returned the system to a baseline value ($[STI]_{-1}$) that is guaranteed to be in either the low state or the high state. Specifically, $[STI]_{-1}$ = 23 μM gives $[Tr]^L_{SS}$, and $[STI]_{-1}$ = 0.5 μM gives $[Tr]^L_{SS}$. To this end, we aimed to perform at least four experiments. One experiment per branch ('thermodynamic branch', $[STI]_{-1}$ = 23 μM and 'kinetic branch', $[STI]_{-1}$ = 0.5 μM), for each $[La^{3+}]$ (0.10 mM and 0.40 mM). The combined results of these experiments in the form of a bistability plot will allow us to demonstrate the ability to control the bistability of a bistable enzymatic system by tuning the concentration of a rate-enhancing metal ion.

Experiment 21 – $[STI]_{-1}$ = 23 μM, $[La^{3+}]_0$ = 0.10 mM (1). The experimental design is shown in **Table A21.1**. The baseline condition ($[STI]_{-1}$) is returned to before and after every $[STI]_0$ step. The experimental results are plotted in **Figure A21.1**.

(Values in μL/h)		$[STI]_{-1}$=23 μM	$[STI]_0$=0.5 μM	$[STI]_0$=6 μM	$[STI]_0$=3 μM
R1	**Tr**	400	400	400	400
	Tg	500	500	500	500
	La	40	40	40	40
	STI	920	20	240	120
	Buffer	140	1040	820	940
R2	R1 Out	2000	2000	2000	2000
	BAPNA	625	625	625	625
	R2 Out	2625	2625	2625	2625

Table A21.1. Experimental design for bistability, $[STI]_{-1}$ = 23 μM and $[La^{3+}]_0$ = 0.10 (1).

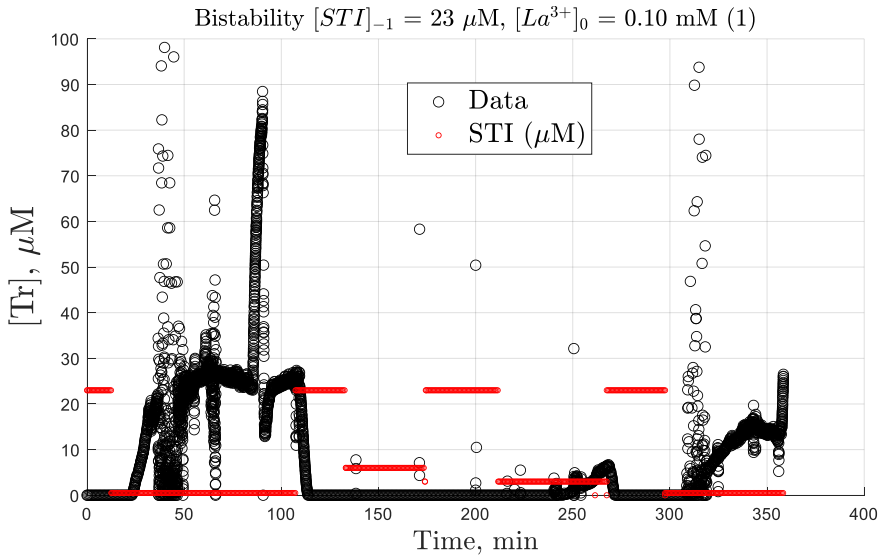

Figure A21.1. Experimental results. Bistability response for $[STI]_{-1}$ = 23 μM, $[La^{3+}]_0$ = 0.10 mM (1).

Experiment 22 – $[STI]_{-1}$ = 23 µM, $[La^{3+}]_0$ = 0.10 mM (2). The experimental design is shown in **Table A22.1**. The baseline condition ($[STI]_{-1}$) is returned to before and after every $[STI]_0$ step. The experimental results are plotted in **Figure A22.1**.

(Values in µL/h)		$[STI]_{-1}$=23 µM	$[STI]_0$=8 µM	$[STI]_0$=6 µM	$[STI]_0$=0.5 µM	$[STI]_0$=4 µM	$[STI]_0$=2 µM	$[STI]_0$=1 µM
R1	**Tr**	400	400	400	400	400	400	400
	Tg	500	500	500	500	500	500	500
	La	40	40	40	40	40	40	40
	STI	920	320	240	320 20	160	80	40
	Buffer	140	740	820	740 1040	900	980	1020
R2	R1 Out	2000	2000	2000	2000	2000	2000	2000
	BAPNA	667	667	667	667	667	667	667
	R2 Out	2667	2667	2667	2667	2667	2667	2667

Table A22.1. Experimental design for bistability, $[STI]_{-1}$ = 23 µM and $[La^{3+}]_0$ = 0.10 (2).

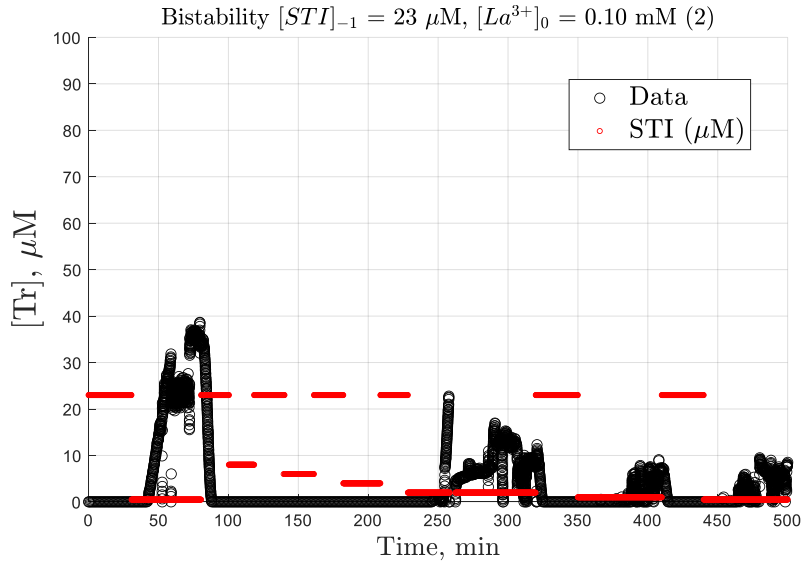

Figure A22.1. Experimental results. Bistability response for $[STI]_{-1}$ = 23 µM, $[La^{3+}]_0$ = 0.10 mM (2).

Experiment 23 – $[STI]_{-1}$ = 23 µM, $[La^{3+}]_0$ = 0.10 mM (3). The experimental design is shown in **Table A23.1**. The baseline condition ($[STI]_{-1}$) is returned to before and after every $[STI]_0$ step. The experimental results are plotted in **Figure A23.1**.

(Values in µL/h)		$[STI]_{-1}$=23 µM	$[STI]_0$=8 µM	$[STI]_0$=0.5 µM	$[STI]_0$=4 µM	$[STI]_0$=2 µM	$[STI]_0$=1 µM	$[STI]_0$=3 µM
R1	**Tr**	400	400	400	400	400	400	400
	Tg	500	500	500	500	500	500	500
	La	40	40	40	40	40	40	40
	STI	920	320	20	160	80	40	120
	Buffer	140	740	1040	900	980	1020	940
R2	R1 Out	2000	2000	2000	2000	2000	2000	2000
	BAPNA	667	667	667	667	667	667	667
	R2 Out	2667	2667	2667	2667	2667	2667	2667

Table A23.1. Experimental design for bistability, $[STI]_{-1}$ = 23 µM and $[La^{3+}]_0$ = 0.10 (3).

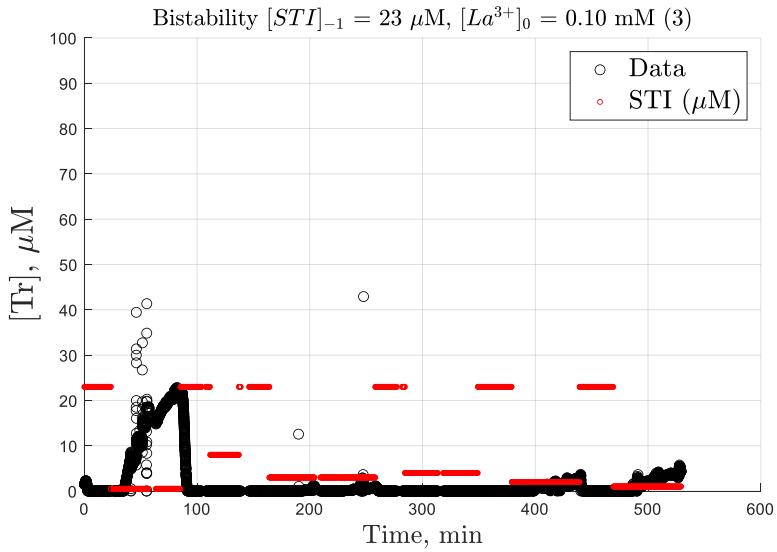

Figure A23.1. Experimental results. Bistability response for $[STI]_{-1}$ = 23 µM, $[La^{3+}]_0$ = 0.10 mM (3).

Experiment 24 – $[STI]_{-1}$ = 23 µM, $[La^{3+}]_0$ = 0.40 mM. The experimental design is shown in **Table A24.1**. The baseline condition ($[STI]_{-1}$) is returned to before and after every $[STI]_0$ step. The experimental results are plotted in **Figure A24.1**.

(Values in µL/h)		$[STI]_{-1}$=23 µM	$[STI]_0$=8 µM	$[STI]_0$=0.5 µM	$[STI]_0$=4 µM	$[STI]_0$=2 µM	$[STI]_0$=1 µM
R1	**Tr**	400	400	400	400	400	400
	Tg	500	500	500	500	500	500
	La	160	160	160	160	160	160
	STI	920	320	20	160	80	40
	Buffer	20	620	920	780	860	900
R2	R1 Out	2000	2000	2000	2000	2000	2000
	BAPNA	667	667	667	667	667	667
	R2 Out	2667	2667	2667	2667	2667	2667

Table A24.1. Experimental design for bistability, $[STI]_{-1}$ = 23 µM and $[La^{3+}]_0$ = 0.40.

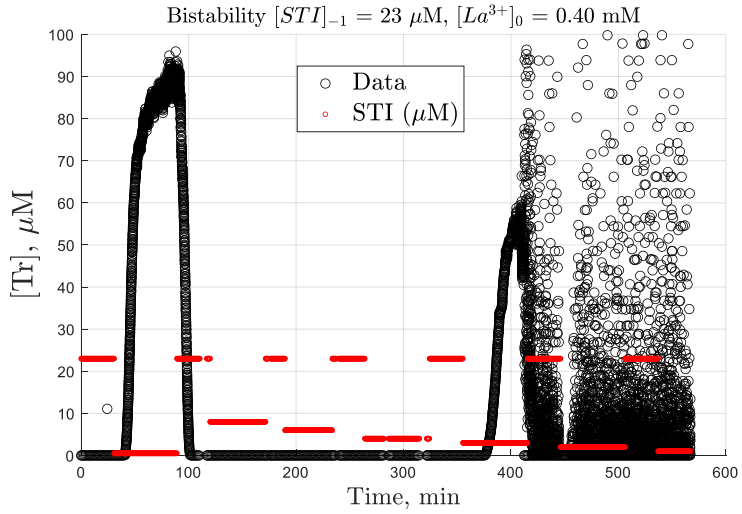

Figure A24.1. Experimental results. Bistability response for $[STI]_{-1}$ = 23 µM, $[La^{3+}]_0$ = 0.40 mM.

Experiment 25 – $[STI]_{-1}$ = 0.5 µM, $[La^{3+}]_0$ = 0.10 mM. The experimental design is shown in **Table A25.1**. The baseline condition ($[STI]_{-1}$) is returned to before and after every $[STI]_0$ step. The experimental results are plotted in **Figure A25.1**.

(Values in µL/h)		$[STI]_{-1}$=0.5 µM	$[STI]_0$=4 µM	$[STI]_0$=8 µM	$[STI]_0$=23 µM
R1	**Tr**	400	400	400	400
	Tg	500	500	500	500
	La	40	40	40	40
	STI	20	160	320	920
	Buffer	1040	900	740	140
R2	R1 Out	2000	2000	2000	2000
	BAPNA	667	667	667	667
	R2 Out	2667	2667	2667	2667

Table A25.1. Experimental design for bistability, $[STI]_{-1}$ = 0.5 µM and $[La^{3+}]_0$ = 0.10.

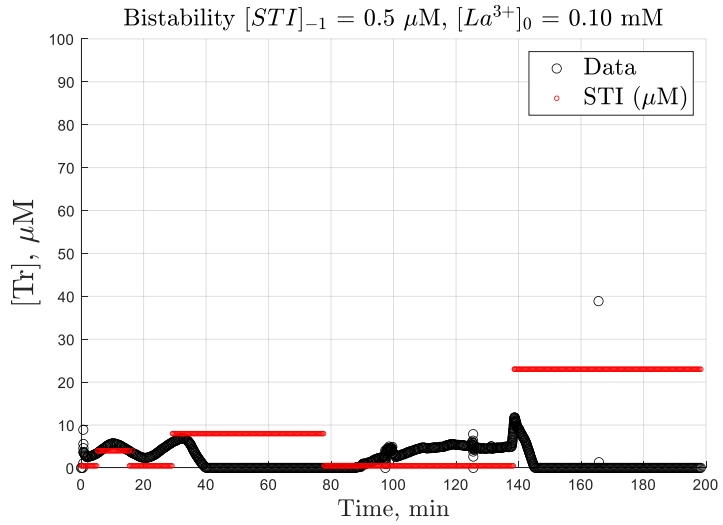

Figure A25.1. Experimental results. Bistability response for $[STI]_{-1}$ = 0.5 µM, $[La^{3+}]_0$ = 0.10 mM.

Experiment 26 – $[STI]_{-1}$ = 0.5 µM, $[La^{3+}]_0$ = 0.40 mM. The experimental design is shown in **Table A26.1**. The baseline condition ($[STI]_{-1}$) is returned to before and after every $[STI]_0$ step. The experimental results are plotted in **Figure A26.1**.

(Values in µL/h)		$[STI]_{-1}$=0.5 µM	$[STI]_0$=4 µM	$[STI]_0$=8 µM	$[STI]_0$=23 µM
R1	**Tr**	400	400	400	400
	Tg	500	500	500	500
	La	160	160	160	160
	STI	20	160	320	920
	Buffer	920	480	620	20
R2	R1 Out	2000	2000	2000	2000
	BAPNA	667	667	667	667
	R2 Out	2667	2667	2667	2667

Table A26.1. Experimental design for bistability, $[STI]_{-1}$ = 0.5 µM and $[La^{3+}]_0$ = 0.40.

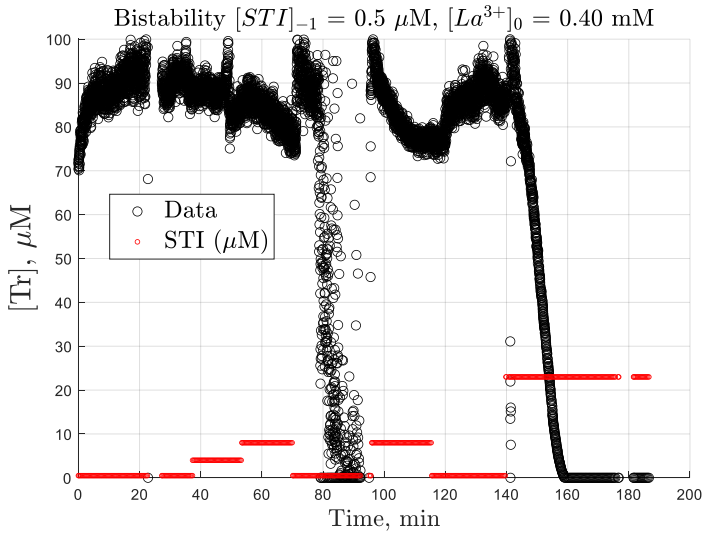

Figure A26.1. Experimental results. Bistability response for $[STI]_{-1}$ = 0.5 µM, $[La^{3+}]_0$ = 0.40 mM.

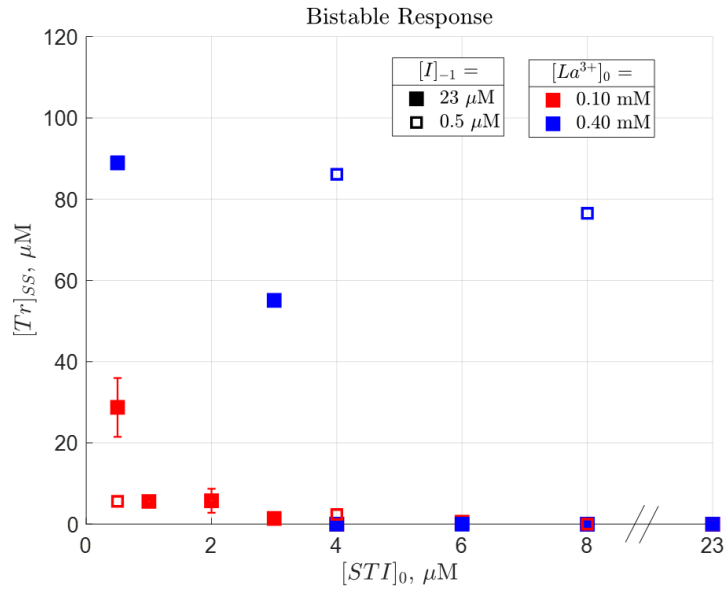

Figure A26.2. Bistability plot of the network's steady states in flow conditions. Combined results from Exp 21–26. Filled squares are $[STI]_{-1}$ = 23 µM, empty squares are [STI] = 0.5 µM. Red squares are $[La^{3+}]_0$ = 0.10 mM, blue squares are $[La^{3+}]_0$ = 0.40 mM.

We now take the steady state [Tr] value for each $[STI]_0$ step for these experiments and plot it against $[STI]_0$ to create the final bistability plot, see **Figure A26.2**. $[Tr]^H_{SS}$ is significantly increased (from ~20 µM to ~80 µM) when we increase $[La^{3+}]$ from 0.10 mM to 0.40 mM. The switching point between $[Tr]^H_{SS}$ and $[Tr]^L_{SS}$ is also significantly impacted by addition of La^{3+}. The thermodynamic branch for $[La^{3+}]_0$ =0.10 mM (filled red squares) has a switching point between $[STI]_0$ = 3-4 µM, and the switching point for the thermodynamic branch for $[La^{3+}]_0$ = 0.40 (filled blue squares) is around the same point. Hence, the $[STI]_{-1}$ = 23 µM branch is not shifted horizontally by addition of La^{3+}. However, the kinetic branch ($[STI]_{-1}$ = 0.5 µM) is affected differently. For $[La^{3+}]_0$ = 0.10 mM (empty red squares), the switching point is between $[STI]_0$ = 4-8 µM, but for $[La^{3+}]_0$ = 0.40 mM (empty blue squares), the switching point is

between $[STI]_0$ = 8-23 μM. This difference is most clearly seen by the fact that, for $[STI]_0$ = 8 μM, the empty blue square is in the high state, and the empty red square is in the low state.

The addition of La^{3+} affects the magnitude of the steady states and the switching point between the two states. We have thus demonstrated the ability to control the bistability of the network by controlling the amount of La^{3+} present, which affects the strength of the chemical feedback loop.

Appendix B – Protocols

B.1 – Preparation of Flow Experiment

1. Clean the microfluidic chips:
   a. Squirt mQ into the openings of the microfluidic chip.
   b. Repeat step 1.a. with EtOH
   c. Tap the microfluidic chip holes down on some paper.
   d. Completely dry the microfluidic chip with a N_2 gas gun.
2. Clean the tubes:
   a. Fill a syringe with mQ and block it with a plunger.
   b. Connect the tube to this syringe.
   c. Empty about 1-2 mL of the syringe into the tube to fully rinse it. Do this with some force to ensure the tube is fully rinsed.
   d. Repeat steps 2.a. – 2.d. with EtOH.
   e. To dry the tubes, flail them around in the air to evaporate the EtOH.
   f. To completely dry the tubes, shoot a N_2 gas gun into the tube until there is no liquid left inside.
3. Clean the syringes:
   a. Empty the syringes' contents.
   b. Fill them partially with mQ while keeping a finger on the outlet of the syringe.
   c. Insert the plunger very slightly to block the wide hole.
   d. Turn over the syringe + plunger so that the mQ falls to the plunger.
   e. Remove the finger.
   f. Slowly push the plunger until the mQ reaches the outlet.
   g. Push the syringe empty using the plunger to wash the entire inside of the syringe.
   h. Repeat steps 3.a. – 3.g. with EtOH.
   i. Rinse the plunger entirely with mQ and then EtOH.
   j. Let them dry on a paper towel.
   k. After some time, completely dry them with a N_2 gas gun.
   l. After the syringes and plungers are dried, insert the plungers into the syringes all the way and store them like this to prevent dust accumulation.
4. Fill the syringes:
   a. Take a hypodermic needle and connect it to a syringe of the desired size.
   b. Suck the desired stock solution into the cleaned syringe by slowly pulling the plunger. Note: proteins in solution are strong surfactants. Take much care to prevent air from being sucked through the needle.
   c. After the syringes are filled, label each appropriately by writing the label on a piece of tape and sticking it on the glass, as close to the outlet as possible.
5. Install the syringes into the setup:
   a. Turn on the syringe holder.
   b. Turn on the computer and log in.
   c. Open QMixElements.
   d. Right click the syringe and select 'configure syringe'.
   e. Select the appropriate syringe size (i.e., 1 mL, 5 mL, 25 mL, etc.).

f. Right click the syringe and select ‘reference move’. The syringe will start moving to the null position. Make sure the module is empty.
g. Connect a tube to the syringe you desire to install.
h. Slowly push the syringe until a small droplet is formed at the tube outlet. Now the tube is filled.
i. Check how much liquid is left in the syringe. Example: 3.85 mL.
j. Right click on the ‘yellow arrow pointing up’ icon and enter the maximum value.
k. Left click on the ‘yellow arrow pointing up’ icon. This will tell the module to retract the syringe holder rapidly. Reminder: the syringe is not inside the holder yet. Stop the movement right before the read volume inside the syringe is reached. Example: 3.7 mL. If you overshoot, right click the ‘blue arrow pointing down’ icon and do the same.
l. Place the syringe into the holder and tighten it. Make sure the plunger and syringe are perfectly horizontal to avoid damaging them.
m. Repeat steps 5.d. – 5.m. for each filled syringe.
n. Ensure all syringes are labeled correctly both physically and in QMixElements.

6. Connect the syringes to the microfluidic chips:
   a. Take the tube of a syringe and stick it into the desired hole in the microfluidic chip.
   b. In QMixElements, right click the ‘blue arrow pointing down’ icon and enter the value ‘6000 µL/h’.
   c. Left click the ‘blue arrow pointing down’ icon and watch the meniscus of the liquid inside the tube enter the microfluidic chip. Stop the movement right when the meniscus reaches the reactor
   d. Repeat steps 6.a. – 6.c. for each syringe.
   e. At every moment when all inlets of a microfluidic chip are used, follow the following steps:
      i. Fill the reactor entirely with the least reactive and most abundant syringe content that is connected to that respective chip. Fill the reactor until a small droplet forms in the outlet of the chip.
      ii. If you desire several reactors in series, insert a connecting tube to the outlet of this reactor. If this is the last reactor, insert the UV-vis-connecting tube to the outlet of this reactor.
      iii. Fill the connecting tube until a small droplet forms at the outlet of this connecting tube.
      iv. Enter the outlet of the connecting tube into an inlet of the next sequential reactor if you desire several reactors in series. If this is the last reactor, insert the UV-vis-connecting tube into the detection machine.
   f. Ensure there are absolutely no bubbles anywhere in the setup. If you see a bubble, re-connect all tubes starting from that point.

7. Rinse the setup:
   a. If, at any point, you are unsure about the signal that the spectrometer is giving or have reason to believe that there is something stuck inside the spectrometer (precipitate or bubbles), then you may rinse the setup. Take a glass syringe that we cleaned in step 3.
   b. Fill this syringe with 100 mM HCl.
   c. Install the syringe in one of the slots.
   d. Connect the syringe to all chips you will use, connect the chips in series, and connect the last chip to the spectrometer.
   e. Close any open ends with stoppers.
   f. Run 3000 µL h^{-1} of 100 mM HCl out of the syringe and into the setup to rinse the setup and the spectrometer. The value that the spectrometer reads out should plateau after a few minutes. This indicates that the setup has been cleaned properly, and nothing is being released anymore.
   g. Ideally, you should perform steps 7.a. – 7.f. before and after every experiment that you run, to maintain the setup for other users, and to prevent buildup from forming.
   h. Note, you can also flush the system manually by connecting a syringe to the setup/spectrometer and pushing the plunger yourself. This is not recommended, as you must take great care to keep the pressure on the spectrometer low. Pushing too hard may break the spectrometer.